PERFORMANCE-BASED FIRE SAFETY DESIGN FOR AUTOMATED VEHICLE PARKING STEEL STRUCTURES

by

Burak Ayva

B.S., Mechanical Engineering, Bogazici University, 2018

Submitted to the Institute for Graduate Studies in
Science and Engineering in partial fulfillment of
the requirements for the degree of
Master of Science

Graduate Program in Civil Engineering
Boğaziçi University
2020

PERFORMANCE-BASED FIRE SAFETY DESIGN FOR AUTOMATED VEHICLE PARKING STEEL STRUCTURES

DATE OF APPROVAL: 25.08.2020

To filter coffee, my engineering fuel

ACKNOWLEDGEMENTS

I would like to extend my sincere gratitude to my supervisor Assoc. Prof. Serdar Selamet for his guidance. His suggestions throughout the research and writing of this thesis have been invaluable. His encouragement made this research possible to achieve a novel fire safety design for tower-type AVPSs. I also wish to acknowledge the engineering ecosystem of Boğaziçi University, which supported my intuition on civil and mechanical engineering.

I would like to pay special thankfulness to Prof. Serdar Soyöz for his kind advice and comments; and to Assoc. Prof. Murat Ergün for his sharp mind and strong hands during these desperate COVID-19 days.

I would like to express my special thanks to my wife Cagla for her delicious cups of coffee at least four times a day. I also want to extend my appreciation and gratitude to my family for their trust and endless encouragement.

ABSTRACT

PERFORMANCE-BASED FIRE SAFETY DESIGN FOR AUTOMATED VEHICLE PARKING STEEL STRUCTURES

Automatic car parking systems, developed to save space and volume in car parks, have become high-capacity car park structures over time. Tower-type automated car parks are prefabricated steel structures included in this class. These structures, which are basically composed of a car lift and slots that parking pallets carrying cars are seated on, have many knowledge gaps regarding fire safety. The effects of vehicle fires and fire spreading mechanism between cars are not known in tower-type automated vehicle parking structures. The design criteria of sprinkler systems to be used in these structures are a matter of debate. The purpose of this thesis is to enable the emergence of accessible and applicable designs by understanding horizontal and vertical fire spreading mechanisms between passenger cars and the structural fire response of tower-type automated vehicle parking structures. There is no automated car park fire or fire test for this kind of structure that has been reported in the world yet. For this reason, studies were carried out through fire simulations and finite element analysis in this thesis. The thermal conditions and times required for the fire in a car to spread to the cars at the side and upper parking pallet were determined by fire simulations. Then, the fire-induced collapse mechanism of the parking pallets was analytically modeled. Current parking pallet – pallet rail design modified to prevent pallet dislodgement. Finally, the behavior of the steel structure under a fire was analyzed by the finite element method, and a design was proposed in which a partial collapse would not occur in the structure and parking pallets as a result of a fire. These studies have been used as analysis tools in the implementation of the three-stepped fire safety doctrine for automated vehicle parking structures. The doctrine steps are respectively preventing the fire spreading from vehicle to vehicle, collapse/dislodgement of parking pallets and partial collapse at the main structure. At the end of the study, different design proposals with and without a sprinkler system were defined by using iterative methods.

ÖZET

TAM OTOMATİK ÇELİK OTOPARK YAPILARINDA PERFORMANS BAZLI YANGIN GÜVENLİĞİ TASARIMI

Otoparklarda alan ve hacim tasarrufu yapmak amacıyla geliştirilen otomatik otopark sistemleri zaman içinde yüksek araç kapasiteli otopark yapıları haline gelmiştir. Kule tipi otomatik otoparklar bu sınıfa dahil olan prefabrike çelik yapılardır. Temelde bir otomobil asansörü ile asansör kovası çevresinde otomobilleri taşıyan park paletlerinin oturtulduğu yataklardan oluşan bu yapıların yangın güvenliği konusunda pek çok bilgi boşluğu bulunmaktadır. Kule tipi otoparklarda araç yangınlarının etkileri ve yangının diğer otomobillere yayılma durumu bilinmemektedir. Bu yapılarda kullanılacak sprinkler yangın söndürme sistemlerinin tasarım kıstasları da tartışma konusudur. Bu tezin amacı, kule tipi otoparklarda otomobil yangınlarının yatay ve dikey yayılımları ile yapının yangın yükü altındaki davranışını anlayarak, erişilebilir ve uygulanabilir tasarımların ortaya çıkmasına olanak sağlamaktır. Dünya üzerinde henüz rapor edilmiş bir kule tipi otomatik otopark yangını ya da yangın testi bulunmamaktadır. Bu nedenle calışmalar yangın simülasyonları ve sonlu elemanlar analizleri aracılığı ile yürütülmüştür. Bir otomobildeki yangının, yan ve üst parklanma paletinde bulunan otomobillere sıçraması için gerekli termal koşullar ve süreler yangın simülasyonları aracılığı ile belirlenmiş ve ardından araçları taşıyan park paletlerinin yangın nedenli göçme modları analitik olarak modellenmiştir. Park paletlerinde göçmenin önlenmesine yönelik tasarim değişiklikleri önerilmiştir. Son olarak, çelik yapının araç yangını altındaki davranışı sonlu elemanlar metodu ile analiz edilmiş ve bir yangın sonucunda taşıyıcı sistemde kısmi göçmenin meydana gelmeyeceği bir tasarım oluşturulmuştur. Bu çalışmalar üç basamaklı otomatik otopark yapılarda yangın güvenliği doktrininin uygulanmasında analiz araçları olarak kullanılmıştır. Doktrin basamakları sırasıyla yangının araçtan araca sıçramasının, park paletlerinin göçmesinin/yerinden çıkmasının ve ana taşıyıcı sistemde göçmenin önlenmesidir. Çalışma sonunda bu koşulları sağlayan biri sprinkler sistemli ikisi de sprinkler sistemsiz üç farklı tasarım örneği iteratif yollarla oluşturulmuştur.

TABLE OF CONTENTS

LIST OF FIGURES

LIST OF TABLES

LIST OF ACRONYMS/ABBREVIATIONS

2D	Two Dimensional
3D	There Dimensional
AFAC	Australasian Fire and Emergency Service Authorities Council Limited
AFAD	Afet ve Acil Durum Yönetimi Başkanlığı
AST	Adiabatic Surface Temperature
AVPS	Automated Vehicle Parking Structure
AVPSS	Automated Vehicle Parking Steel Structure
BC	Boundary condition
BEV	Battery Electric Vehicle
BRE	Building Research Establishment
EC3	Eurocode 3
FDS	Fire Dynamics Simulator
HRR	Heat Release Rate
HPC	High-Performance Computing
NFPA	The National Fire Protection Association
NIST	the National Institute of Standards and Technology
SHS	Square Hollow Section
SUV	Sport Utility Vehicle
TBEC	Turkey Building Earthquake Code
TRFP	Turkey’s Regulation on Fire Protection
WWII	World War II

LIST OF SYMBOLS

α	Thermal expansion coefficient
ε	Emissivity
ε_s	Emissivity of structural steel
ρ	Gas density
σ	Stefan-Boltzmann coefficient
$\sigma_{\mathrm{y},\Delta\mathrm{T}}$	Temperature-dependent yielding strength
$\emptyset_{i-j}$	View factor of surface j to surface i
δ	Safety margin for bracket drag
$\delta_{\Delta\mathrm{w}}$	Drag length due to vertical deflection
τ	Viscous tension
A	Cell area
c_p	Specific heat
D	Diffusion coefficient
E	Young’s Modulus
g	Gravitational acceleration in the Earth
h	Enthalpy
h_c	Convective heat transfer coefficient
$\dot{\mathrm{h}}_{\mathrm{net,R,i-j}}$	Radiative net heat transfer rate from surface j to i
I	Equivalent moment of inertia of parking pallet
k	Coefficient of heat conduction
$\mathrm{k}_{\mathrm{p},\theta}$	Temperature-dependent proportionality limit modifier
$\mathrm{k}_{\mathrm{y},\theta}$	Temperature-dependent yielding strength modifier
$\mathrm{k}_{\mathrm{E},\theta}$	Temperature-dependent Young’s Modulus modifier
L_{a}	Length of the wheelbase of passenger car
L_{P}	Length of parking pallet
$\mathrm{L}_{\mathrm{P},\Delta\mathrm{T}}$	Thermally expanded length of parking pallet
M	Molar weight
m_W''	Local mass of water per unit area

$\dot{m}'''$	Rate mass change in unit volume
$\mathrm{q}_{\mathrm{i-j}}$	Convective heat transfer rate from cell j to i
q_{k}	Heat transfer rate from adiabatic surface to medium
$\dot{\mathrm{q}}_{\mathrm{up}}$	HRR during ascending of fire
$\dot{\mathrm{q}}_{\mathrm{down}}$	HRR during descending of fire
$\dot{q}''$	Heat release rate per unit area
$\dot{q_o}''$	Predefined heat release rate per unit area
$\dot{q}'''$	Power of combustion in unit volume
p	Pressure
R	Ideal gas constant
Δx	relative change of the distance
t	Time
Δt	Time interval
T	Temperature
ΔT	Change in temperature
T_{AST}	Adiabatic surface temperature
$T_{k,out}$	Outer surface temperature (k$^{\mathrm{th}}$)
$\mathrm{T}_{,\mathrm{z}}$	Temperature gradient at parking pallet
u	Gas velocity vector
w	Width of heat transfer interface in 2D
Δw	Total vertical deflection of parking pallet
$\Delta \mathrm{w}_{\mathrm{P}}$	Vertical deflection of parking pallet due to gravity load
$\Delta \mathrm{w}_{\mathrm{T}}$	Vertical deflection of parking pallet due to thermal bowing
W_{car}	Curb weight of passenger car
W_{pl}	Plastic section modulus

1. INTRODUCTION

1.1. General

Passenger cars have a history of more than a hundred years. Before the revolution of inline mass production method so-called Fordism, they were expensive and unreliable machines. Developments in mass production methods occurred with passenger car inflation. Parallel to this increase in the number of cars in cities, an emerging lack of parking area enforced civil engineers to create robust and applicable solutions. The basic principle of the solution is that the available volume is limited laterally, but the sky is the limit vertically. As a result, designs have emerged where cars are parked on top of each other. Even, these vehicles were brought to the places where they would be parked via pallets and rails. As automated systems developed, these systems also have been improved. The first example of these systems was built in Paris in 1905. Garage Rue de Ponthieu was a multistory concrete structure, but there was a rail&pallet system inside its atria to deliver passenger cars. It also had a car elevator, and electric motors on rails drove the pallets. This garage is shown in Figure 1.1. However, the system was not fully-automatic. It has been controlled by operators as can be seen in the figure. The technology has waited until the end of WWII. Techniques for mechanism control developed for war machines were opened to public use. Then the first tower-type car stacking system was launched in 1951 in Washington, D.C. (Greater Greater Washington,2015). It was the ancestor of modern automatic car parking buildings.

When the computer era started, automated parking systems turned from automatic to robotic. The first robotic parking garage of the humankind was launched in New Jersey in 2002 (USAtoday, 2007). On the other hand, Japan has also adopted the technology and developed it more. Due to the enormous population on the small Japan Island, the tower-type automated vehicle parking systems (AVPS) are very common. A 16-floor tower-type AVPS from Japan is shown in Figure 1.2. It is a simple externally braced steel structure with embedded elevator and parking pallets to store and retrieve passenger cars. The structure may be constructed with either open or closed façade.

Figure 1.1 The first car stacker: Garage Rue de Ponthieu, 1905, Paris (Parking-net, 2020)

Figure 1.2 Modular tower-type AVPSS with an orientation of 2x1 (closed and open façade) (Web-japan, 2017)

Tower-type AVPSs are generally constructed from steel. Even if the primary structural system is made from concrete; pallets, rails and elevator systems are still steel. High material strength, uniformity, elasticity, ductility and weldability are some of the main reasons for the usage of steel in the construction of tower-type AVPSs. However, as a construction material, the fire resistance of steel is weak. The material loses its strength and integrity at higher temperatures. Parallel to this, passenger cars have lots of combustible materials. An ordinary passenger car fire can lead to structural collapse. Thus this fire load density existence in AVPSs causes these structures to be highly risky for fire. Fire induced collapse of AVPSs not only causes loss of the structures but also loss of stored cars. To prevent these loses, fire mechanism and fire-induced structural behavior of steel-framed AVPSs should be analyzed during the design phase of the structure, and necessary precautions should be taken. However, passenger fires in tower-type AVPSs and their structural effects have not been studied yet. A few knowledge gaps also appear in this field such as fire spreading between passenger cars vertically, the effectiveness of sprinkler systems, fire behavior at stacker systems with three or more levels, effect of wind for open façade AVPSSs, specific fire risks for stacker systems and response time requirements. Thus the same gaps exist in national fire safety codes. For example, NFPA 13 Standard for the Installation of Sprinkler Systems does not cover all types of car stacking and automated vehicle parking structures (2019). The same situation is also valid for The Turkish Buildings Fire Safety Regulations.

Modern design methods implement performance-based analysis approaches to observe more realistic fire-induced behavior of structures. On the other hand, this approach is the only way for structures like AVPSs, which are not covered by prescribed methods or national codes. Fire simulation and structural analysis under elevated temperatures are the two main steps of the performance-based structural fire safety methods. The complexity of the structural mechanism causes a considerable need for reliable analytical modelling approaches for performance-based structural fire safety concept. A semi-analytic method can be obtained by decoupling the main problem, then some part of it is solved by simulations while the remaining part is modelled by analytical methods.

In this study, a new framework is followed for fire simulations and structural analyses of tower-types AVPSs. Due to several knowledge gaps, new assessment methods are proposed for vertical fire spreading between passenger cars and structural integrity of parking pallets under fire events. The vertical fire spreading is examined thermochemically, whereas thermo-mechanical principles are employed for the structural integrity of parking pallets. The assessment method for vertical fire spreading is based on a detailed passenger car fire simulation specially developed for the analysis. The assessment method for the structural integrity of parking pallets is actually very straightforward and understandable; thus, any verification work is not performed.

The entire study in this thesis is based on computational modellings and some analytic simplifications. Real-size or reduced-scale fire and structural tests are not employed. Fire Dynamic Simulator with PyroSim (ThunderHead, 2019) is used for fire modelling. Sap2000 (CSI America, 2019) is employed for structural calculation with finite element methods. Matlab (Mathworks,2019) is also used for simple heat transfer analyses and the assessment method for the structural integrity of parking pallets. Results of this study include lateral and vertical fire spreading between passenger cars and its suppression methods, and fire responses of main structures and parking pallets in AVPSs.

1.2. Thesis Outline

This thesis focuses on the development of an assessment method for fire safety of automated vehicle parking structures (AVPSs) and consists of five chapters. In Chapter 1, the background and general structure of the thesis are outlined. Chapter 2 then reviews some of the relevant literature available on the topics pertinent to car fires and fire safety of carparks. The methodology and theoretical approach used for the study are detailed in Chapter 3. In Chapter 4, the analysis and results of the iterative design study for fire-safe automated-type parking structures are provided. Lastly, Chapter 5 presents the conclusions of the study and general suggestion for fire safety design along with some recommendations for areas of future research.

2. LITERATURE REVIEW

2.1. Car Fires, Spreading and Suppression

Automobile fires are an important issue in terms of structural fire safety. The high level of thermal power released during the fire and the probability of the surrounding vehicles to ignite increases collapse risk of structure. For a classic car park, fire scenarios are based on lateral fire spreading between cars. Then most of the fire spreading tests between cars are based on lateral fire spreading scenarios in the literature. Even the recent studies of Park et al. (2019) and Weisenpacher et al. (2016) are based on lateral fire spreading. Weisenpacker et al. (2016) focused on temperature levels around and inside of burning cars and did not measure heat released rates. The test set up of Weisenpacker et al. is given in Figure 2.1. On the contrary, Park et al. (2019) measured HRR by using large-scale calorimeter and maximum HRR for the single-car fire was estimated as 3.5 MW. Experimental and numerical results coincide with each other in both two studies. There are also other studies in this field. Some of them are studies of Joyeux et al. (2002), Mohd (2015), Okomato et al. (2009), Part et al. (2019) and Schleich et al. (1999). HRR curves adapted from all these studies are given in Figure 2.2. As can be seen in the figure, there is no apparent similarity at HRR characteristics for different passenger car fires. Parallel to this, engineers of Combustion Science and Engineering Inc. (CSE, 2020) have analyzed HRR curves of passenger cars for decades from 1970s, and revealed that there is no clear correlation for HRR and aged of vehicles. A few selected HRR curves for each decades are given in Figure 2.3. Fire characteristics of passenger cars depend on vehicle size and age, ignition source and location, environmental conditions and ventilation level.

Figure 2.1. Fire test setup lateral fire spreading retrieved from Weisenpacker et al. (2016).

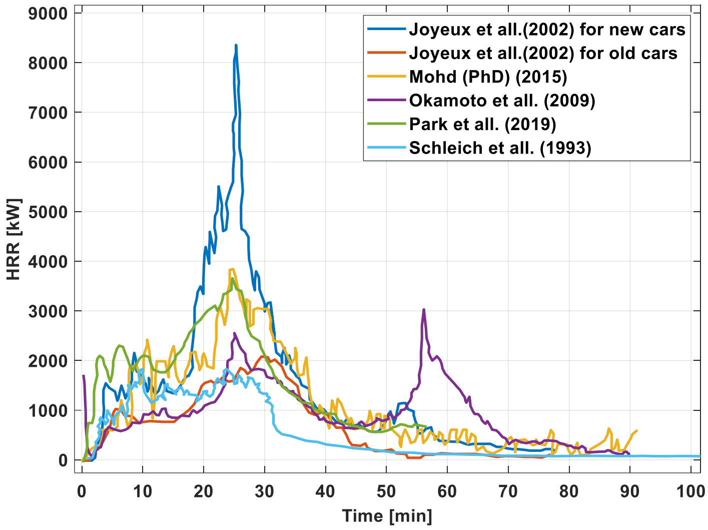

Figure 2.2. HRR curves adapted from literature for passenger car fires

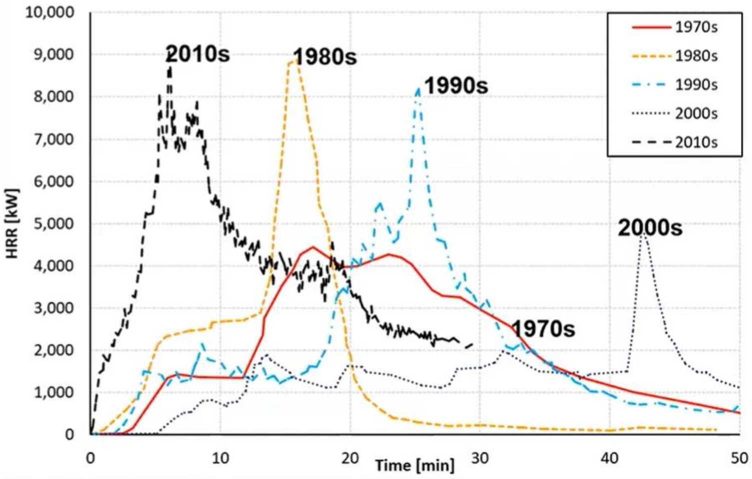

Figure 2.3. Change in severity of passenger car fire throughout decades (CSE, 2020)

First of all, the types and dimensions of automobiles vary. This diversity comes up with different HRR curves. HRR curves can also change with fire scenarios. This diversity is the most challenging issue of designed car fires. As can be seen in Figure 2.2 and 2.3, peak HRR levels vary in a wide spectrum, from 1900 kW to 8500 kW. At this point, a commonly-held observation is that the peak HRR is higher for new cars because of relatively more combustible material used in cars. While Schleich et al. (1999) estimated Peak HRR as around 1.9 MW; in more modern studies such as Park et al. (2019) and Okomato et al. (2009), Peak HRR was estimated more than 3 MW. In literature, the calorific potential of burning cars is categorized as five in terms of heat release rates and total combustion energy. Adapted data for cars manufactured between 1995-2000 is tabulated in Table 2.1.

Table 2.1. Calorific Potential Classification of Cars Manufactured Between 1995-2000 (Joyeux et al., 2002; Schleich et al., 1999; Pope, 2005)

Manufacturer	**Category I**	**Category II**	**Category III**	**Category IV**	**Category V**
Fiat	Punto	Bravo	Tempra	Croma	Ulysse
Renault	Clio	Megane	Laguna	Safrane	Espace
Volkswagen	Polo	Golf	Passat		Sharan
Ford	Fiesta	Escort	Mondeo	Scorpio	Galaxy
Opel	Corsa	Astra	Vectra	Omega	Frontera
Citroen	Saxo	ZX	Xantia	XM	Evasion
Peugeot	106	306	406	605	806
Theoretical Energy Containment [MJ]	6000	7500	9500	12000	12000
Peak HRR [kW]	5242	6553	8300	10448	10448
Total Mass [kg]	850	1000	1250	1400	1400
Mass Loss [kg]	200	250	320	400	400

As can be seen in Table 2.1, the calorific potential classification of passenger cars is generally based on vehicle size and curb weight. Peak HRR levels are also dependent on ventilation conditions and fires first propagation location. The estimated values in the table are valid for European passenger car fleet in between 1995-2000. Old cars are used in fire experiments because of availability and cost.

Joyeux et al. (2002) have present equivalent HRR curves for the calorific potential classifications of passenger cars. The curves can be seen in Figure 2.4. The characteristics and trends of the HRR curves are identical. Generally, Joyeux et al.’s (2002) approach is based on the amplification of HRR values. For example, the minute of Peak HRRs are identical, and only Peak HRR values change with respect to the calorific potential classification.

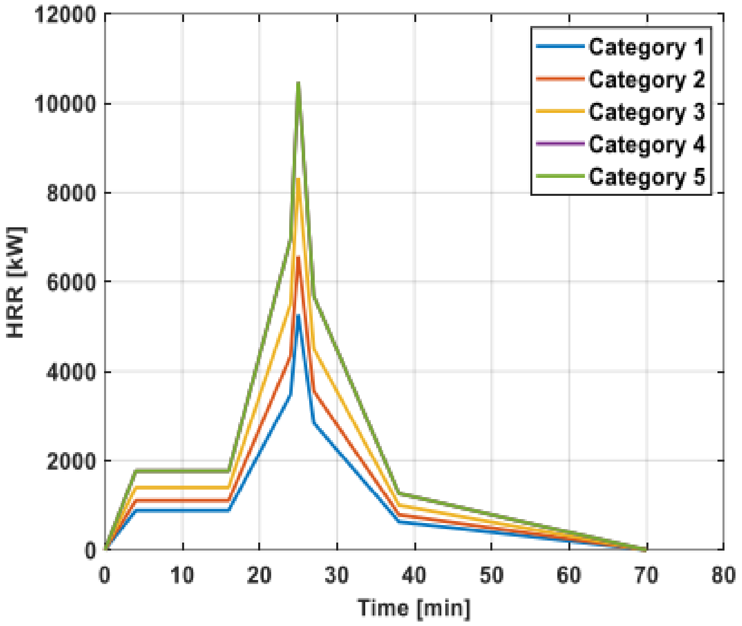

Figure 2.4. Equivalent HRR curves for the calorific potential classification of cars, adapted from Joyeux et al. (2002)

Parallel to the overall calorific heat potential of passenger cars, ignition mechanisms of individual component in vehicles are also essential to understand car fires. After the 1990s, use of plastic components in passenger cars has increased. Whereas the total plastic weight corresponds to 5.1% of the total weight, the ratio increased to 8.8% in 2018 (CSE, 2020). In addition to this, the average combustion energy per mass of plastic components within passenger cars has increased. Although the change in the mass of plastic materials is 42%, the total combustion energy has increased by 91% since the 1970s. The main reason of this situation is changing the type of plastics used in passenger cars. Plastic components of vehicles of the 1970s was produced with hard plastics with low heat of combustion like polyvinyl chloride. However, a trend on using soft plastics like polyurethane for components using especially inside the cabin has emerged after the early 1990s. Hard plastic materials have also been preferred for exterior parts such as bumpers, mirrors after this decade. The overall change in plastic usage and combustion energy are summarized in Figure 2.5 and 2.6.

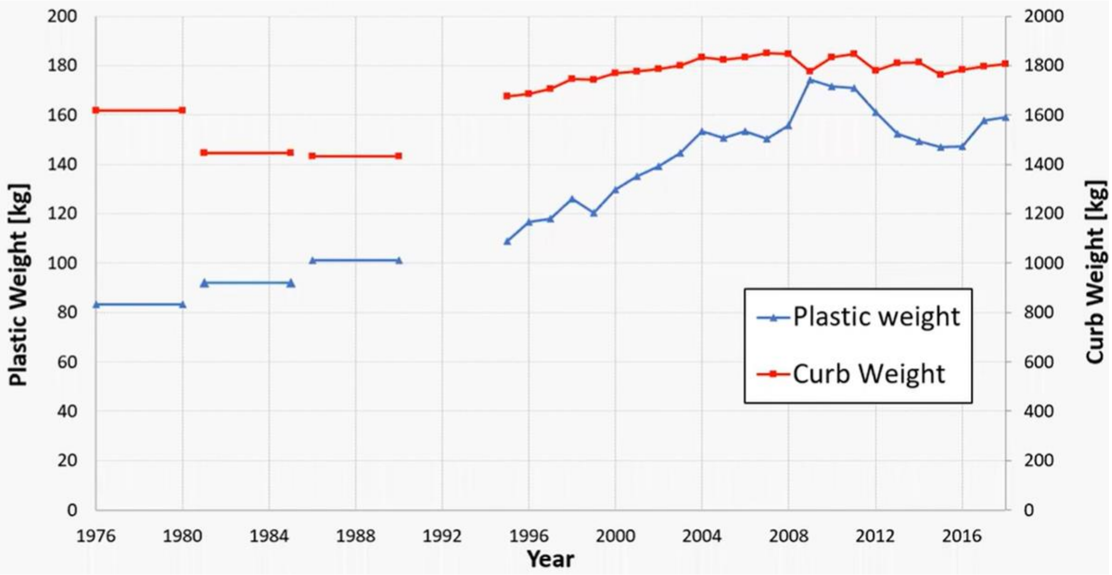

Figure 2.5. Curb weight and plastic use

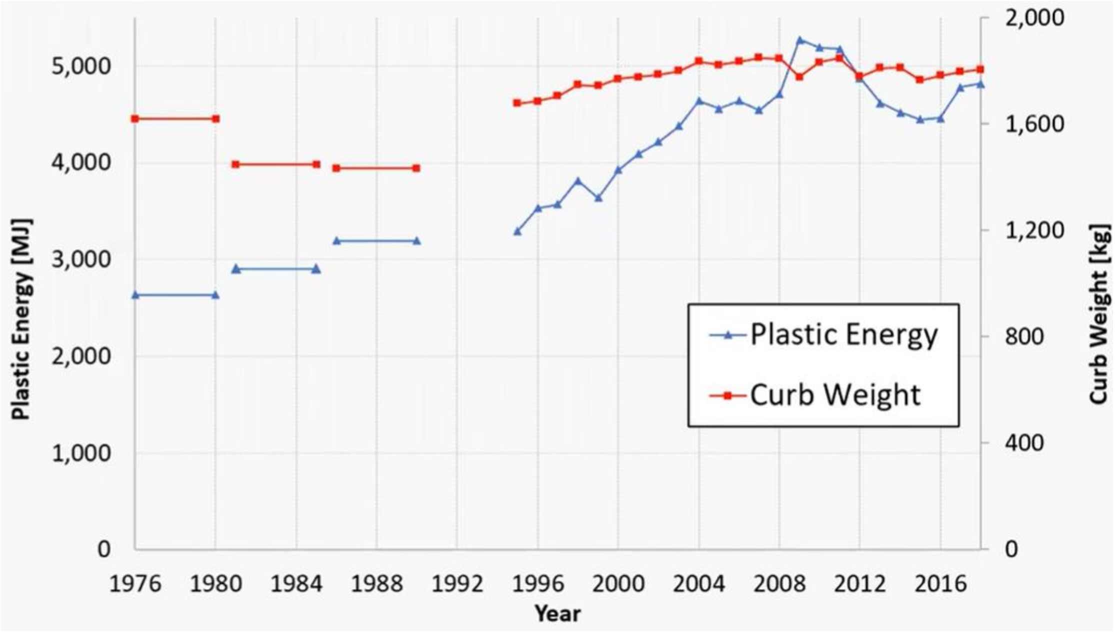

Figure 2.6. Curb weight and total combustion energy of plastic components

The risk of fire spread from one car to another has risen with the increase in the use of plastic materials for exterior parts of passenger cars. Plastic material can be ignited by direct flame contact, radiation, convection and rarely conduction. The occurrence of ignition can be forecasted with a calculation of surface temperature if the substance is heated by convection and conduction. A high level of conductive heat transfer mode without a radiative heat source is not applicable. However, radiative heat transfer is more dominant during passenger car fires for closer objects or other passenger cars. Then ignition mechanisms under radiation should be tested. A set of test results of plastic vehicle components that used on outmost surfaces of passenger cars are given in Table 2.2 (BRE, 2010). Ignition times under different irradiance levels and critical irradiance levels of plastic components have been determined by tests. All exterior plastic components excluding tires can be ignited by an irradiance level of 20 kW/m^2 in 7.5 minutes, whereas it takes lower than one minute with an irradiance level of 30 kW/m^2. On the other hand, the ignition of tires takes much more time, but its critical irradiance level is not high.

Table 2.2. Ignition times of plastic passenger car components with different irradiance levels (BRE, 2010) (NI: not ignited)

	Time to ignition (seconds) (NI=no ignition) Irradiance level				**Critical irradiance level (kW/m^2)**
Sample	**10 kW/m^2**	**20 kW/m^2**	**30 kW/m^2**	**40 kW/m^2**	
Hub cap	NI	205	58	28	17.5
Mud flap	380	57	29	16	10
Wheel arch	NI	81	44	25	12
Bumper	NI	450	89	43	18.5
Bumper grill	NI	114	44	19	17.5
Bumper trim	415	83	30	16	11.5
Fuel tank	NI	354	114	59	16.5
	10 kW/m^2	**12 kW/m^2**	**15 kW/m^2**	**20 kW/m^2**	
Tire	NI	1100	597	240	11

Fire spreading between passenger cars is also an important part of fire safety of car parks. Communities and Local Government Sustainable Buildings Division in the United Kingdom have appointed the Building Research Establishment (BRE) to conduct a set of fire tests on fire spreading modes between passenger cars (BRE, 2010). All possible fire spreading patterns between passenger cars have been tested during the project. The patterns are side by side fire spreading, nose to nose firer spreading and vertical fire spreading at car stacker. Before and after photographs of tests are shown in Figure 2.7. All results given in the figure indicates that fire can spread adjacent cars in all directions. The gas temperature close to the ceiling has reached 1100 °C during side by side fire spread test. Heat flux levels have also peaked at 140 kW/m^2 during the same test. This level can ignite all combustible components of passenger cars quickly. In the nose to nose test, a fire started in the engine compartment of a passenger car then the bonnet was closed. A second car was located with its front bumper 50 cm from the front bumper of the vehicle at that the fire started. The fire has jumped to the next vehicle at approximately at the 5th minute of the test. In 30 minutes, both two vehicles were engulfed by flames. Another test for vertical fire spreading between passenger cars has been conducted with a simple car stacker mockup. A car stacker allows two passenger cars to be parked on the parking area for a single vehicle. This increases the fire load and fire spreading risk. Development of fire in the test has been summarized as follow: *"The fire grew rapidly once started and quickly reached the underside of the car above. Flame entered the wheel arch of the upper car igniting the tire. The fire developed within the passenger compartment of the lower car while growing in the engine of the upper car. Eventually the fire spread to the passenger compartment of the upper car."* (BRE, 2010). Flames have engulfed both two cars at the car stacker mock-up. The situation that is 21 minutes from the first ignition can be seen in Figure 2.7 (bottom right corner).

Figure 2.7. Fire spreading between passenger cars (BRE, 2010)

To control or suppress a passenger car fire, sprinkler systems are a simple, cheap and applicable choice. Car park fires are defined as an ordinary hazard in most of national fire safety codes such as BS EN 12845:2015 (2015), AS 2118:2017 (2017), NZS 4541:2020 (2020) and Turkey's Regulation on Fire Protection (2009). BRE has also conducted tests on the efficiency of sprinklers on passenger car fires for ordinary car parks and stacker systems (BRE, 2009) (BRE, 2010). The test setup for ordinary car parks is given in Figure 2.8. The setup represents a closed car park, but ventilation is enough for a fuel-controlled car fire. K Factor of 115 $L/min\sqrt{atm}$ sprinkler heads per 12 m^2 floor area have been placed at the top of the cars. The fire was started at the rightmost passenger car. The first sprinkler has been activated after 4 minutes, then all of six sprinklers have actuated at the early stage of fire. The fire has not been extinguished, and its thermal power has reached around 7000 kW. However, the fire has not spread to the next vehicle. Cooling and transport effect of water droplets from sprinklers has also caused the smoke to drag down.

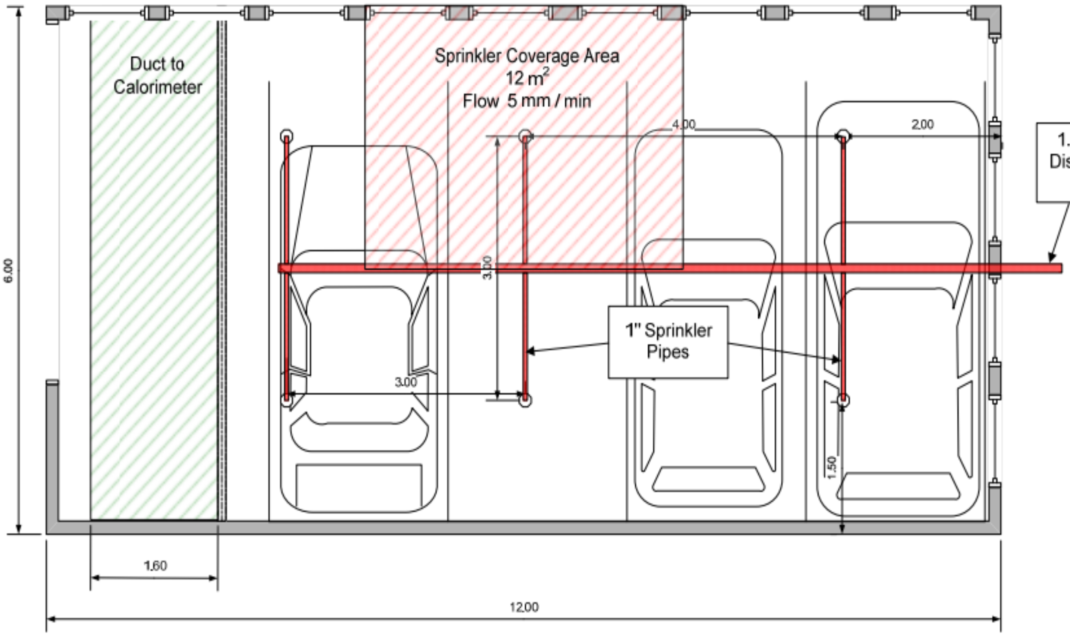

Figure 2.8. Tested sprinkler layout (BRE, 2010)

One of the most critical knowledge gaps in the topic of suppression of passenger car fires is the effectivity of sprinkler systems in car stackers. BRE has carried out a test to fill the gap on 17th September 2009. Four sprinkler heads per passenger car have been placed, and sprinkler application principles were reported as follow (BRE, 2009):

- Four sprinkler heads should be located in the vicinity of each corner above cars in stackers.
- Sprinkler heads are not to be installed directionally.

Eight sprinkler heads that have a K-factor of 80 $L/min\sqrt{atm}$ with 68 °C temperature rate have been used in the test. The test rig is given in Figure 2.9a, and an SUV and a sedan passenger car had been used. The fire was started at the driver seat of the lower car. Although the fire was initiated at the lower car, the sprinkler, that was located at the front right side of the upper car, actuated firstly in 13 minutes. Due to the steel ceiling that was located on top of the test rig, hot gasses accumulated under it led the sprinkler to actuate. Sprinklers around the lower car have started to actuate at 23rd minute of the test. The sprinkler system has been turned off 73 minutes after the ignition. The fire has still been alive after they were turned off. The state of fire at 83rd minute of the test is shown in Figure 2.9b. After the test, nearly all combustible materials in the lower passenger car had been burnt. The upper car had been damaged to its underside and engine bay.

Figure 2.9. Effect of sprinklers on vertical fire spreading (BRE, 2009)

2.2. Open-façade Car Park Fires and Fire Safety Fire Safety Requirements

The CTCIM center in France has carried out passenger car fire tests and determined a reference HRR curve with 8300 kW peak value for a single vehicle (Joyeux, 1997). The experimental campaign has also revealed that fire spread occurs at every 12 minutes between cars. It is one of the current assumptions for the fire safety design of open car parks. Another assumption is that fire severity is mitigated by ventilation in open car parks (Marton et al., 2016). Most of national fire safety codes on car parks adopt these assumptions, thereby fire safety requirements for open car parks are reduced. Structural fire resistance ratings of open car parks differ from 0 to 90 minutes in Europe, and an overview is shown in Figure 2.10. NFPA 88A and Turkey's Regulation on Fire Protection are good examples of this reduction in safety requirements. Fire requirements for open car parks in these codes are summarized in Table 2.3. Ventilation systems, fire alarms systems and fire protections at vertical openings are not compulsory by both codes (TRFP, 2009) (NFPA88A, 2019). Fire resistance ratings are 15 minutes for constructions with a total height of 30.5 m or lower, and 60 minutes for taller structures in Turkey's Regulation on Fire Protection. On the other hand, NFPA 88A refers to NFPA 220 on fire resistance ratings of open façade steel car parks. If an open car park structure meets the following conditions, fire resistance is not compulsory:

1- *"The height does not exceed 25 m."*

2- *"The horizontal distance from any point on any parking level to an exterior wall opening on a street, an alley, a courtyard, or other similar permanent open space does not exceed 60 m."* (NFPA 88A, 2019)

Table 2.3. Comparison of Fire Safety Requirements for Open Carpark

	Turkey's Regulation on Fire Protection (2009)	**NFPA 88A (2019)**
Sprinkler system	not compulsory	compulsory only for AVPS refers NFPA 13
Ventilation system	not compulsory	not compulsory
Protection at vertical openings	not compulsory	not compulsory
Fire alarm system	not compulsory	not compulsory
Fire resistance ratings	15 min. for construction height lower than 30.5 m, otherwise 60 min.	refers NFPA220 not compulsory for Type II (000) constructions

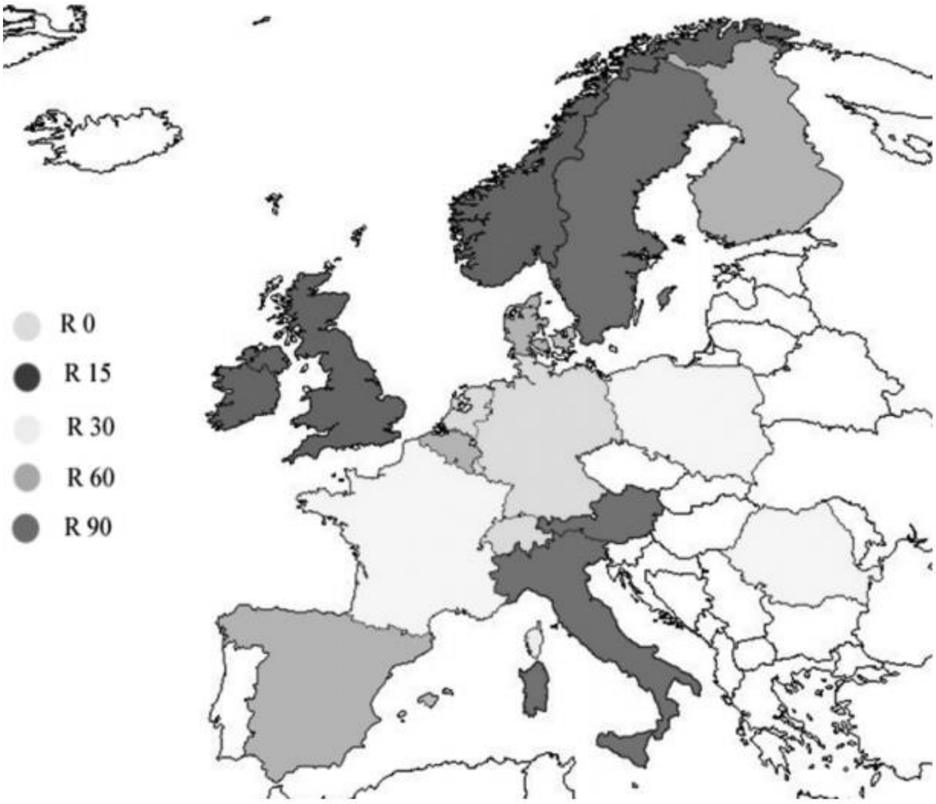

Figure 2.10. Structural fire resistance ratings in European Countries in 1993 (Zanon et al., 2010)

All in all, another primary concern in fire safety of open car parks is the installation of sprinkler systems. Turkey’s Regulation on Fire Protection does not mandate the installation of sprinkler systems on open car parks including AVPSs. Similar to this, NFPA 88A also does not set any condition for sprinkler systems on open car parks. It only suggests sprinkler systems for AVPSs in accordance with NFPA 13. However, NFPA 13 Standard for the Installation of Sprinkler Systems does not define application principles of sprinkler systems for AVPSs (NFPA 13, 2019). In contrary, Australian AS 2118.1:2017 ‘Automatic fire sprinkler systems, Part 1: General systems’ defines principles of sprinkler systems in AVPSs (AS 2118.1:2017, 2017). The related clause in the code is as follow:

C10.6.2: The design of car stackers can vary considerably and the intent of the design and installation requirements in this clause is the provide sprinkler coverage for the front and rear of each vehicle are at least coverage for the space between each vehicle from the front or rear. (AS 2118.1:2017, 2017)

Sprinkler design criteria are also defined in AS 2118.1:2017. According to C10.6.2.2.1, sprinkler systems must be provided within open frame AVPSs, where passenger cars are parked side by side. Sprinklers are positioned at every corner of all individual parking space (AS 2118.1:2017, 2017). The ceiling of an AVPS should be covered with a sprinkler mesh. A typical arrangement of sprinklers at an AVPS is given in Figure 2.11. The AVPS presented in Figure 2.11 is a multiple row stacker, and AVPSs in some cases have single row similar to the one in Figure 1.2. The same Australian standard defines a design rule of sprinkler systems for this kind of AVPSs. The related clause in AS 2118.1:2017 is as follow: *"10.6.2.2.2: Where cars are stacked individually, with walls bounding the front, side and rear of the car, or cars are arranged in a single row nose to tail, sidewall sprinklers shall be provided on the walls of structure, covering the front and rear of each car."*(AS 2118.1:2017, 2017). The related arrangement is also given in Figure 2.12. It is basically a simple tower-type AVPS. However, the code defines the application principle of sprinklers only for closed tower-type AVPSs. Due to the absence of exterior walls at open façade tower-type AVPSs, the arrangement in Figure 2.12 may not be applicable to it. In addition to this, simple tower-type open façade AVPSs is not covered by the code correctly. The clause 10.6.2.2.1 is for multiple row stackers, whereas AVPSs like in Figure 1.2 have single rows.

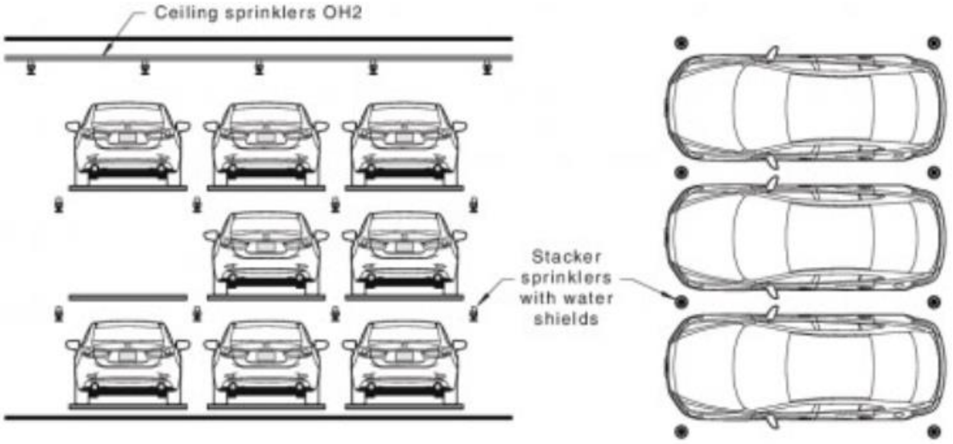

Figure 2.11. Typical arrangement of open frame AVPS sprinklers (AS 2118.1:2017, 2017).

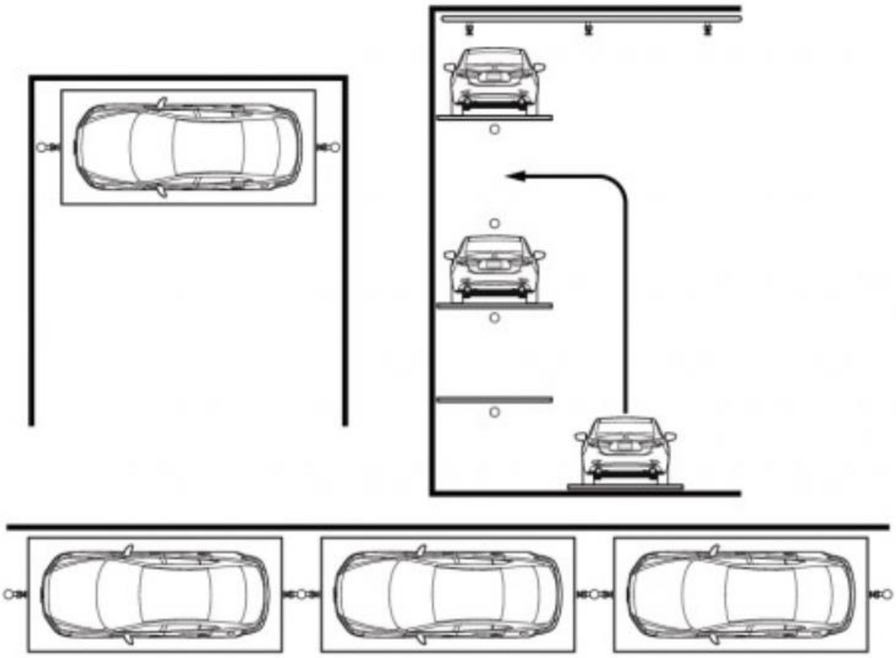

Figure 2.12. Typical sprinkler arrangement for single or multiple nose to tail AVPS (AS 2118.1:2017, 2017)

Sprinkler types for AVPSs are also defined at 2118.1:2017. Sprinklers at ceilings of main structures should be designed according to requirements of Ordinary Hazard Level 2 (OH2) (AS 2118.1:2017, 2017). The OH2 refers to maximum operation area of 144 m^2 and the minimum water density of 5 mm/min. Sprinklers within parking slots must have a minimum K Factor of 115 $L/min\sqrt{atm}$ and a nominal temperature rating of 68 °C. They are also fast response sprinklers that have conventional deflectors.

An open car park fire can be a catastrophic event. After the 2000s, the severity of open car park fires has been increased. Some of the crucial open car park fire events in Europe are given in Table 2.4. A fire has started in Schiphol Airport, Amsterdam in 13/12/2002. Nearly 30 passenger cars were on fire at the same time; thus, the fire could spread much faster than the rule of 12 minutes (Noordijk and Lemaire, 2005). The cars on fire were owned by a car rental company and, they are brand new and with filled fuel tanks. Because brand new cars contain more plastic and even plastic fuel tanks, circumstances in the Schiphol car park have caused a dangerous fire and fast fire spread. Around 101 passenger cars have been damaged during the fire consequently. The car rental company has parked cars very close to each other, that the parking layout is very similar to the one in multi-row AVPSs. The fire debris at the parks is shown in Figure 2.13b, that reveals the parking layout. The structure has had no sprinkler system, and the debris gives an idea about the destruction level of fire in unprotected or unsprinklered AVPSs. Another important fire event in an open car park is Kings Dock car park fire in 31/12/17 in Liverpool (MF&RS, 2018). The fire started in a car on level 3 and led to a total loss of 1150 passenger cars. Firemen have reported rapid lateral fire spread and vertical fire spread through both downward and upward. This event is an excellent example of the importance of vertical openings on slabs and sprinkler system in open car parks. The absences of sprinkler systems and fire protection in vertical openings in Kings Dock car park sparked off a disaster. The debris after the fire is shown in Figure 2.13a. The fire has spread not only upper floors but also lower ones.

Table 2.4. Severe car park fires after 2000 in Europe.

Date	**# of burned vehicles**	**Location**
08/01/2020	300	Stavanger, Norway
31/12/2017	1150	Liverpool, UK
13/11/2002	101	Amsterdam, Netherlands

The most recent open car park fire has occurred on 08/01/2020 in Stavanger, Norway (FESG,2020). The fire started in a 15-year-old car and spread to the nearest cars quickly. With the effect of strong wind, flames have engulfed the structure partially. Then a partial but significant structural collapse has happened, as shown in Figure 2.13c. Around 300 passenger cars, including BEVs, were destroyed, and any significant impact of the presence of many BEVs on fire severity has not been observed.

Carpark fires are also a significant safety problem in US. Although injuries are very rare because occupants in car parks are few and typically awake, the economic cost of property losses in US due to carpark fires is 22.8 Mill. USD annually (CSE, 2020).

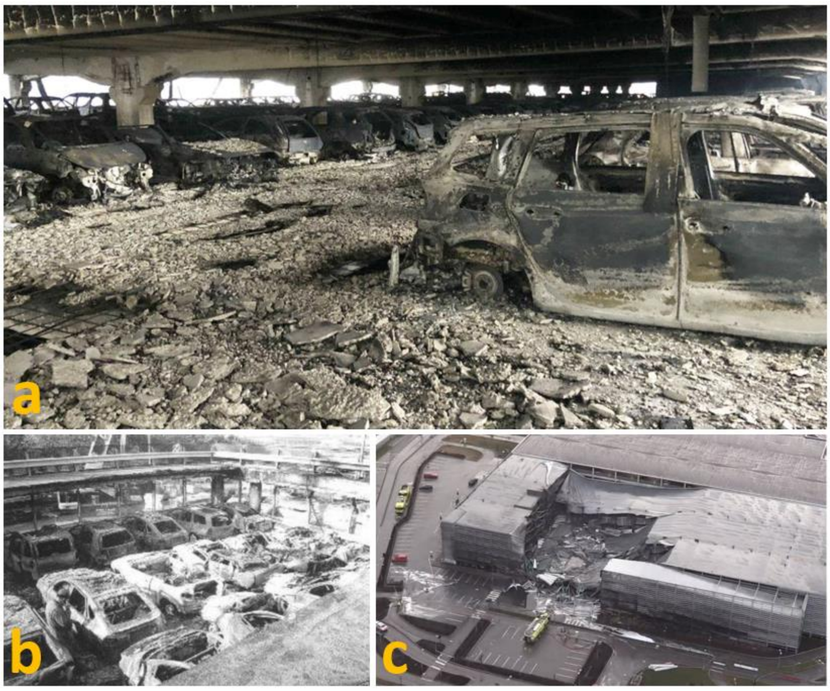

Figure 2.13. (a) 2017 Liverpool car park fire (MF&RS, 2018); (b) 2002 Amsterdam car park fire (Noordijk and Lemaire, 2005); (c) 2020 Stavanger car park fire (FESG, 2020).

2.3. Structural Performance of Steel Car Parks Under Fire

A formal definition of open car parks is given in NFPA 88A as follow (NFPA 88A, 2019):

- *C5.5.1: "Each parking level shall have wall openings open to the atmosphere, for an area of not less than 0.4 m*^{2} *for each linear meter of its exterior perimeter."*
- *C5.5.2: "Such openings shall be distributed over 40 percent of the building perimeter or uniformly over two opposing sides."*
- *C5.5.3: "Interior wall lines and column lines shall be at least 20 percent open, with openings distributed to provide ventilation."*

A typical open car park structure is like as given in Figure 2.14. Open car parks are over-ground buildings that provide natural ventilation through openings along facades. Thus, a possible fire event in an open car park is probably fuel controlled. In addition to this, wind may penetrate directly into structures and drag the fire to ahead; consequently, it can spread to adjacent passenger cars. On the other hands, an open façade may ensure that the heat is exhausted out, and temperature levels inside the structure can not increase as much as the levels in closed car parks.

Open car parks can be a steel or concrete structure, no matter what slabs are generally made by concrete at steel-framed ones. In most of the cases, steel is used in columns, beams and bracings. Modern tower type AVPSs do not contain concrete slab, but rather steel parking pallets. However, early examples of AVPSs could include concrete slabs, as shown in Figure 2.15.

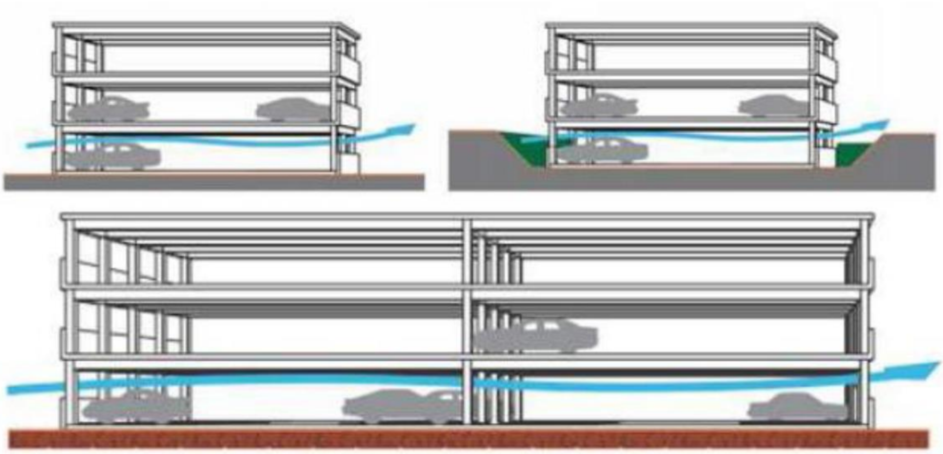

Figure 2.14. Design of a typical open car parking structure (ArcelorMittal, 2007)

Figure 2.15. An early example of concrete AVPS in the 1970s (Dobson, 1974)

Fire events within open-deck car parks were summarized adequately by Zanon et al. (2010) as follow: *"In the case of open car parks, it was experimentally observed that the fire* *concerns the structure only locally, affecting the structural elements in inverse proportion to their distance from the flames. The steel beams next to fire heat up quickly and consequently loose their mechanical properties, while the temperature increase in the slab appears moderate and slower due to its bigger thermal inertia. The reinforcement bars present in the slab usually are not significantly heated, due to their consistent concrete cover. As well, the part of the building enough far from the fire (which means about 10 meters) can be considered as not affected."*

Temperature levels at structural members such as beams, columns and slabs can be either calculated or measured by tests. However, calculations must be validated before use widely. A few passenger car fire tests in full-size open car parks have been carried out (Bennetts et al., 1986), (Kitano et al., 2000), (Joyeux et al., 2001), (Zhao et al., 2004). A prototype of two-story open car park constructed of unprotected steelwork has been tested under real passenger car fires at the BHP Melbourne Research Laboratories to determine the need of fire protection (Bennetts et al. 1986). The prototype structure was not damaged, and Bennets et al. concluded that structural fire protections are not necessary for open deck car parking structures. The peak gas temperature at above a burning car was measured 575 °C if the fire does not spread to other vehicles whereas the peak gas temperature has reached 750 °C while several passenger cars were burning. The maximum surface temperature at steel beams was also measured as 340 °C.

Kitano et al. (2000) have carried out a large scale passenger car fire test in a 4-story open car park with 2.9 m floor height that is shown in Figure 2.16.

Figure 2.16. Open-deck 4-storey steel car park (Kitano et al., 2000)

They measured the maximum steel temperature around 600 °C at the beam located just above burning vehicles. Overall temperature levels around burning cars and structural response were published later by Hirashima et al. (2003) for the same test. The response is given in Figure 2.17. The full developed fire has not caused any collapse, and steel temperatures at lower flanges of beams above burning cars reached around 550 °C whereas the ones at upper flanges were under 350 °C. The test also indicated that temperature levels at columns are dependent on relative positions of them. Temperature levels at surfaces that do not face to radiation of the fire such as Temp.9 in the figure are quite low. In contrary, temperature levels at columns engulfed by flames have reached about 350 °C. On the other hand, thermal elongations of exposed members have influenced the entire structure. In addition to this, the total length of the structure was increased due to thermal elongations at exposed columns. Hirashima et al. (2003) have concluded the test as follow:

- *“A steel frame exposed to a car fire without fire protection is stable in case of members connected rigidly and designed against seismic load in Japan.”*

- *“When the column bases of a frame are restrained for the horizontal displacement by footings, large curvature is developed at the top and bottom of outer columns due to the thermal elongation of the fire exposed beam and it remains after a fire.”*

- *“Calculated values of the displacements of frame approximately agreed with the experimental values.”*

Zhao and Kruppa (2004) made two fire tests in an open car park built with unprotected steel columns, beams and a composite slab, as shown in Figure 2.18. The structure was with a floor area of 15 m x 32 m and a height of 3m. The columns have sections of HEA180 at edges and HEB200 at the inner space. Sections used for beams were IPE400, IPE500 and IPE550. The beams have carried a composite slab with a thickness of 12 cm.

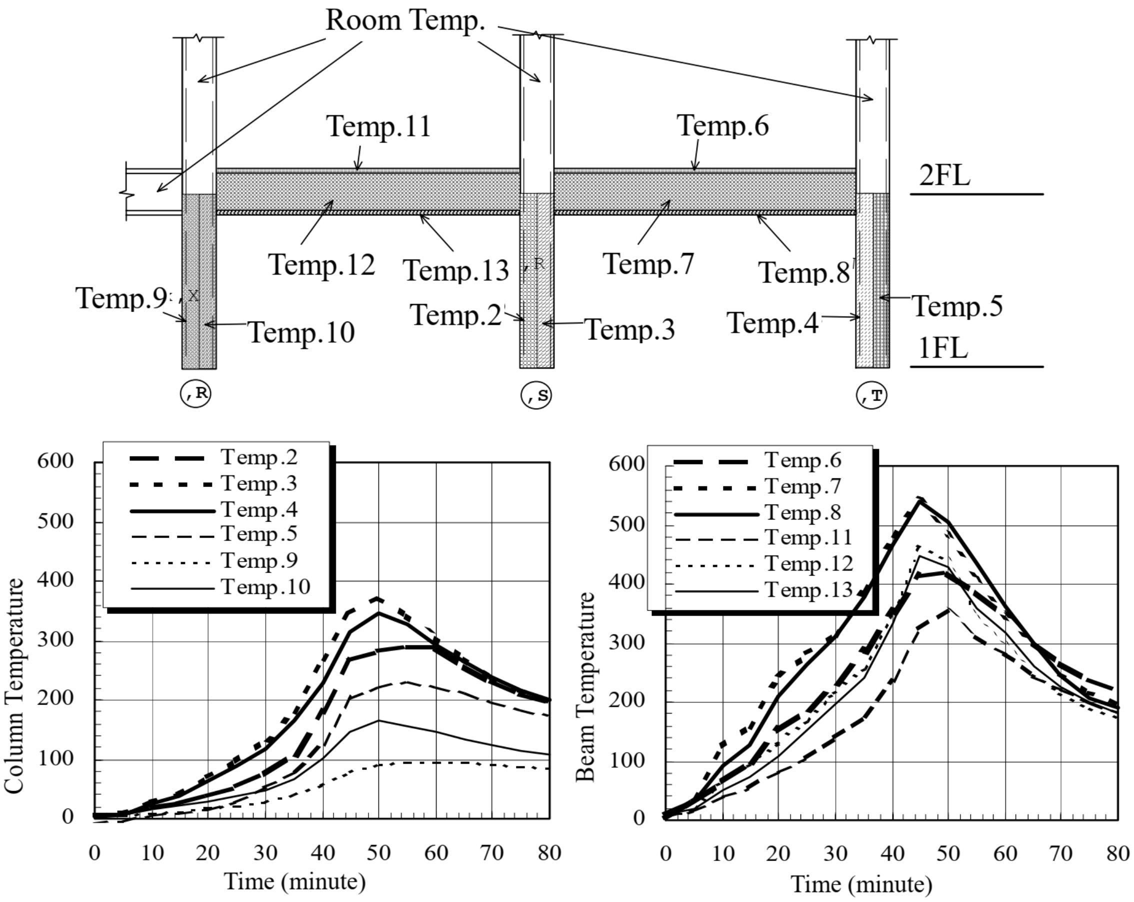

Figure 2.17. Structural response during the test conducted by Kitano et al. (2000) (adapted from Hirashima et al. 2003)

Figure 2.18. Open steel car park (Zhao and Kruppa, 2004)

In both two tests, there were three vehicles in an average parking distance. The test conditions included a strong wind that varied in both direction and velocity, which enhanced fire spreading between cars. Zhao and Kruppa (2004) recorded gas and surface temperatures at beams above burning cars. Temperature and displacement levels of beams are given in Figure 2.19. Locations of thermocouples and passenger cars on the ground floor of the car park are also shown in the figure. The gas temperature near beams has reached to about 1000 °C, and steel temperature levels were around 700 °C. Vertical deflection levels at midpoints of beams have differed from 6 to 15 cm, that the fire response of structure has been dependent on wind direction and strength. Zhao and Kruppa (2004) have also constructed setups of numerical 2D and 3D analyses to estimate the structural fire response. The study revealed the following findings (Zhao and Kruppa, 2004):

- 3D numerical modelling agrees well with experimental results in terms of structural response for both heating and cooling phases.
- 2D numerical modelling can give more severe outputs than experimental results for both vertical and axial displacements

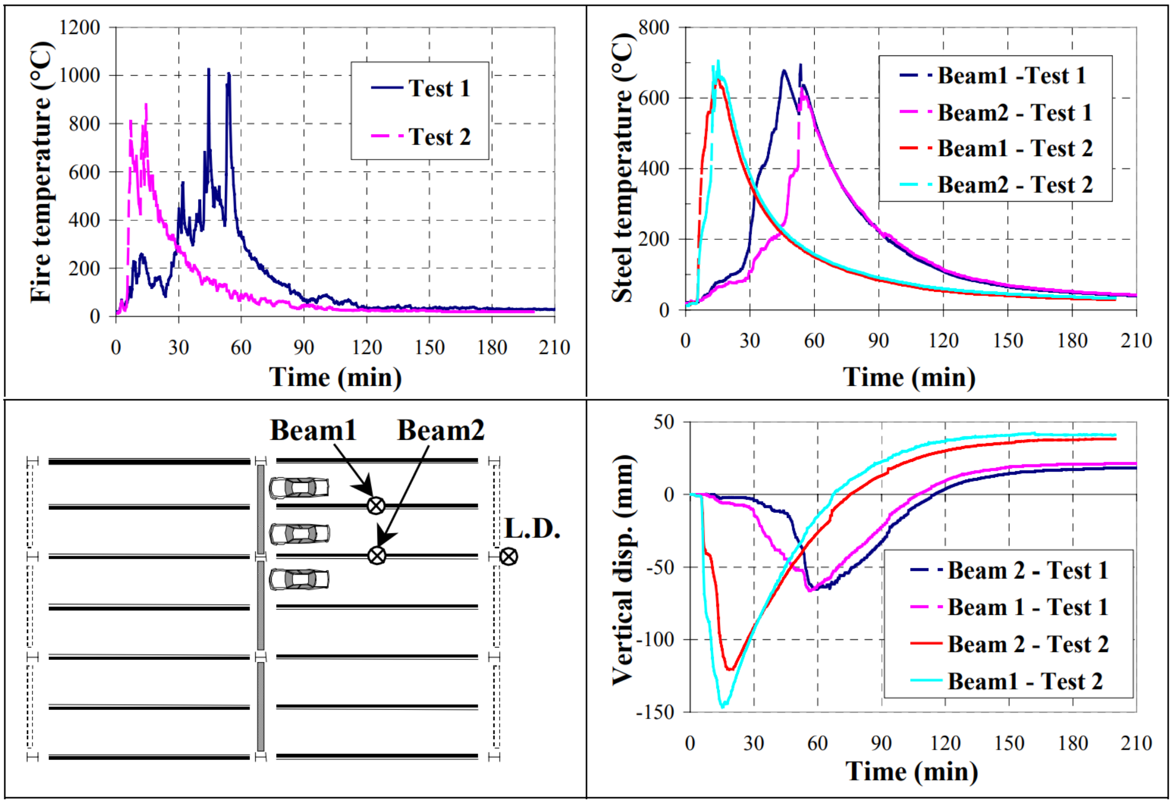

Figure 2.19. Temperature and displacement levels during passenger car fire test (Zhao and Kruppa, 2004)

Once fire levels at structural member are measured carefully, and the temperature data is enough to represent overall thermal characteristics of the fire event, obtaining realistic structural responses is possible with 3D finite elements method. Fraud et al. (2003), modelled the structural effects of a vehicle fire just under the midspan of a main IPE400 beam. The scenario was very severe for an unprotected steel open car park with a composite concrete slab. SAFIR (Franssen, 2005) has been used for the finite element simulation, and the model is given in Figure 2.20. SAFIR involves not only a mechanical calculation module but also a thermal calculation module in 3D. Any collapse has not been detected during the simulation, although the maximum midspan deflection reached to 60 cm. The result of simulation in SAFIR was very similar to findings in full-size fire tests mention before. The midspan deflection is a bit high, but the fire location was chosen as just under the midspan, whereas in the study of Zhao and Kruppa (2004) it was the end of the beam.

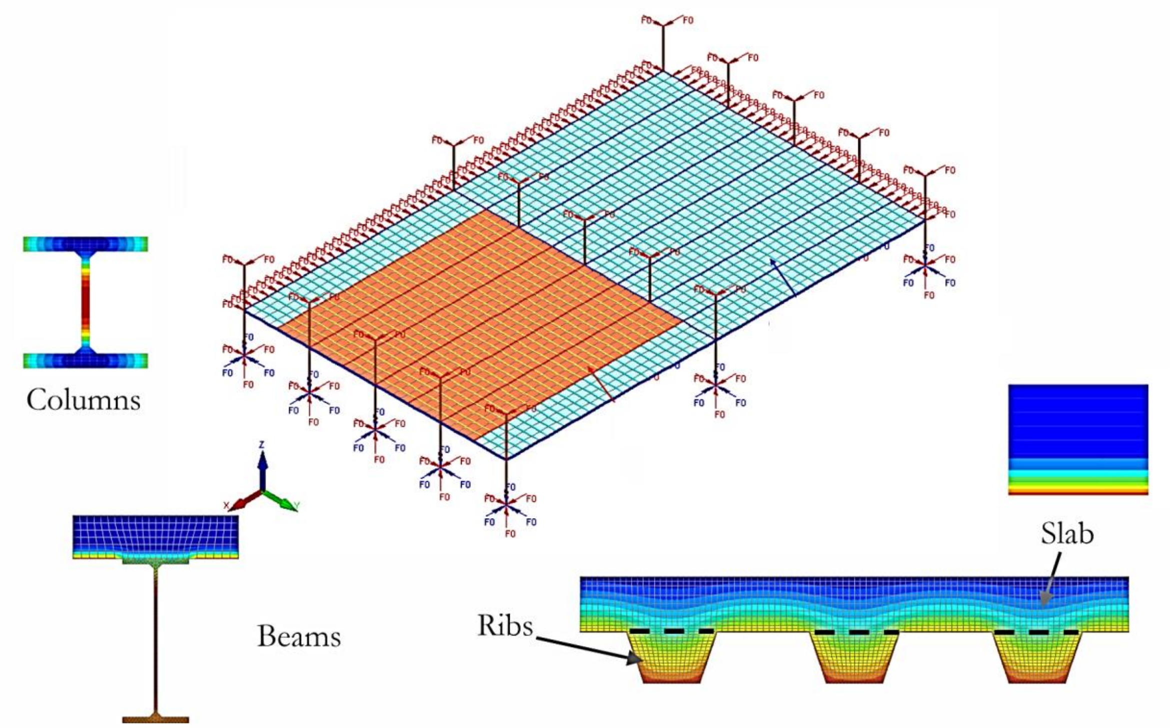

Figure 2.20. Fraud et al.'s (2003) finite element model in SAFIR

Cook and Pessiki (2008) from Lehigh University have conducted a research project on the development of realistic fire loads for open-deck steel car parks. Their structural model was based on the typical structural design provided in the AISC Design Guide 18: Steel-Framed Open-Deck Parking Structures (Churches et al. 2003), and Fire Dynamics Simulator

(FDS) was employed for thermal analyses. The project started with a passenger car model as a burnable vehicle on which all surfaces were considered to be inert. The model based on 2000 Ford Taurus is shown in Figure 2.21, which is 4.5 m in length, 1.75 m in width and 1.65 in height. It contains a small plate, 0.125 m thick, 1.75 m long and 1.5 m wide, as a car ceiling at the top of the main body. A flammable solid vent with a specified time-varying heat release and in size of 2x1.75 m was located on the main body of car model symmetrically. The peak HRR of the burnable car has been defined about 5 MW. The time interval between ignitions of adjacent vehicles was selected to be six minutes based on the findings of Strenchock (2008). Lastly, the burnable car models are located in the structures that are given in Figure 2.22 with mesh layout in FDS. The columns were reinforced concrete and slabs were modelled as steel-concrete composite. Default material library of FDS was used for properties of materials in the model. Cell sizes in mesh have been 0.125 m in all three principal directions (a cube with 0.125 m edge length). Large Eddy Simulation with Radiation Transport Solver was employed. Two different architectural models have been taken into account in the project: staggered and level. Six different cases have been simulated in total.

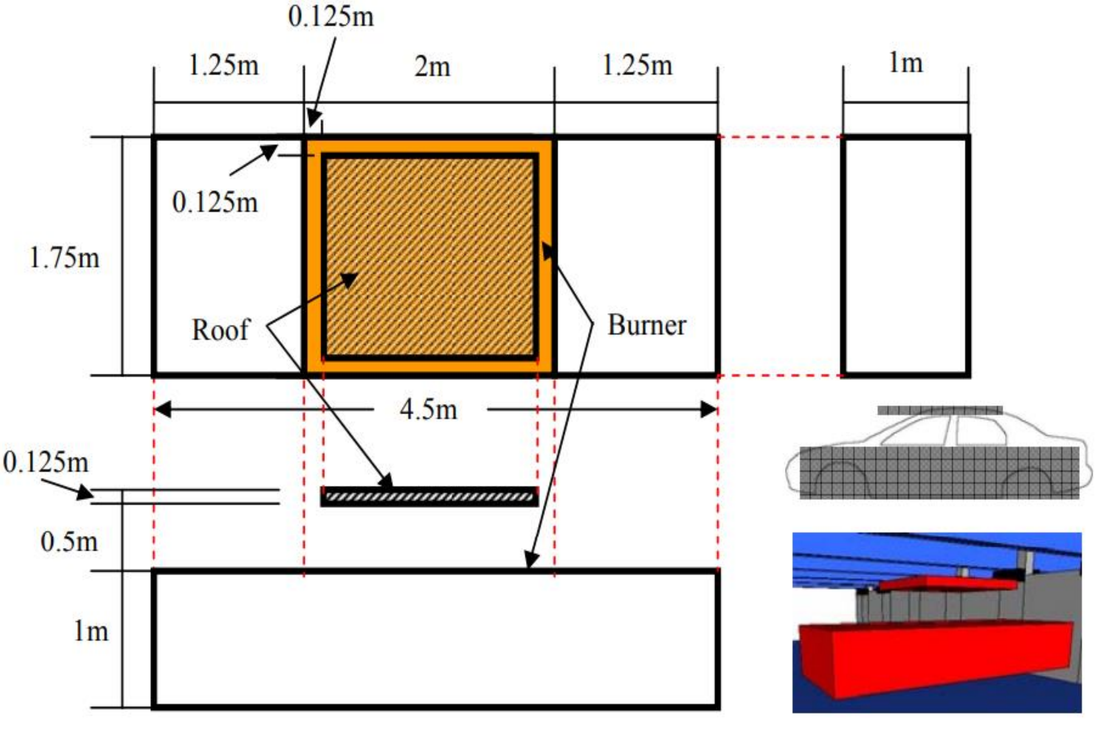

Figure 2.21. Passenger car model in FDS (Cook and Pessiki, 2008)

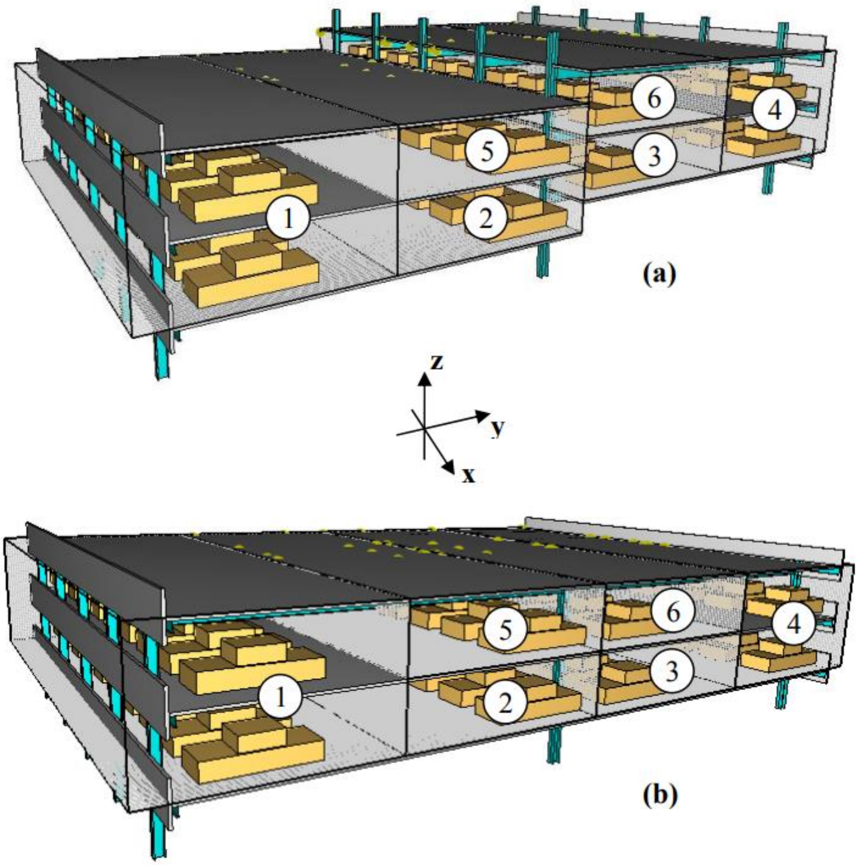

Figure 2.22. Geometrical model and mesh layout in FDS: (a) staggered; (b) level (Cook and Pessiki, 2008)

After the thermal analyses with FDS, Cook and Pessiki (2008) have transferred results to a finite element analysis program to estimate temperature distribution within beams close to burning cars. Followings were concluded after the FE analyses:

- Variations in framing and member geometry affect heat transmission and heat fluxes into members close to the fire.

- Variations in floor elevation affect ceiling temperatures and heat transmission through structural elements.

- Increases in internal member temperatures cause more significant reductions in the mechanical strength of steel members.

Changes in mechanical properties of construction steel such as the yielding strength, the proportional limit and the Young’s Modulus depending on internal temperature levels are defined in EC3. Reduction factors based on average temperatures at flanges and web of the closest beam to the fire are tabulated in Table 2.5, according to EC3. The bottom flange is more vulnerable to fire because it faces to flames and radiation from the fire directly. The reduction in the tension capacity of the bottom flange is 12% during a single passenger car fire, whereas the value increases to 88% in the course of multiple vehicle fires. On the other hand, webs fall into a more vulnerable situation, because they block ceiling jets and are exposed to hot gaseous severely. Mechanical properties of the web have decreased by about 90%. However, any structural calculation was performed; hence, the structural integrity of the composite slab was not addressed.

Table 2.5. Eurocode-defined reduction factors for the steel members adjacent burning vehicle/vehicles (Cook and Pessiki, 2008) (PT: post tension; RC: conventional reinforced concrete; LS: long span; SS: short span)

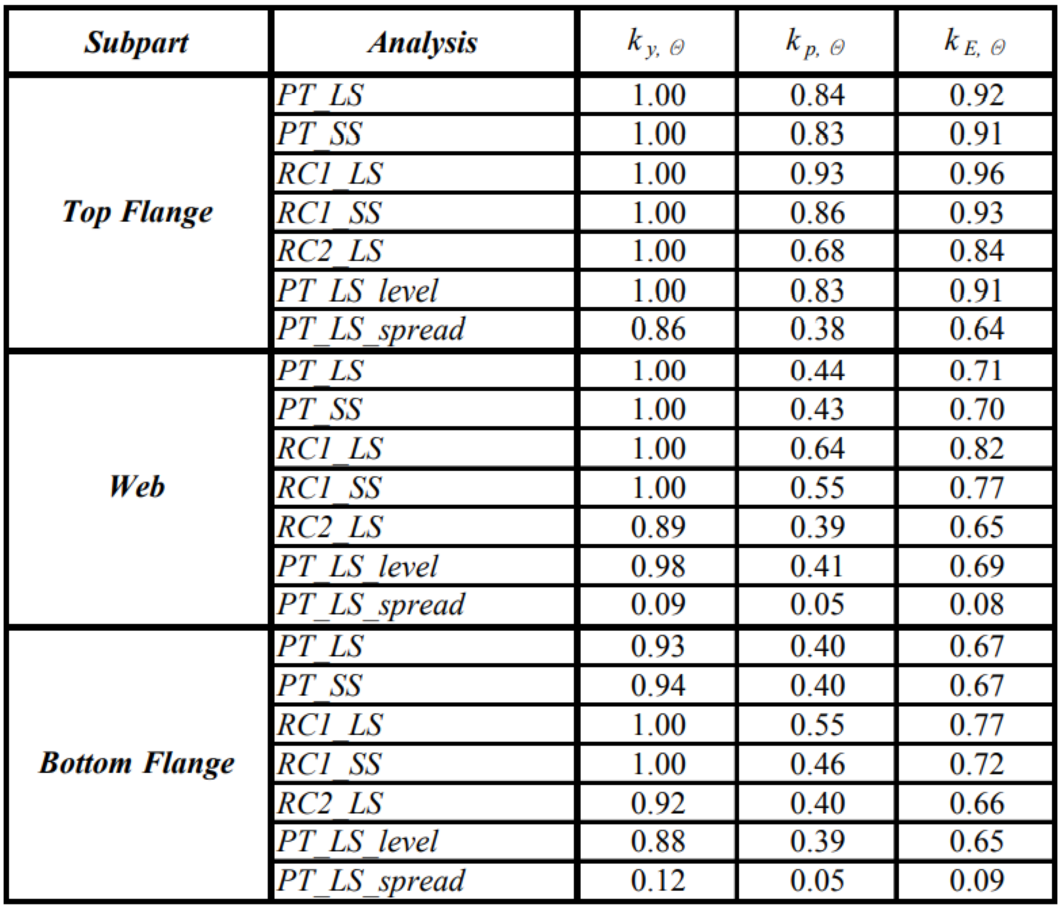

Subpart	***Analysis***	$k_{y,\Theta}$	$k_{p,\Theta}$	$k_{E,\Theta}$
Top Flange	*PT_LS*	1.00	0.84	0.92
	PT_SS	1.00	0.83	0.91
	RC1_LS	1.00	0.93	0.96
	RC1_SS	1.00	0.86	0.93
	RC2_LS	1.00	0.68	0.84
	PT_LS_level	1.00	0.83	0.91
	PT_LS_spread	0.86	0.38	0.64
Web	*PT_LS*	1.00	0.44	0.71
	PT_SS	1.00	0.43	0.70
	RC1_LS	1.00	0.64	0.82
	RC1_SS	1.00	0.55	0.77
	RC2_LS	0.89	0.39	0.65
	PT_LS_level	0.98	0.41	0.69
	PT_LS_spread	0.09	0.05	0.08
Bottom Flange	*PT_LS*	0.93	0.40	0.67
	PT_SS	0.94	0.40	0.67
	RC1_LS	1.00	0.55	0.77
	RC1_SS	1.00	0.46	0.72
	RC2_LS	0.92	0.40	0.66
	PT_LS_level	0.88	0.39	0.65
	PT_LS_spread	0.12	0.05	0.09

2.4. A full-size passenger car fire test within a steel frame in similar dimensions to tower-type AVPS units.

Structural designs of tower type AVPSs are based on dimensions of passenger cars. In other words, span lengths in AVPSs are close to the length or width of an average car. Floor heights are also smaller relative to conventional car parks. The height of a family-size sedan car is around 1.7 m, and the floor height of an ordinary AVPS is at most 2 m. Tramoni et al. (2019) have conducted a full-size vehicle fire test within a steel dummy frame that was in similar dimensions with individual parking spaces in AVPSs. The experimental setup of Tremoni et al. (2019) is given in Figure 2.23. The frame has contained nine columns in total; HEA300 columns were used at edges and one full square section of 160x160mm column in the center of the frame. Seven IPE450 beams have used. Span lengths of beams were 2.5 and 5 m. The top of the frame was covered with a non-combustible plate. The frame has also been equipped with 200 thermocouples for steel and gas temperatures, and the distance between passenger cars was about 70 cm.

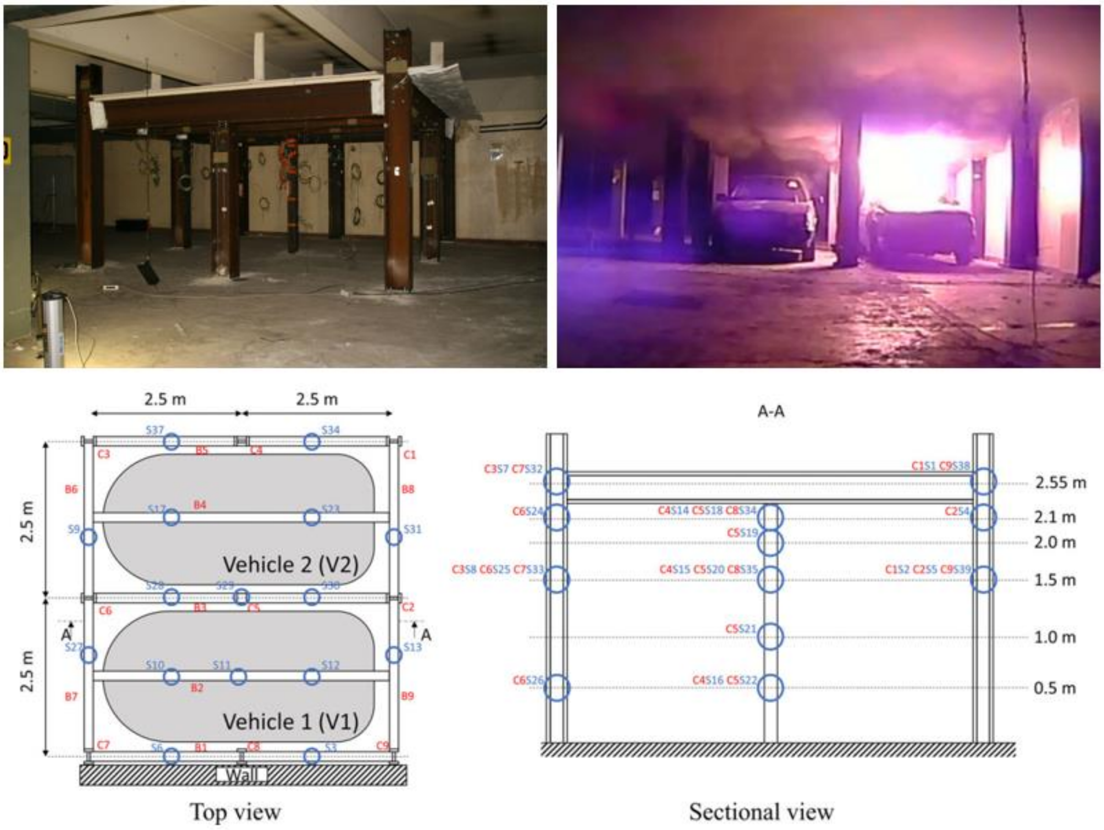

Figure 2.23. Experimental setup of Tramoni et al. (2019)

Two medium diesel passenger cars of the 1990s have been used in the fire test. The was initiated at the vehicle V1, and then it spread to the vehicle V2 at the 26th minute of fire. The beams most affected by heat and flames were just above the burning vehicles, which can be seen in Figure 2.24b. The maximum temperatures in the beams increased up to 920 °C, and temperature levels did not increase much more in places far from the center. Temperature values also decreased up to 150 °C in external beams. As seen in Figure 2.24a, temperature levels in beams remained constant for a certain period, and they started to increase after the fuel tank ruptured. Meanwhile, the fire spilled to another car. Regarding the columns, only a few sections at columns have reached a temperature of more than 500 °C. The most affected sections were located back sides of the vehicles, and at the top of the columns on the sides of the vehicles due to the ceiling jet. The central column placed between cars reached a maximum temperature of 474 °C. The test has also indicated that one of the main causes of the high temperature at columns is the ceiling jet, and steel members with smaller section factors are more robust against fire.

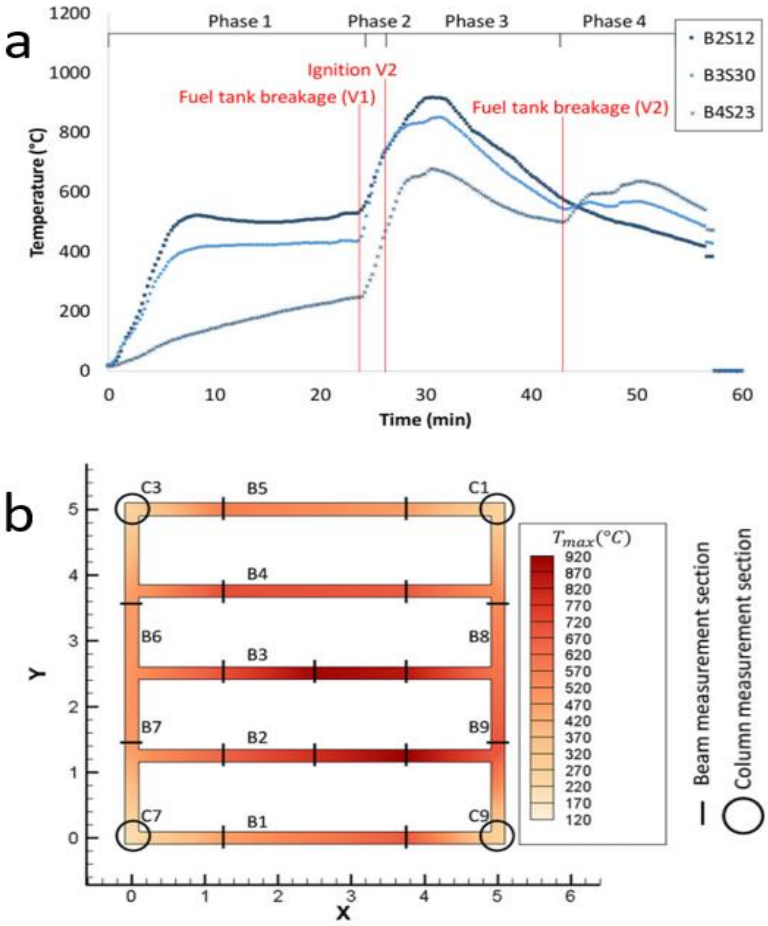

Figure 2.24. Experimental results of internal combustion engine fires: (a) beam temperatures above the cars; (b) maximum temperature field on the frame.

3. METHODOLOGY

3.1. Structural Design of an 8-floor AVPS unit

AVPSSs are modular structures. Each unit has an elevator/lift column and parking slots on the left and right sides of the lift. An individual unit can expand vertically. An example of tower type AVPS produced in Turkey is shown in Figure 3.1 (Polipark, 2020). S235 grade HEA180 beams were used as columns. Floor heights were varying between 1.75 and 2 m for different size of passenger cars. Architectural drawings of another AVPS that under usage in Balıkesir are given at Appendix C. The car park contains four identical tower type AVPS units side by side, and its total capacity is 56-cars. In general, dimensions of parking bays are similar for all kind of AVPSs due to the same aspects of passenger cars.

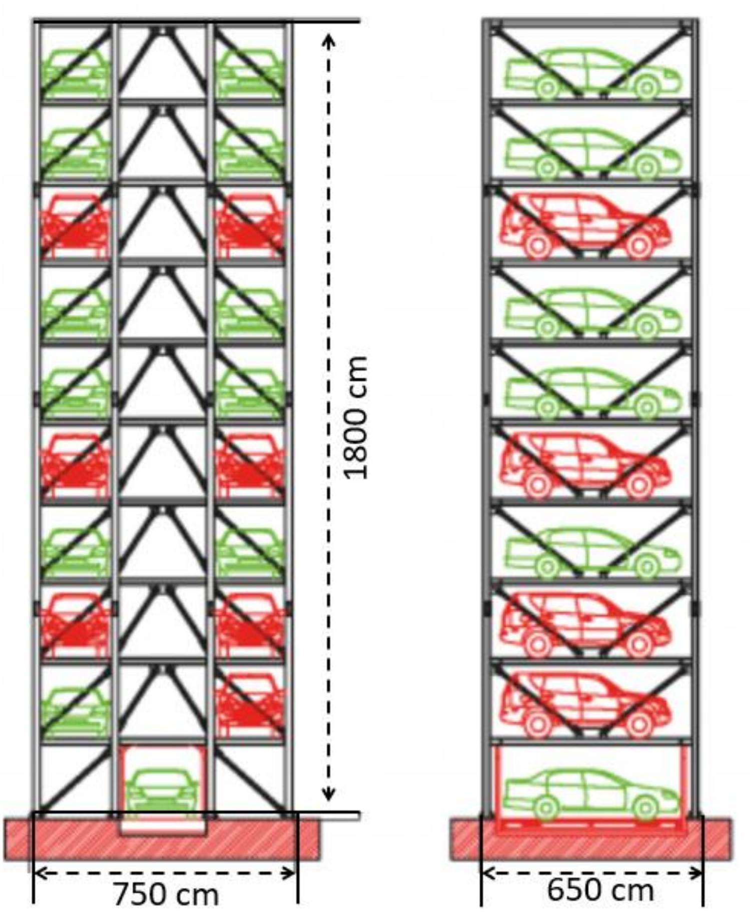

Figure 3.1. A tower type AVPS design from Turkey (Polipark, 2020)

An 8-floor open-facade AVPSS unit with the capacity of 14 car has been designed according to the Turkey Building Earthquake Code 2018 and Eurocode 3 (TBDY, 2018)(European Committee for Standardization, 2005). The design was also based on dimensions and structural properties of existing AVPSs that were in Balikesir and Bursa. However, the cross-section of columns was chosen as square hollow section (SHS) rather than I beams. Sizes of the unit are 19.8 m in height, 6x7.6 m in plan. Construction material has been chosen as S235 grade carbon steel. The structure contains external cross-bracings in the cross-section of TUBO 80x80x8 in the short side whereas D=10 mm cable in the long side. The entrance gate to car lift takes place on the ground floor, where the strongest bracings with the section of TUBO 160x160x10 are employed on the long side of the ground floor. All columns are also TUBO 160x160x10 in cross-section. TUBO 80x80x8 beams between columns are placed only near to short edges of car pallets. The beams are connected to columns by pins to release moment transfer during an earthquake, as given in Figure 3.2. The beams in the cross-section of TUBO 160x160x10 are also placed in every three floors between inside columns. Design and general views of the unit are shown in Figure 3.3. Member sections used at the structure are also tabulated in Table 3.1.

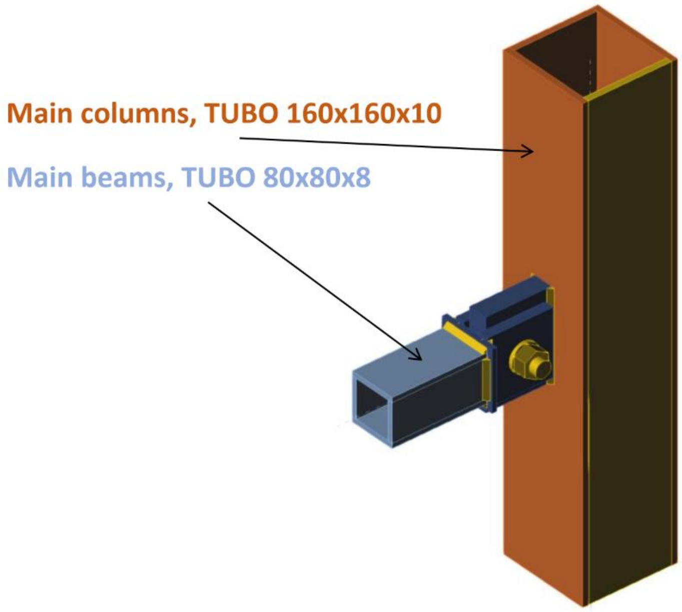

Figure 3.2. Pin joint between main column and main beam

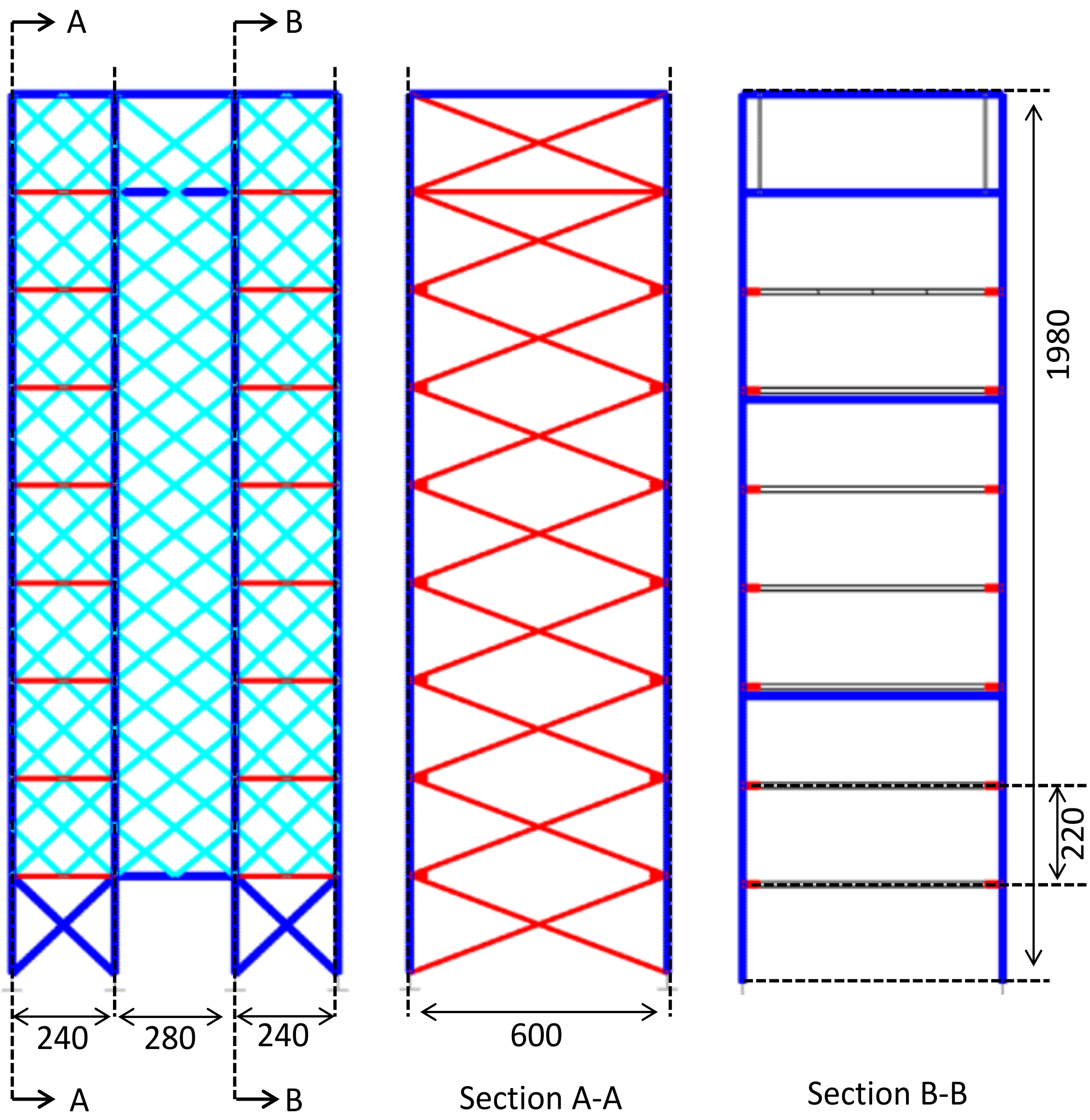

Figure 3.3. Structural design of the 8-floor AVPS unit (lengths in cm)

Table 3.1. Member Sections in Figure 3.3.

Member	**Section**	**Colour**
Column	TUBO160x160x10	**Dark Blue**
Strong beam	TUBO160x160x10	**Dark blue**
Weak beam	TUBO80x80x8	**Red**
Ground bracing	TUBO160x160x10	**Dark blue**
Strong bracing	TUBO80x80x8	**Red**
Weak bracing	Ø20 cable	**Turquoise**
Parking pallet at the Section B-B	Detailed in Figure 3.4	**Grey**

Parking pallets stay on wheels, like a short but wide train car. The wheels are mounted to short cantilever beams fixed to columns. In the design, the cross-section of cantilever beams is chosen as HE160A. Boundary conditions of car pallet are shown in Figure 3.4. The only purpose of car pallets is to carry passenger cars. Kerb weight of an ordinary large size SUV is at most 2 tons. Its wheelbase is also at least 2.7 m. The main assumption for vehicle loading on car pallets is based on a perfectly symmetric car with 19.6 kN in total weight and 2.7 m length of the wheelbase. The pallet contains four IPE120 longitudinal beams to carry to vehicle load and four TUBO 90x45x3.6 crossbeams. The frame of the pallet is also covered with sheet metal with a thickness of 2 mm. The design of car pallet is also shown in Figure 3.4.

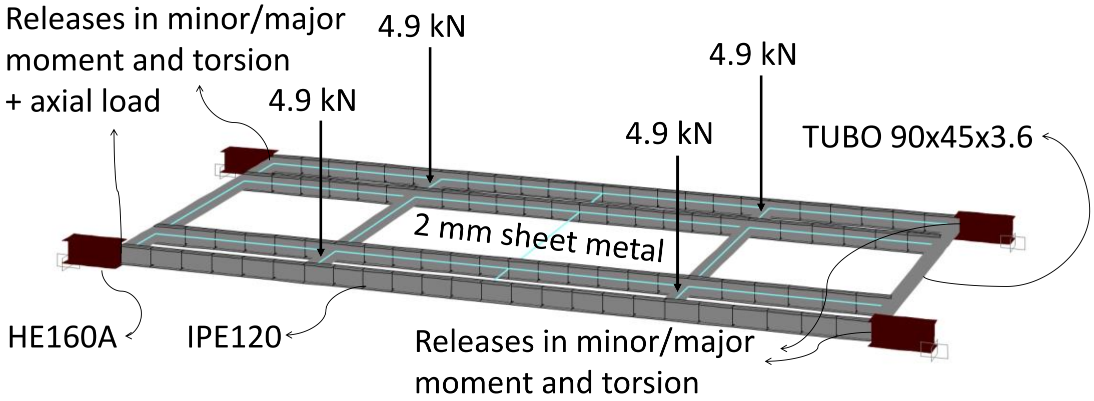

Figure 3.4. Structural design and design load of parking pallet

Earthquake performance was determined before the fire analysis of the prototype structure. According to TBDY-2018, equivalent earthquake load has been applied to the building. There are parameters to be determined before these analyses. These variables are specific to the type of building and the region where the building is being built. Regional earthquake properties can be determined through AFAD's website (AFAD, 2019). The parameters depending on the building type are also determined through the TBDY-2018 standard. Structure specific parameters are response modification, R, system overstrength, D and occupancy importance, I. There are no people inside the AVPSs. Therefore, in the event of a disaster, the risk of loss of life is very low in the building, and the occupancy importance takes the value 1. In addition, all earthquake loads should be carried through eccentric bracings because AVPS systems are modular structures. The number of identical floors can be increased. As the building height increases, the moment of the earthquake in the lower floors increases too. To overcome this problem, bracing members on the lower floors can be strengthened. As a result, a single column type and different cross-section elements are produced according to the building height and earthquake conditions in order to simplify production. This strategy will reduce the marginal cost of mass production. The parameters *R* and *D* can be defined as 8 and 2.5 for a tower-type AVPS like in Figure 3.3. Site-specific parameters such as long-period transition period and soil classification are also given in Table 3.2. These values belong to a randomly selected point in the Marmara region. The site class was also chosen arbitrary.

Table 3.2. Parameters for seismic load (TBDY-2018)

Ss	0.981
S1	0.271
Long-period transition period	6
Earthquake Ground Motion Level	DD-2
Site class (arbitrary chosen)	ZD
Response modification, *R*	8
System overstrength, *D*	2.5
Occupancy importance, *I*	1

Load combinations to be used for steel structures are also determined in TBDY-2018 code. Since there are no ground surveys in this thesis, those related to the ground in load combinations have not been evaluated. The load combinations used in the earthquake calculations of the AVPS are given in Table 3.3. Parameters in combinations are dead load, *G*, live load, *Q*, earthquake load in *x*, *Ex*, earthquake load in *y*, *Ey* and vertical effect of the earthquake, *Ez*. These individual loads are calculated automatically by SAP2000.

Table 3.3. Design load combinations

#	**Load combination**
1	G+1.2Q+Ex+0.3Ey+0.3Ez
2	G+1.2Q+Ex-0.3Ey+0.3Ez
3	G+1.2Q-Ex+0.3Ey+0.3Ez
4	G+1.2Q-Ex-0.3Ey+0.3Ez

#	**Load combination**
5	G+1.2Q+Ey+0.3Ex+0.3Ez
6	G+1.2Q+Ey-0.3Ex+0.3Ez
7	G+1.2Q-Ey+0.3Ex+0.3Ez
8	G+1.2Q-Ey-0.3Ex+0.3Ez

The deformed shapes obtained by the earthquake analysis made with SAP2000 are given in Figure 3.5. The structure is oscillating homogeneously, and the deflection at the tip of the structure is less than 1/200 of the total height. Structural elements do not form plastic hinges. The structure is more flexible against earthquake loads that are parallel to the long axis. Steel cables gave a more elastic result. Utility ratios of structural elements were also calculated. Utility rates are determined in accordance with EC3. Utility ratios in all columns and beams are less than 0.5. Yielding has been observed in some of the cables on the front facade, but the cables have not been broken. The utility level varies from floor to floor in TUBE 80x80x8 cross-section bracing members. The levels are up to 0.9 in the first three floors. Utility ratios are between 0.5 and 0.7 in the middle floors, and below 0.5 in the upper floors. Utility rations are seen in Figure 3.6.

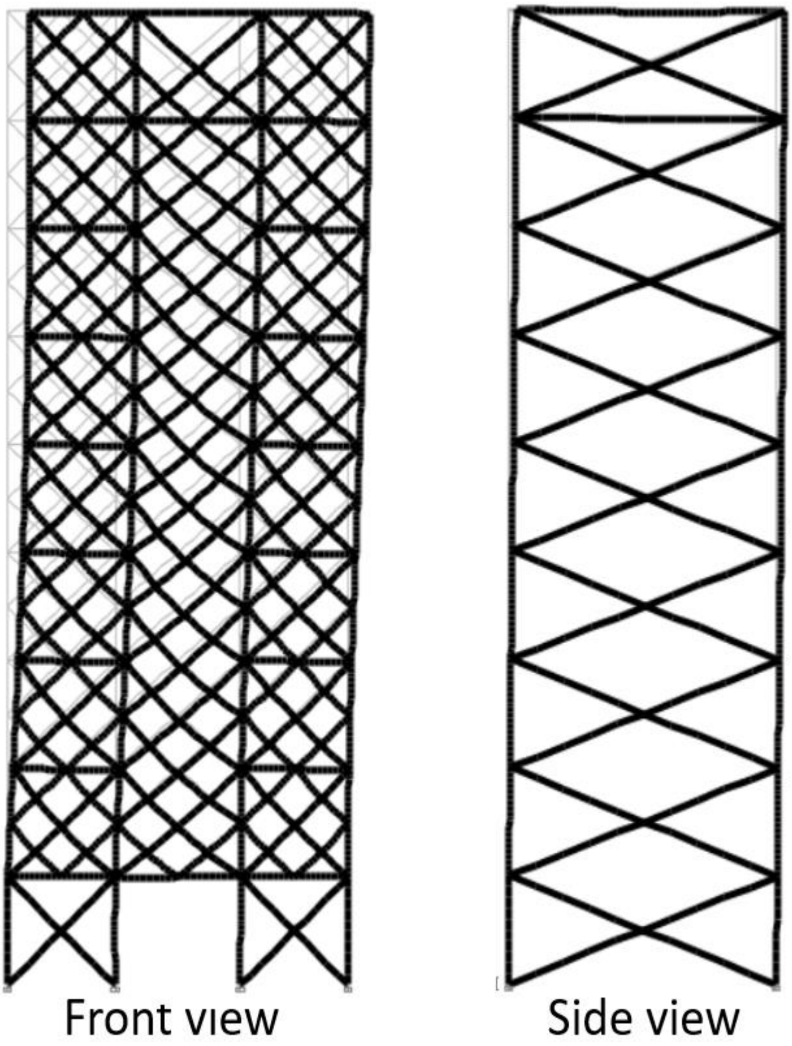

Figure 3.5. Earthquake load response, load in the long axis in front view, load in the short axis in side view

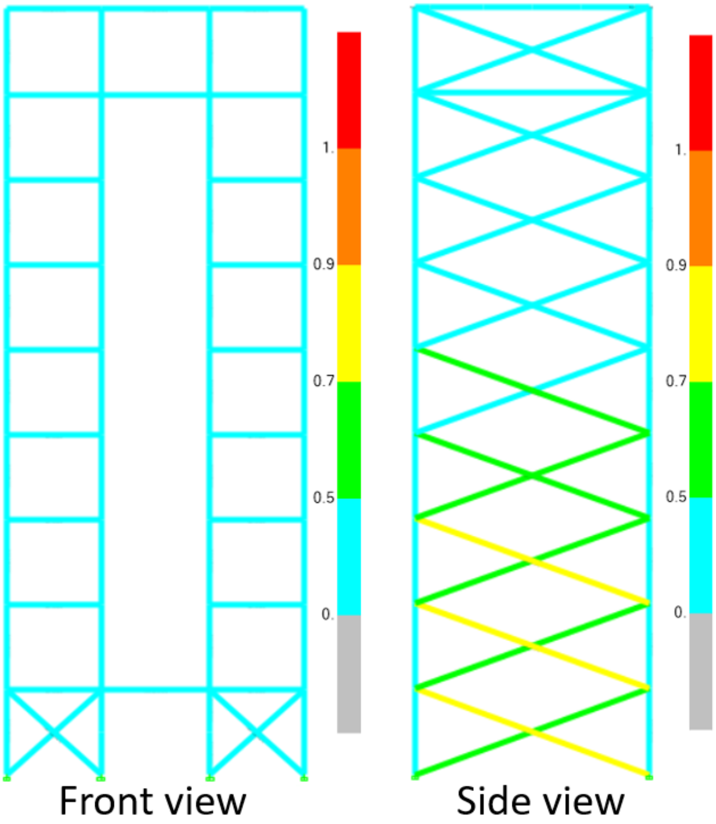

Figure 3.6. Utility ratios of steel members according to EC3

3.2. Fire Simulation Method with FDS

Fire Dynamic Simulator (FDS) developed by the National Institute of Standards of Technology (NIST) is a computational fluid dynamics software specialized for fire dynamics. FDS solves fire-driven low-Mach flows on a computationally uniform grid (McGrattan et al., 2015). Because of this uniformity, solid objects in the FDS is modelled by a composition of rectangular obstructions in the level of resolution determined by a uniformly spaced 3-D grid. Partial derivatives of the conservation equations of energy, momentum and mass are solved by finite differences technique for every cell in the grid. The thermal radiation is also solved using finite volumes technique. Because of the nonignorable turbulences in fire-driven flows, FDS treats turbulence via the Smagorinsky form of Large Eddy Simulation, and for more specific problems, Direct Numerical Simulation can be employed (McGrattan et al. 2015). Fundamental equations in FDS software are detailed in the 'Fire dynamics simulator technical reference guide volume 1 : mathematical model' by McGrattan et al. (2015). These equations are within the Navier-Stokes equation, and they are given in Eq. 3.1-5. These are the continuity equation, the momentum equation, the energy equation, the chemical composition equation and the equivalent pressure equation, respectively.

$$\frac{\partial \rho}{\partial t} + \nabla \cdot \rho u = 0 \tag{3.1}$$

$$\frac{\partial (\rho u)}{\partial t} + \nabla \cdot (\rho u^2) + \nabla p = \rho g + \nabla \cdot \tau \tag{3.2}$$

$$\frac{\partial (\rho h)}{\partial t} + \nabla \cdot (\rho u h) = \frac{\partial (p_o)}{\partial t} + \nabla \cdot (k \nabla T) + \dot{q}''' \tag{3.3}$$

$$\frac{\partial (\rho Y_i)}{\partial t} + \nabla \cdot (\rho u Y_i) = \nabla \cdot (\rho D_i \nabla Y_i) + \dot{m}_i''' \tag{3.4}$$

$$p_o(t) = \rho T R \sum_i^N \frac{Y_i}{M_i} \tag{3.5}$$

Where, ρ is the gas density, p is pressure, τ is the viscous tension, h is enthalpy, T is the temperature of the gas, k is the heat conduction term, u is the velocity of the gas, g is the gravitational acceleration, t is time, R is the ideal gas constant, D is the diffusion coefficient, M is the molecular weight, $\dot{m}_i'''$ is the mass change in unit volume and $\dot{q}'''$ is the combustion power in unit volume. Fire simulations, as can be understood from Eq. 3.3, give consistent results in streams where the MACH number is small.

3.3. Heat Transfer Analysis and Material Modeling at Elevated Temperatures

3.3.1. SHS Sections

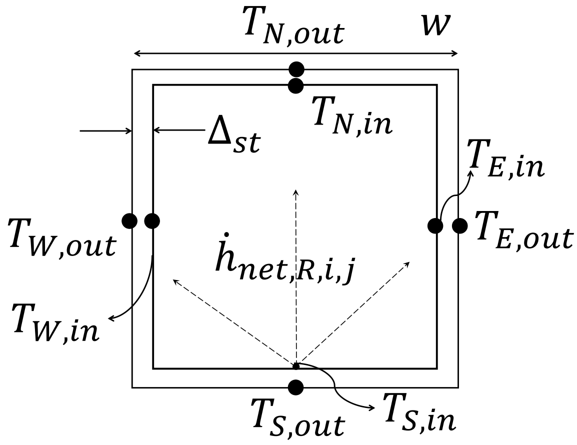

Figure 3.7. SHS section schematic for heat transfer analysis

Some portion of the heat generated by combustion reactions is transferred by radiation or convection to steel members. Transferred net heat causes temperature rise at them.

However, the direct calculation of member temperature with FDS requires much more time for modelling and mesh optimization for square hollow sections. Apart from this, a very refine computational domain with small cell sizes that can represent a SHS section comes up with an enormous computational load. However, fire and structural models can be decoupled by calculation of adiabatic surface temperature by the fire model (Wickstrom et al. 2007). Hence, the thermomechanical analysis can be simplified. Once adiabatic surface temperature data on square hollow sections are extracted from the fire model, the total heat transfer rate penetrating the member is calculated by Eq. 3.6. The equation is written for two dimensional or cross-sectional analysis. Thus, q_k is in W/m, and k refers to the direction such as north side (N) or west side (W) of the member. The equation contains the following parameters: width of the member in m, w, surface emissivity ratio, ε_s, Stefan-Boltzmann constant equal to 5.67x10^{-8} W/m^{2}K^4, σ, adiabatic surface temperature in °C from fire model, T_{AST}, convective heat transfer coefficient in W/m^2°C, h_c, and surface temperature in °C, $T_{k,out}$. Steel members can be a square hollow section in a conventional tower type AVPS. The schematic of a SHS section is shown in Figure 3.7. It is also modelled specifically for this research to develop a heat transfer calculation model. Sign conventions and terms for the calculation model are also shown in the same figure.

$$\mathrm{q_k} = \mathrm{w}\varepsilon_s\sigma\left[(T_{AST}+273)^4-\left(T_{k,out}+273\right)^4\right]+\mathrm{w}h_c(T_{AST}-T_{k,out}) \tag{3.6}$$

Once the heat input is defined, dissemination of the heat inside the member can be calculated by the finite difference method. The cell configuration in the finite difference method on the section is two parallel cells per flange and one cell per temperature point T. Thus, eight cells are modelled within the SHS section. The finite difference method and principles of heat transfer are explained at the heat transfer book written by Çengel (2004). All equations except Eq. 3.6 are based on the Çengel's book (2004). The air inside hollow sections may cause a cooling effect by natural convection. This phenomenon has been neglected to obtain a conservative approach. On the other hand, heat transfer by radiation between inner surfaces of the SHS section has been taken into account by employing the Eq. 3.7. $\dot{\mathrm{h}}_{\mathrm{net,R,i-j}}$ refers to the net heat transfer rate by radiation from surface i to j, in W/m. Terms of $\emptyset_{i-j}, y_j, \varepsilon_i, \varepsilon_j, T_i\ and\ T_j$ refer to view factor, the width of the surface which absorbed the heat in m, the emissivity of surface i and j, surface temperatures in °C. Radiative heat transfers to an inner surface from the other three surfaces are taken into account, as shown in Figure 3.7. Additionally, conductive heat transfer rate inside the steel member is calculated by Eq. 3.8. q_{i-j} refers to heat transfer rate from cell i to j in W/m in the finite difference model. ‘k’ is the convective heat transfer coefficient in W/mK. Δy_j and Δx_{i-j} refer to the width of the heat transfer boundary and distance between point i to j. After heat transfer rates in conduction, convection and radiation are defined for a cell j in 2D finite difference model, the temperature in the cell is calculated by Eq. 3.9. Δt refers to time increments which stored in the data of T_{AST} from fire model. $\rho, A\ and\ c_p$ are density in kg/m^3, cell area in m^2 and specific heat constant in J/kgK. $'T_j^{t+\Delta t} - T_j^{t}{}'$ term also refers to temperature change in cell j during a heating or cooling duration of Δt. By solving equations Eq. 3.6 to 3.9 for every point by the finite difference model of the cross-section, time-dependent temperature curves are obtained.

$$\dot{\mathrm{h}}_{\mathrm{net,R,i-j}} = \emptyset_{i-j}\, \mathrm{y_j} \varepsilon_i \varepsilon_j \sigma \left[(T_i + 273)^4 - \left(T_j + 273\right)^4\right] \tag{3.7}$$

$$\mathrm{q_{i-j}} = \mathrm{k}\Delta \mathrm{y_j} \frac{T_i - T_j}{\Delta \mathrm{x_{i-j}}} \qquad \text{...(3.8)}$$

$$\rho A c_p \frac{\mathrm{T_j^{t+\Delta t} - T_j^t}}{\Delta \mathrm{t}} = \textstyle\sum_i (\mathrm{q_k} + \mathrm{q_{i-j}} + \dot{\mathrm{h}}_{\mathrm{net,R,i-j}}) \tag{3.9}$$

After temperature curves of the points marked in Figure 3.7 are obtained by the transient finite difference analysis; average temperature change curve of the steel section, ΔT, and time-dependent temperature gradients in principle directions, $T_{,S-N}$ and $T_{,W-E}$, are calculated by Eq.3.10-12. Once the time-dependent average temperature of the cross-section is determined, change in mechanical properties of steel can be found with the assumption of homogenous temperature change in the section. Temperature-dependent mechanical properties of construction steel are also defined in EC3. Changes with temperature in coefficients of proportionality limit, $k_{p,\theta}$, yielding strength, $k_{y,\theta}$, and Young Modulus, $k_{E,\theta}$, are shown in Figure 3.8b. Mechanical properties of steel stay constant up to body temperature of 100 °C, then, proportionality limit and Young Modulus start to decrease. On the other hand, construction steel does not lose its yielding strength, while its temperature is under 400 °C. Temperature rise in a steel member leads to additional mechanical stress due to the thermal elongation. The thermal elongation occurs at every level of temperature rise, which is also defined in Eurocode 3. The thermal elongation, according to EC3, is shown in Figure 3.8a. This phenomenon should be taken into account in structural fire calculations.

$$\Delta T = \frac{1}{8}\left[T_{E,in} + T_{E,out} + T_{W,in} + T_{W,out} + T_{S,in} + T_{S,out} + T_{N,in} + T_{N,out}\right] \tag{3.10}$$

$$T_{,S-N} = \frac{1}{2W}\left[\left(T_{N,in} + T_{N,out}\right) - \left(T_{S,in} + T_{S,out}\right)\right] \tag{3.11}$$

$$T_{,W-E} = \frac{1}{2W}\left[\left(T_{E,in} + T_{E,out}\right) - \left(T_{W,in} + T_{W,out}\right)\right] \tag{3.12}$$

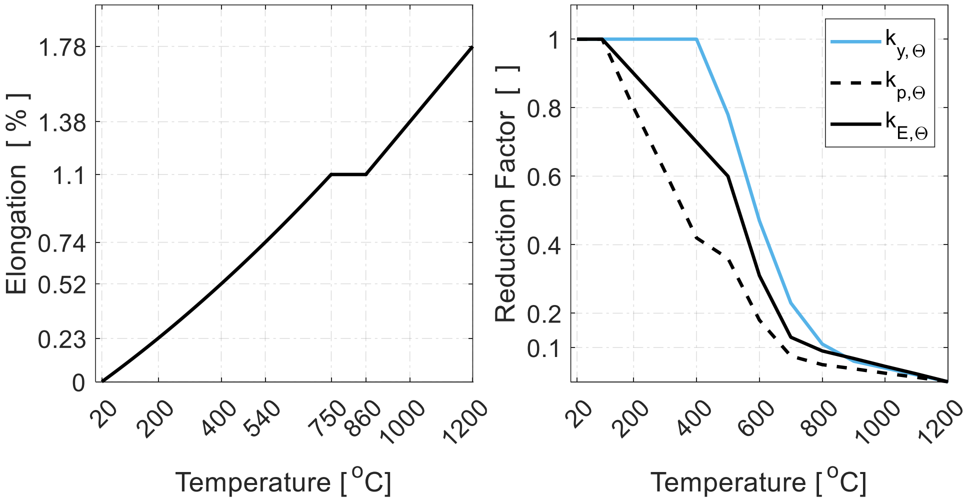

(a) (b)

Figure 3.8. Temperature-dependent mechanical properties of structural steel in EC3 (European Committee for Standardization, 2005)

To test the validity of the method for member temperature calculation given in this subchapter, a numerical test setup in FDS has been developed. The configuration contains a section of TUBO160x160x10 steel beam surrounded by uneven heating surfaces. The section view with dimensions is given in Figure 3.9. Yellow pieces in the figure represent heating surfaces with 75 kW/m^2 peak heat release rate per unit area. The temporal characteristic of the heat release rate is also similar to the Category III fire curve for passenger cars. However, the design curve used in this setup was downsized in the time domain to lower the computational cost. The total duration of the simulation is 720 second, whereas the value for Category III fire curve is 72 minutes. This modification in the time domain can not cause any misestimation. Because the purpose is to compare two different methods that calculate temperature levels, not to find temperature levels in a fire scenario.

Locations of heater surfaces have been chosen arbitrarily to simulate an uneven heating condition. All heater surfaces are in a distance of 10 cm from the member. A very refine computational domain with 1 cm cubic cells are also used to solve geometric detail of TUBO160x160x10 section of which the shortest dimension is 10 mm. A 1-cm mesh is unpractical for fire simulations of buildings, due to computational cost. Cell sizes differ from 10 to 50 cm in simulation setups with FDS for closed compartment or open space fires. After validation of the method, block elements in dimensions that are similar to external dimensions of steel members will be used in fire simulations of AVPSs.

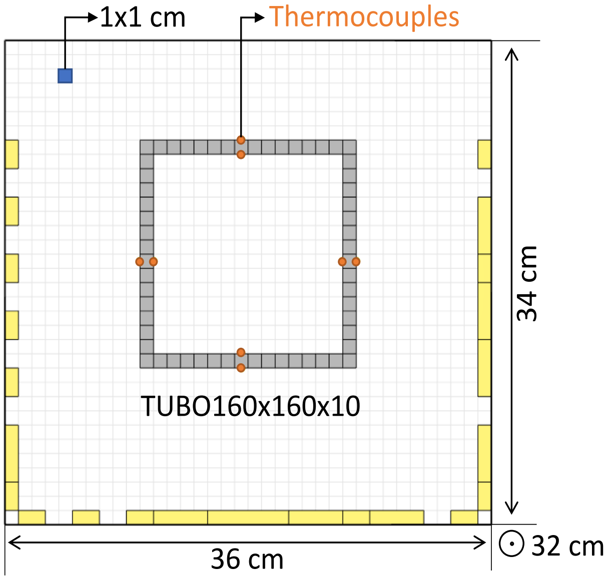

Figure 3.9. FDS setup for validation of proposed heat transfer calculation (section view)

Boundary conditions of the validation setup are very critical because of the compact design of the installation. Distances between opposing boundaries are 32, 34 and 36 cm as can be seen in Figure 3.9. Symmetric boundary conditions were implemented at ends of the square hollow section beam. A steel beam with an infinite length was obtained by the symmetric boundaries mathematically. Additionally, other four faces of the computational domain were chosen as the open boundary surface. Open boundary surface is a unique boundary condition in FDS, that it imitates open atmospheric conditions such as constant pressure and an unlimited source of fresh air (McGrattan et al., 2013). Boundary conditions and heater surfaces are shown in Figure 3.10. After the simulation, calculated adiabatic surface temperature curves for each face of the beam are given in Figure 3.11. The AST of the upper surface does not increase as expected. Because the top flange is an unexposed surface and it can be heated by internal surface radiation from other flanges or convective heat transfer through internal space of the beam. On the other hand, the highest AST levels are between 600 and 850 °C.

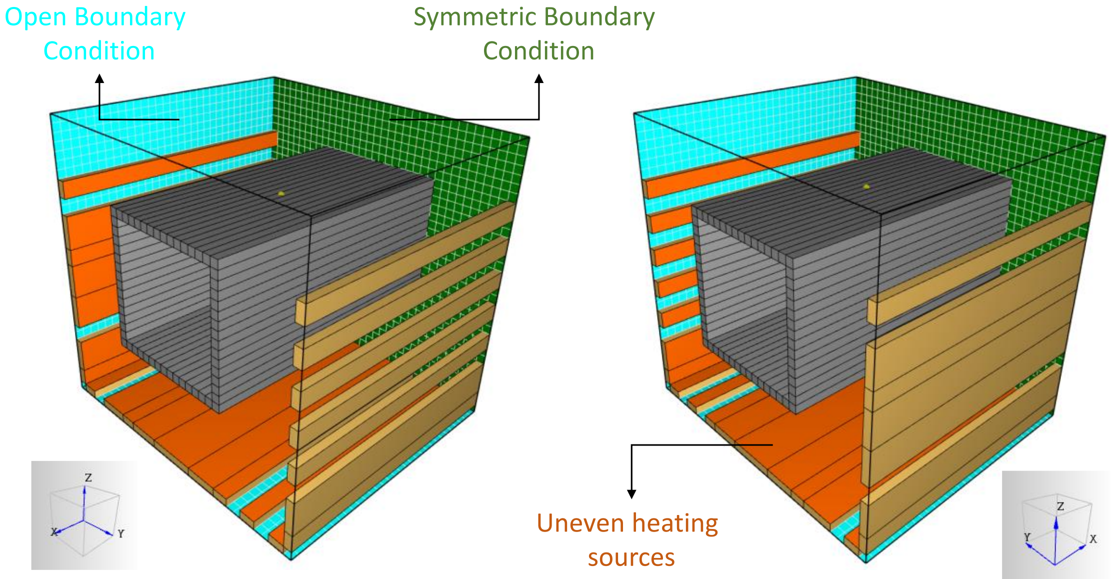

Figure 3.10. FDS setup for validation of proposed heat transfer calculation (3D views and BCs)

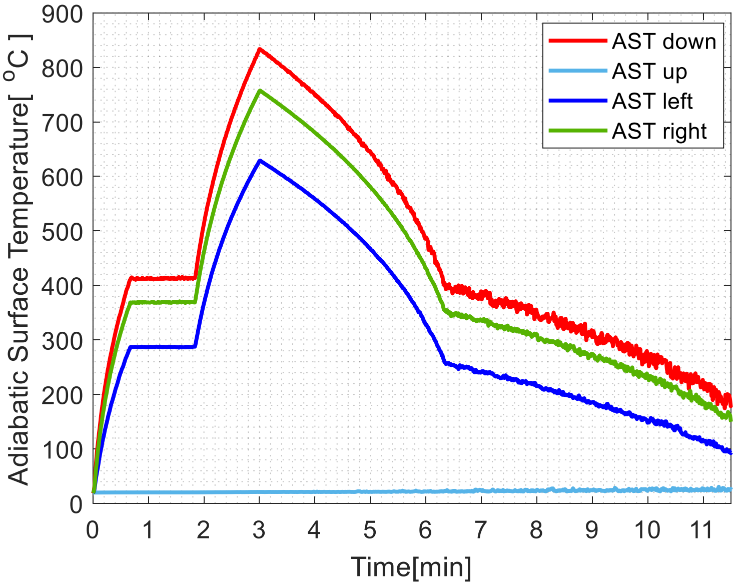

Figure 3.11. Calculated adiabatic surface temperature levels

Average temperatures of flanges of the beam obtained by both FDS simulation and the method given in this subchapter are presented in Figure 3.12. Before the criticizing of results, it should be noted that the calculation method does not consider the thermal effect of air inside the square hollow section beam, whereas the air was modelled in FDS. The thermal inertia and capacity of air can be expected to decelerate the cooling phase of the beam, if the air is incarcerated in it. Otherwise, an airflow inside a hollowed member can lead the member to cool faster. As can be seen in Figure 3.12, the temperature of the right flange decreases faster in the proposed method during the cooling phase. However, the peak temperatures are the same in both curves, around 280 °C. Parallel to this, peak temperatures of left and lower flanges were calculated as very close to levels obtain from FDS results. Temperature levels for all flanges except the upper one are parallel with FDS result in the heating phase. The proposed method overestimates mean temperatures for unexposed flanges by about 35%. However, it is expected that temperature levels at unexposed surfaces are relatively low. Although the overestimation ratio can be seen unacceptably high at first glance, it is under 30 °C, which can be considered as negligible in fire engineering calculations. Resultant member temperature and temperature gradients in the section are also given in Figure 3.13. Errors in peak levels are 1% for member temperature, ΔT, 5% for horizontal temperature gradient, $T_{,horizontal}$ and 9.6% for vertical temperature gradient, $T_{,vertical}$. The misestimation is relatively high in the vertical temperature gradient due to the overestimation in the unexposed flange. By considering all of these results, the proposed method in this chapter for heat transfer calculation can be applicable for determining peak temperature levels.

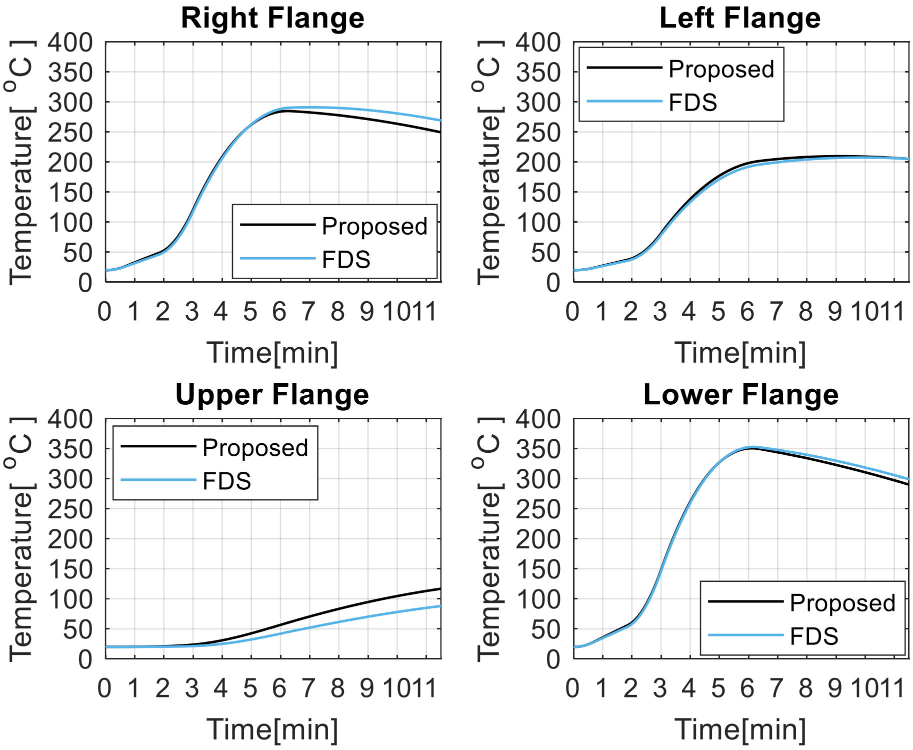

Figure 3.12. Comparison of temperature levels at flanges

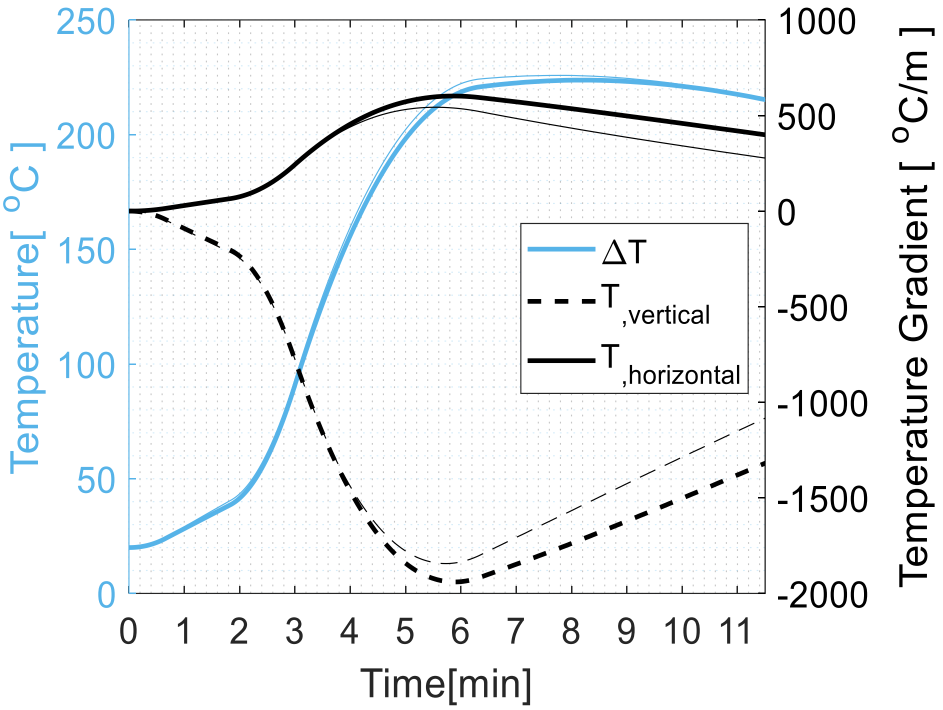

Figure 3.13. Comparison of member temperature and temperature gradients (thick lines from FDS, thin lines from proposed method)

3.3.2. Parking Pallets

The design approach of '*pallet on wheels'* can not provide a fixed boundary condition for parking pallets during a fire. Relative change in positions of cantilever beams carrying a parking pallet may cause a loss of contact at pallet wheels. A typical parking pallet-rail coupling design is shown in Figure 3.14. The parking pallet slides on four wheels which are fixed to the main structure. During stationary positions, the parking pallets just stay on the small wheels. On the other hand, deformation of parking pallets during a fire can cause dislodgement. There is only a small safety margin of 5 or 6 cm for the coupling, as shown in Figure 3.14. Besides, the material of pallet wheels is chosen as polyamide or polyurethane in some designs. These polymers are not robust against high temperature. Thus, the wheel itself can cause unsafe situations.

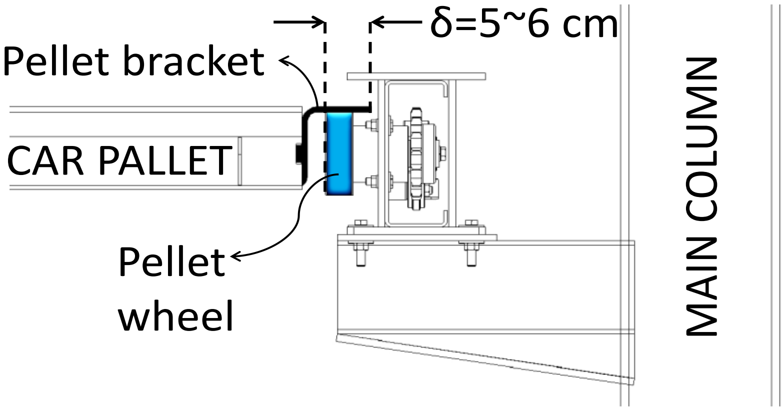

Figure 3.14. The detail of parking pallet docking design

Some designs also contain a locking mechanism for parking pallets against earthquake. An example of such designs is given in Figure 3.15. In the design, a brake track with a cylindrical notch is mounted underside of the parking pallet. A locker mechanism that drive a pin in a linear path is mounted on the main structure. Then the locking pin with a cylindrical head rises up and contacts the milled recess in the form of a circular segment. The performance of the locking mechanism against fire is also unknown.


Locked

Unlocked

Figure 3.15. An example of parking pallet locking mechanism under the pallet and parallel to the rail (Hrabovský et al., 2019)

The failure mechanism of the pallet dislodgement can be divided into two distinct modes. The first mode is related to parking pallet itself. Plastic and elastic deformation due to thermal load causes a deflection, and this deformation can lead pallet bracket to drag on the pallet wheel. This failure mode called ‘Mode 1’ is shown in Figure 3.16. The latter failure mode is the deformation of the main structure, which is shown in Figure 3.16 and named as ‘Mode 2’. The mathematical model of failure modes is based on basic structural mechanics and some geometrical constraints. First of all, the relative change of the distance between opposing cantilever beams, Δx, is taken from the structural model of AVPSS directly. Thermal elongation of the parking pallet is also taken into account as a positive effect. Thermally elongated length of the parking pallet, $L_{P,\Delta T}$, with average temperature change, ΔT, is calculated by Eq. 3.13 α refers to thermal elongation coefficient which defined in Eurocode 3, and L_P is the initial length of parking pallet. Once the thermally elongated length, $L_{P,\Delta T}$, is calculated; the next steps of the mathematical model can be employed. The Mode 1 is based on vertical mid-deflection of the parking pallet, Δw. There are two main causes of the vertical displacement, vehicle load and thermal gradient. The deflection is calculated by Eq. 3.14, where Δw_P refers to the vertical displacement driven by gravitational loads, and Δw_T is the vertical displacement due to the thermal bowing. The term of Δw_P is calculated by Eq. 3.15., which is originally based on the deflection formula of the simply supported beam under two symmetric and equal loads. L_a refers to the length of the wheelbase of a passenger car with a weight of W_{car}. I is the equivalent moment of inertia of parking pallets. E also refers to temperature dependent Young's Modulus of structural steel which defined in EC3. Derivation of Eq. 3.15 is given in Appendix A. In addition to this, Δw_T is calculated by Eq. 3.16. The term of $T_{,z}$ in the equation refers to the temperature gradient causing thermal bowing.

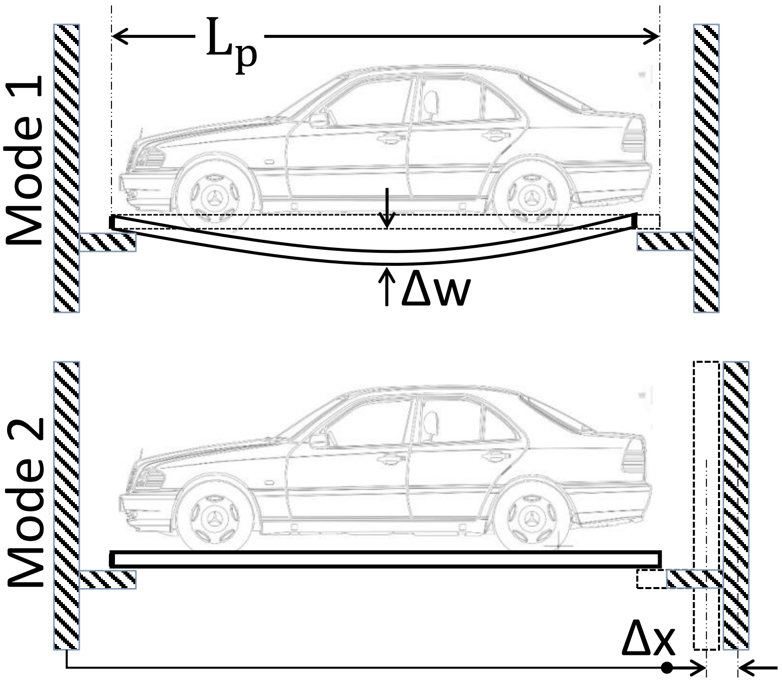

Figure 3.16. Parking car pallet failure modes

$$\mathrm{L_{P,\Delta T}} = \mathrm{L_P}(1 + \alpha\Delta \mathrm{T}) \tag{3.13}$$

$$\Delta \mathrm{w} = \Delta \mathrm{w_P} + \Delta \mathrm{w_T} \tag{3.14}$$

$$\Delta \mathrm{w_P} = \frac{W_{car}}{96\mathrm{EI}}\left[\left(\mathrm{L_{P,\Delta T}} - \mathrm{L_a}\right)\left(2\mathrm{L_{p,\Delta T}}^2 - \mathrm{L_a}^2 + 2\mathrm{L_{P,\Delta T}}\mathrm{L_a}\right)\right] \tag{3.15}$$

$$\Delta \mathrm{w_T} = \frac{\alpha \mathrm{L_{p,\Delta T}}^2 \mathrm{T_{,z}}}{8} \tag{3.16}$$

The vertical displacement of parking pallets can be used to calculate the drag length of pallet bracket on the pallet wheel. If the resultant deformed shape of parking pallets is reckoned as a triangle, the drag length due to vertical displacement, $\delta_{\Delta w}$, can be calculated with Eq. 3.17. Derivation of Eq. 3.17 is also given in Appendix A. The value of $\delta_{\Delta w}$ can be negative due to the thermal elongation. The resultant drag length is the summation of $\delta_{\Delta w}$ and Δx. Also, it should be smaller than the safety margin for the bracket drag, δ, shown in Figure 3.14. These calculations are also based on the assumption that a bracket on one side of the parking pallet is dragging on pallet wheels, while the other bracket on the opposite side stays stationary on other wheels. As a last remark, the global plastic strength of the parking pallet should always be higher than the demand caused by gravity loads The Eq. 3.19 checks for this situation. The term of W_{pl}, refers to equivalent plastic section modulus of the parking pallet, and $\sigma_{y,\Delta T}$ is the temperature-dependant yielding strength. While overall state of the parking pallet meets the conditions of Eq.3.18 and 19, it is assumed that the pallet dislodgement does not occur.

$$\delta_{\Delta \mathrm{w}} = \mathrm{L_p} - 2\sqrt{\frac{\mathrm{L_{p,\Delta T}}^2}{4} - \Delta \mathrm{w}^2} \tag{3.17}$$

$$\delta \geq \delta_{\Delta \mathrm{w}} + \Delta \mathrm{x} \tag{3.18}$$

$$W_{\mathrm{pl}}\, \sigma_{\mathrm{y,\Delta T}} \geq W_{car}\, (\mathrm{L_{p,\Delta T}} - \mathrm{L_a})/2 \tag{3.19}$$

3.4. Modified Passenger Car Fire Curve to Reduce Computational Time

Although passenger cars are generally C segments, it would be more realistic to model a car slightly above C segment to avoid a misestimation of fire destructiveness. Nevertheless, selecting a current D segment car can be a more conservative choice in terms of fire load. For this reason, an old car between the C and D segments matching the existing fire test results can be preferred. Mercedes-Benz C 180 Classic Sedan manufactured in 1998 is a suitable passenger sedan car as a C segment Category III vehicle. Although the Mercedes-Benz C180 Classic is a C segment passenger car, it can be assumed as a D segment medium car in terms of fire severity because of its luxury interior design and insulation, and curb weight. Parallel to this decision, Peak HRR levels and total energy containment of D segment passenger cars were examined by Mohd (2015). Adapted data for medium passenger cars are tabulated in Table 3.4. Peak HRR varies between 4 to 10 MW. This inconsistent information is hard to use as a design parameter. However, diversity between the total energy released is not much as Peak HRR. The total energy released values can be considered as a design variable. The total energy containment given in Table 2.1 for Category III cars is much higher than the maximum value in Table 3.4. In Table 3.4, listed passenger cars under Category III are generally medium-size passenger cars such as Passat, Mondeo, etc. Category III fire curve is chosen as a basis for design curve.

Table 3.4. Medium-size passenger car fire tests (Mohd, 2015)

Experiment ID	Peak HRR [kW]	Total Energy Released [MJ]	Total Mass Loss [kg]	Curb Weight [kg]	Ignition Location
1	4073	6144	192	1380	driver seat
2	8283	7000	255	1382	under gear box
3	9854	6806	262	1454	under gear box
4	3650	5960	186	1470	driver seat
Average	6465	6477	224	1421	-

The computational load of CFD solvers like FDS is high and running simulations on an ordinary computer with 4 or 8 physical cores is unpractical for detailed analyses. In order to ease fire simulations computationally, there are two possible methods, such as decreasing the detail level of the model and redefining fire design curve. The former method is already employed in FDS simulations easily during model construction. At this point, the latter method can be employed to shorten total simulation time. Before analyses for an AVPSS, the Category III fire curve has been slightly modified and justified. The modification mainly focuses on the ascent and descent parts around the peak point of the Category III fire curve. The new ascent part starts to increase exponentially 4 minutes before. The peak HRR level is decreased from 8300 to 7375 kW and first 11 minutes stay the same. Equations of ascent and descent parts of the Modified Category III fire curve are given in Eq. 3.20 and Eq. 3.21. where t is time in minutes and $\dot{q}_{\mathrm{dec}}$ and $\dot{q}_{asc}$ are heat release rate in kW. A comparison between modified and normal cases are also given in Figure 3.17.

$$\dot{q}_{asc} = 11.8\,t^2 \qquad 11 \le t \le 25 \quad \text{:ascent part} \tag{3.20}$$

$$\dot{q}_{\mathrm{dec}} = \dot{q}_{\mathrm{asc}}(25) * e^{-(t-25)/6} \qquad 25 \le t \le 70 \quad \text{: descent part} \tag{3.21}$$

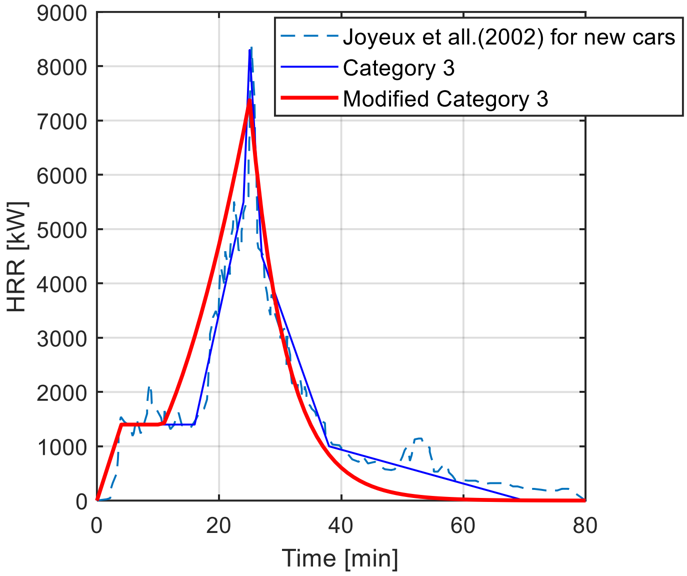

Figure 3.17. Modified Category III fire curve based on Category III and Joyeux’s test result

As can be seen in Figure 3.17, cumulative thermal energy shifted left in the Modified Category III fire respect to the original curve. The decreasing phase is also faster so that the dying out of fire occurs quickly. This situation comes up with the flexibility to stop simulation earlier. The predefined stopping point of simulation is when the fire curve drops to 5% of its peak value at 43rd minute. Conserving the total heat level of an HRR curve is another issue during curve modification. Comparison of cumulative oxygen consumption of modified and normal Category III fire curve is given in Figure 3.18. The Modified Category III fire curve consumes available energy earlier, and simulation is stopped just before the running out of fuel.

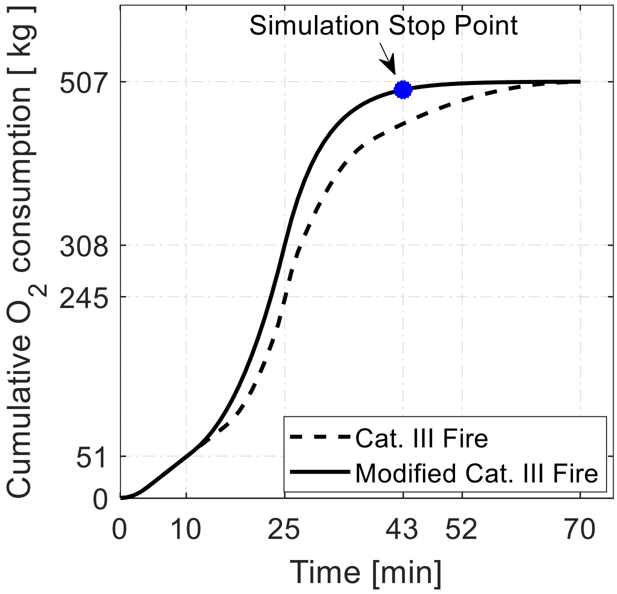

Figure 3.18. Oxygen need of category III and modified category III car fire

To determine the effects of the modification of the Category III fire curve on temperature levels, a simple FDS model has been constructed as given in Figure 3.19. Fire scenario is based on a pool fire under a steel ceiling 2 mm in thickness. The 1.4x3.1m fire surface is placed 0.5 m above the ground level. The steel ceiling is located 1.5 m above the fire surface, and the conduction coefficient is defined as 40 W/mK. The computational domain contains a single mesh with 160,000 cells. Cell size is defined as 10 cm in all principle directions. The FDS model has been run on a single-core for both modified and original Category III fire curves; thus, parallel processing was not employed. When computational loads of two distinct design curves are compared, minimum time steps are similar for both two cases, 0.0054 second for original curve and 0.0056 seconds for Modified Category III fire curve. Trends on time steps which can be checked from Figure 3.20 are similar in the first 660 seconds. Time step drops earlier than rises quickly for the modified case as expected. However, the increase in the minimum time step, which is increasing with 3.7%, is an unsatisfying result. Anyhow, the overall effect given in Figure 3.20 results with a 28% reduction in the total iteration number. Total iteration number is directly proportional to the waiting period for simulation results.

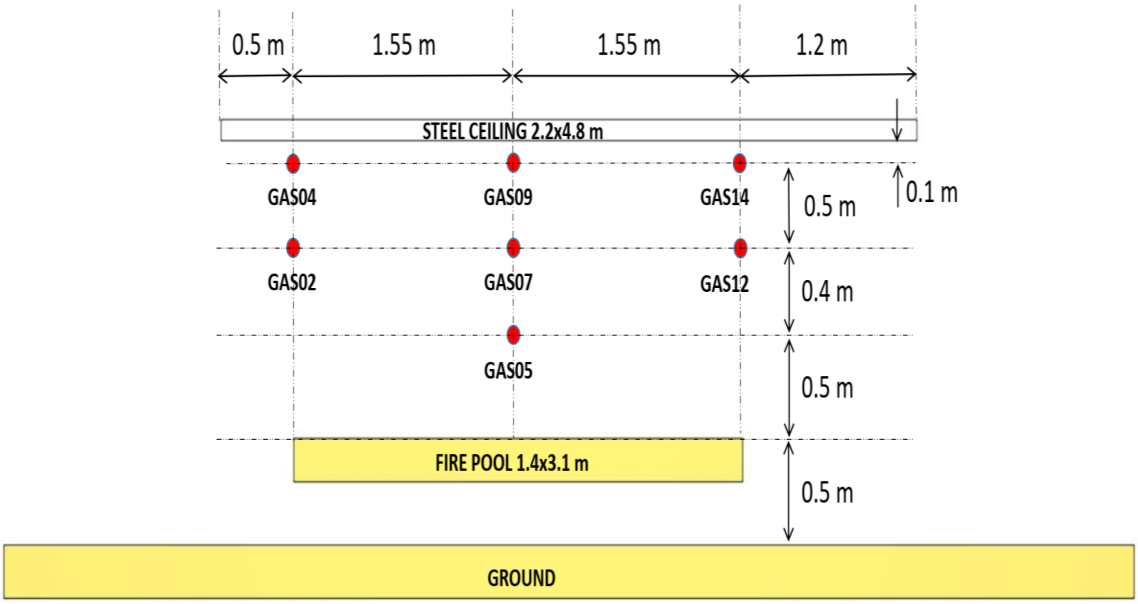

Figure 3.19. Thermocouple positions in FDS model

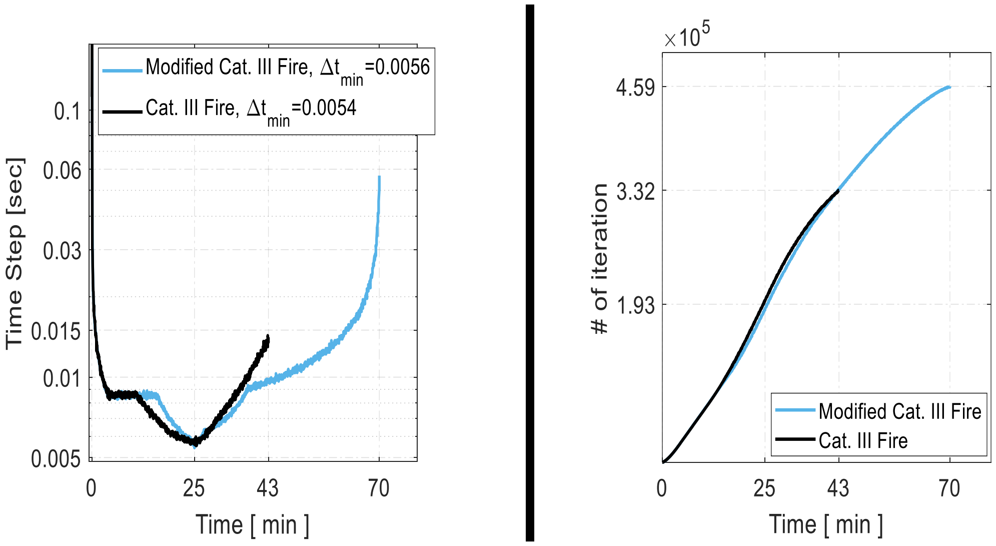

Figure 3.20. Computational cost (Step time, left; iteration number, right)

Although the effect of the modification in the Category III fire curve on overall computational load is essential, the main thing is the similarity level between thermophysical results. Seven thermocouples for gas temperature have been defined to test the similarity level, of which positions and labels are given in Figure 3.19. Differences between maximum gas temperatures at thermocouples GAS04 and GAS14 are lower than 50°C for modified and original Category III fire curve. The results also revealed that maximum gas temperatures occur at GAS07 and GAS09 are same for both cases. Overall changes in gas temperature levels are similar for both cases, and all results are given in Table 3.5.

Table 3.5. Maximum Gas Temperatures

Thermocouple ID	**Category III Fire [°C]**	**Modified Category III Fire [°C]**
GAS2	312	342
GAS4	808	804
GAS5	994	1010
GAS7	1010	1010
GAS9	929	935
GAS12	321	301
GAS14	815	774
Max	1010	1010

Temperature maps are also used to compare both normal and modified category III passenger car fire curves. Surface temperature maps for the 25th minute of the underside of the steel ceiling for both cases are shown in Figure 3.21. Maximum surface temperature is around 800 °C hot regions appear in similar places in both cases. It is also very similar to the temperature distribution characteristic. The gas temperature around the steel ceiling is also mapped. The temperature of the gas rising from roof edges is directly related to the ignition of the car on the upper floor. This situation must be preserved while the fire curve is modified. In Figure 3.22, the gas temperature maps around the steel ceiling are given. The map shows between 50 and 1250 °C. The results obtained in both cases are similar. The temperature of the gases that will wrap the upper layer reaches over 1000 °C.

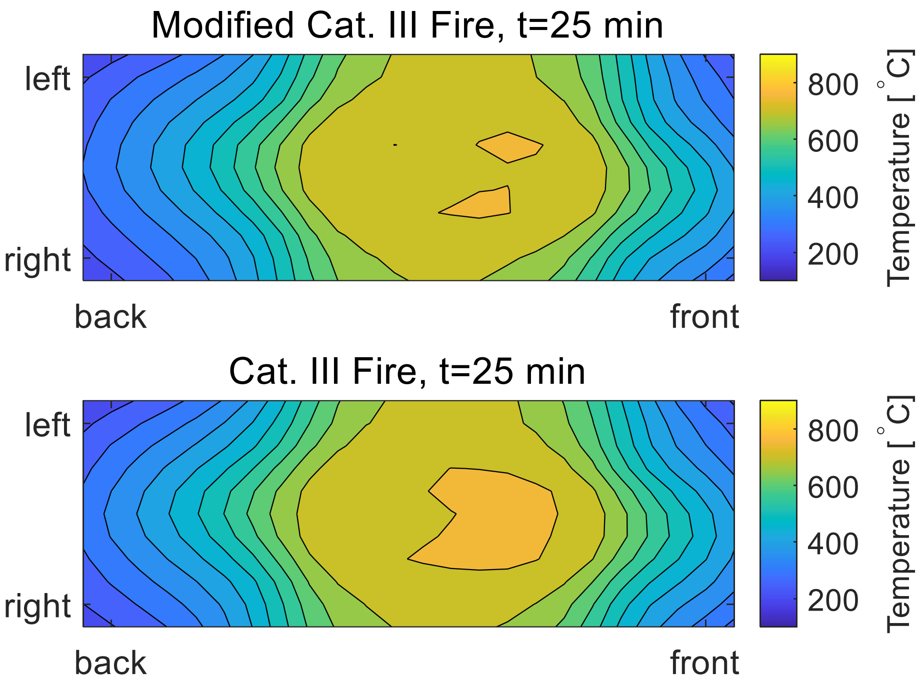

Figure 3.21. Surface temperature map of the steel ceiling

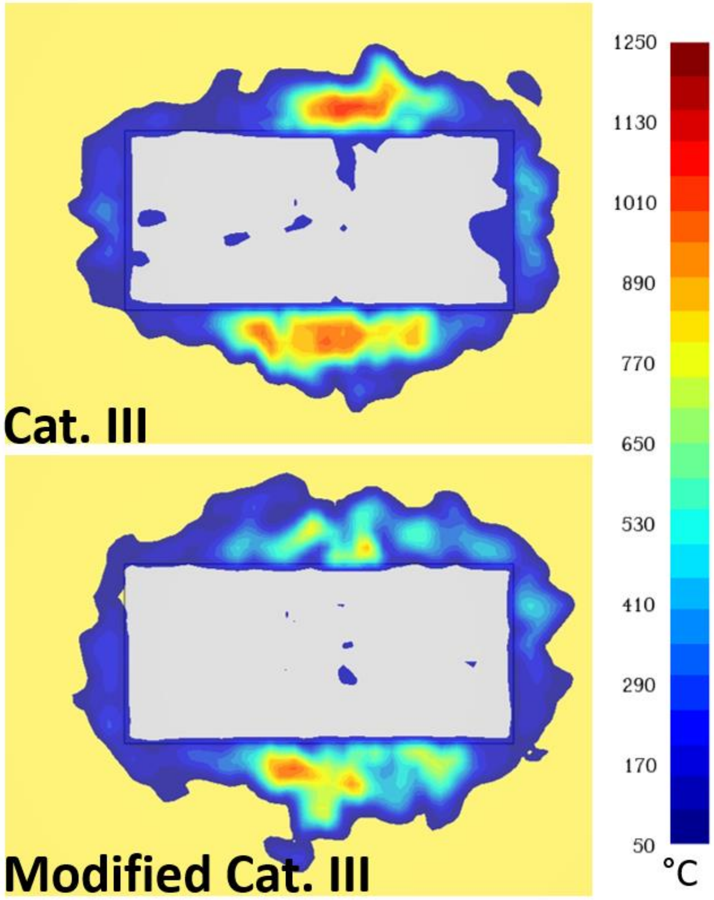

Figure 3.22. Gas temperature map around the partial ceiling at t=25 min. (z=2m)

3.5. Passenger Car Modelling

After guaranteeing a sufficient similarity between two cases in terms of thermo physics, effects of car bodies and windows have also been examined. A car body similar to a compact size hatch has been designed with a resolution of 0.1 m in FDS environment. Metal parts in the car body are defined as 0.001 m steel sheet with 40 W/mK of heat conduction coefficient. Windows are ordinary glass 0.003 m in thickness and 1 W/mK of heat conduction coefficient. The general view and dimensions of the car body are given in Figure 3.23a. The car body engulfs the fire pool shown in Figure 3.19 basically. To sustain a continuous air ventilation, small gaps have been left on the front grille and front-wheel splash guards, and the right-front window is 1/5 open to release hot gas pressure. A fire scenario is also designed for glass breakage, in which the method is based on the paper of Weisenpacher et al. (2016). It was foreseen that glass breakages occur at the windshield at first then side windows and rear window sequentially. Predefined glass breakage times are given in Table 3.6. It is assumed that when the last window breaks, the overall HRR level starts to rise again. There is a flat zone between 4th and 11th minutes on the Modified Category III fire curve, in which time interval all glasses break.

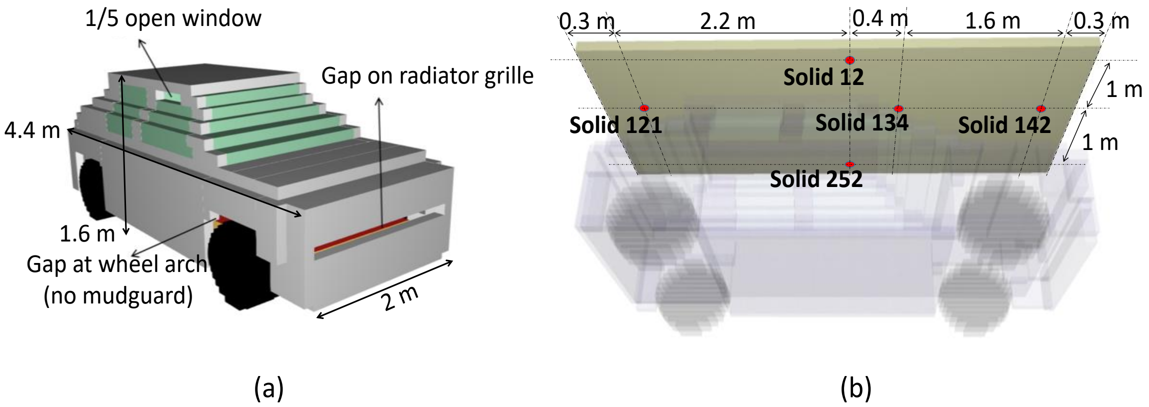

Figure 3.23. Setup of the numerical experiment in FDS for the effect of car body

Table 3.6. The scenario for fire cases enclosed by car body

Event	**Time**
Fire start	0.min
Windshield breakage	4. min
All side windows breakage	5. min
Back window breakage	11. min

Fire simulation with the car body has been run for only The Modified Category III fire curve. Thermophysical results have been followed by numerical surface temperature sensors located under the same steel ceiling given in Figure 3.19. Exact locations of the sensors marked as Solid 12, 121, 134, 142 and 252 respect to the steel ceiling are also given in Figure 3.23b. Conductional and convectional heat transfer between the underside of the steel ceiling and its upper side was calculated during the FDS simulation, and maximum temperatures occur during the simulation are given in Table 3.7. The overall top temperature level is the same for pool fire and pool fire with the car body, 761.4 °C and 762 °C respectively. These two similar values have occurred at the same surface temperature sensor, Solid 134. The most significant change was captured at the Solid 121, in where the temperature level equals 355.1 °C for pool fire whereas 654.8 °C for the one engulfed by car body. The cause of this phenomenon is the car body design itself. The ceiling of car body blocks convectional heat transfer to upward, then the airflow entering to the inside of car body from gaps at the front grille and splash guards wafts the hot gas under the car ceiling to the backward. Then the temperature distribution is stretched to the back side of the passenger car. This change can also be seen in Figure 3.24. The location of maximum temperature stays the same, whereas temperature levels at the back end of the ceiling increase significantly.

Table 3.7. Under surface temperature of the steel ceiling

	Max. Surface Temperature [°C]	
Point ID	**Modified Category III Fire**	**Modified Category III Fire with Car Body**
SOLID12	713.4	633.4
SOLID121	355.1	654.8
SOLID134	761.4	762.0
SOLID142	462.8	329.1
SOLID252	719.8	588.9
Max	761.4	762.0

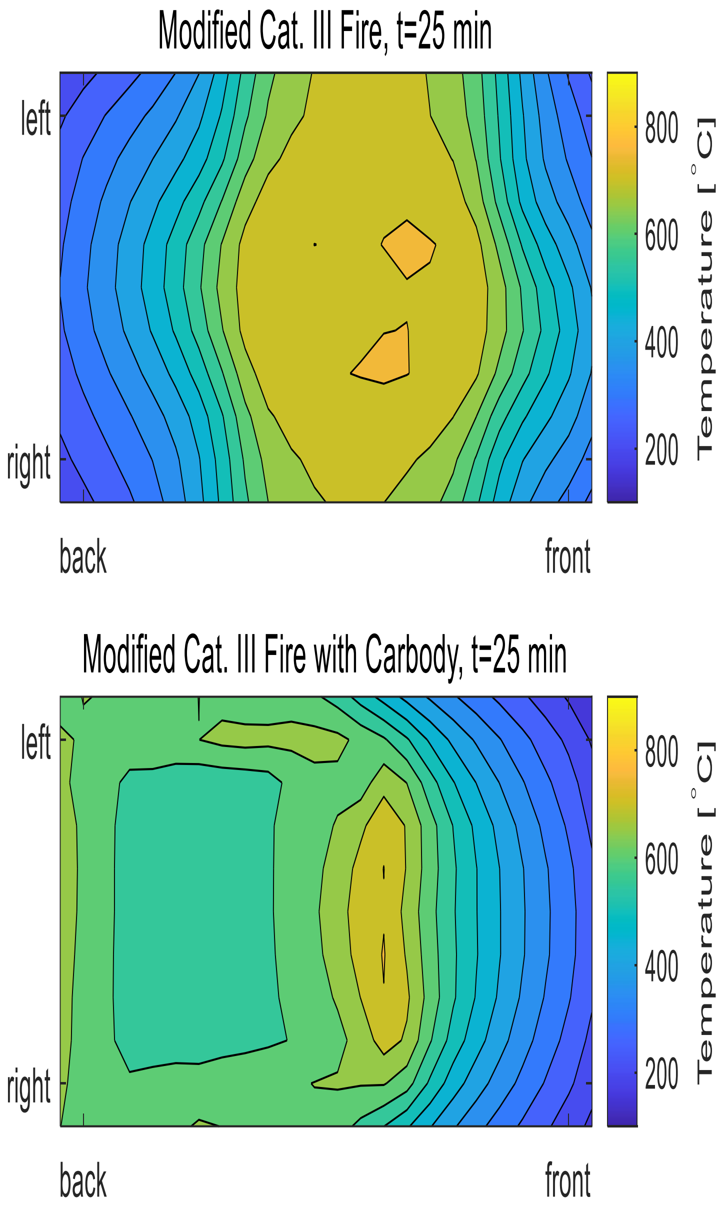

Figure 3.24. Surface temperature map of steel ceiling (effect of car body)

3.5.1. Lateral and vertical fire spreading between passenger cars

It is hard to estimate fire spreading conditions and required time for passenger car fires without full-size tests. Joyeux (2001) estimated the time duration needed for lateral fire spreading between passenger cars as 12 minutes. In contrary, Li et al. (2017) assessed the period as approximately 20 minutes, whereas Park et al. (2019) reported the first fire spread to an adjacent car at 500th second of their full-size fire test. On the other hand, full-size tests for vertical fire spreading are infrequent. There are two main test reports on vertical fire spreading by The *Building Research Establishment* (*BRE*) (BRE, 2009) (BRE, 2010). These tests have been performed with simple car stackers with and without a sprinkler system. According to results, fire can spread to the underside of the upper car in approximately 5 minutes at the unsprinklered case. However, the car stackers in tests did not contain a plate similar to parking pallets between two passenger cars, two parallel steel beams just under the tires were placed. Thus, flames have reached to the underside of the upper vehicle directly. A plate wide enough between two cars may retard the fire to spread vertically.

To assess criteria for vertical fire spreading, undercover, tires, and front bumper of the car body model given in Figure 3.23 have been altered with combustible polymers in the FDS environment. The new car model has been placed on the steel ceiling shown in Figure 3.19. Heat flux meters have also been added under the cover and tires. The partially flammable car model is given in Figure 3.25. The material of the undercover and bumper is chosen as polypropylene and rubber for tires. Thermal properties of materials used in the model are given in Table 3.8.

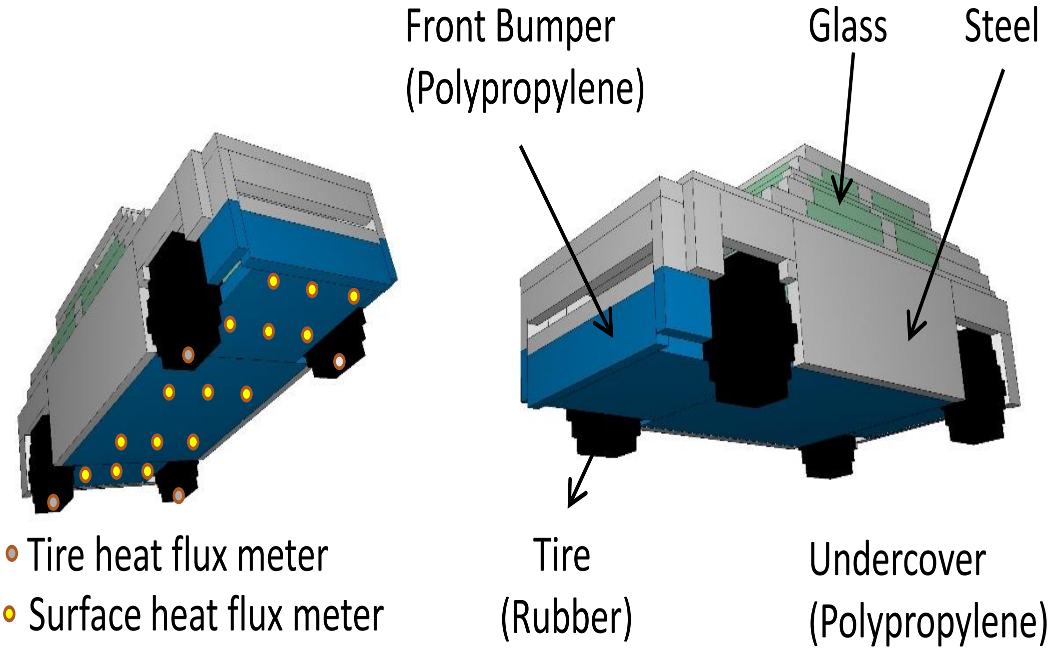

Figure 3.25. Numerical design of ignitable passenger car in FDS

Table 3.8. Thermal properties of materials in ignitable passenger car model

	Thermal Properties					
Material	**Ignition Temp. [°C]**	**Specific Heat [kJ/kg.K]**	**Conductivity [W/m.K]**	**Heat of Combustion [kJ/kg]**	**Emissivity**	**Density [kg/m^3]**
Rubber (Pearce,1985)	350	1.88	0.13	50	0.9	910
Polypropylene (Pearce, 1985)	388	1.75	0.15	46	0.9	946
Steel (FDS default)	-	0.46	45.8	-	0.95	7850
Glass (FDS default)	-	0.792	1	-	0.05	2500

The fire simulation for vertical fire spreading has been run with the Modified Category III fire curve, and cell size was chosen as 10 cm in all axes. The first ignition occurred at the undercover of car, which is similar to the unsprinklered car-stacker test of BRE (BRE, 2010). However, the undercover cached fire at 728th second which 7 minutes later the BRE Test. In contrast to the BRE test on car stacker systems, 2 mm steel ceiling in the FDS model prevents flames from reaching to the upper car directly. After the ignition of undercover, front tires have also started to burn at 975th second. Overall ignition history of the FDS simulation is given in Figure 3.26. When the first ignition occurs, the instantaneous incident heat lux map of the undercover is shown in Figure 3.27. The result indicates that an around 10 kW/m^2 of incident surface heat flux is enough to start combustion, and this can happen in the first 12 minutes. On the other hand, boundary conditions, the orientation of the combustible material and continuity of heating are also essential parameters that affect the ignition. The undercover may ignite earlier under higher incident surface heat flux. In contrast, a well-insulated parking pallet can stop vertical heat transfer. There is also no accessible test report about fire tests of car parking pallets. Apart from the undercover, the simulation reveals that tires can start to burn at their closest points to the undercover. In other words, the heat generated from the combustion of undercover stepped up the ignition of tires. Thus, the data collected from heat flux meters under tires can not provide clear knowledge of the effects of designed fire on ignition of tires. Incident surface heat flux curves for tires are shown in Figure 3.28. When tires started to burn, the incident surface heat flux level equals to nearly 20 kW/m^2 under front tires and 10 kW/m^2 under back tires.

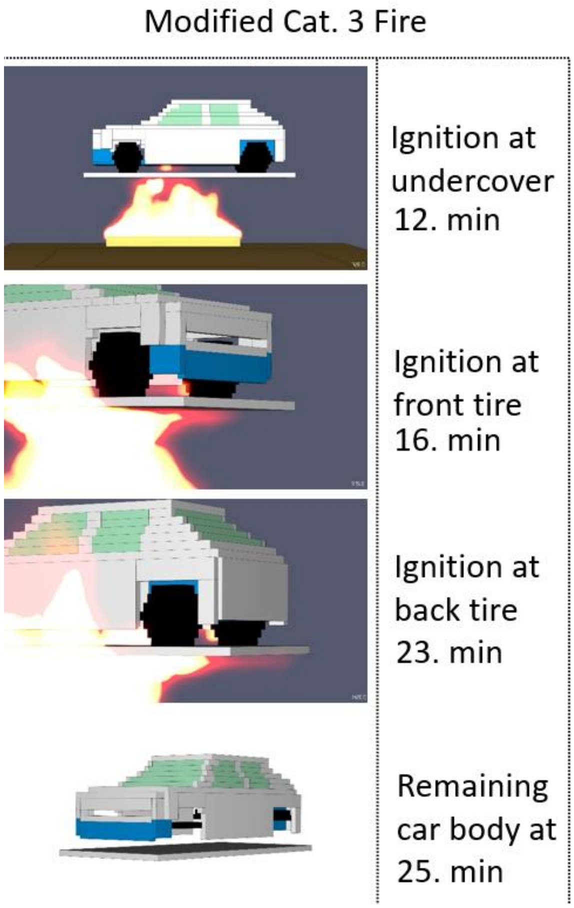

Figure 3.26. Vertical fire spreading

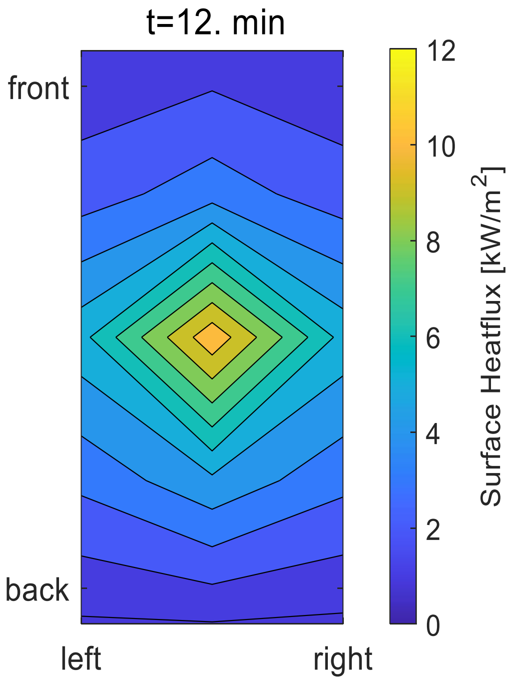

Figure 3.27. Incident heat flux over the undercover of passenger car

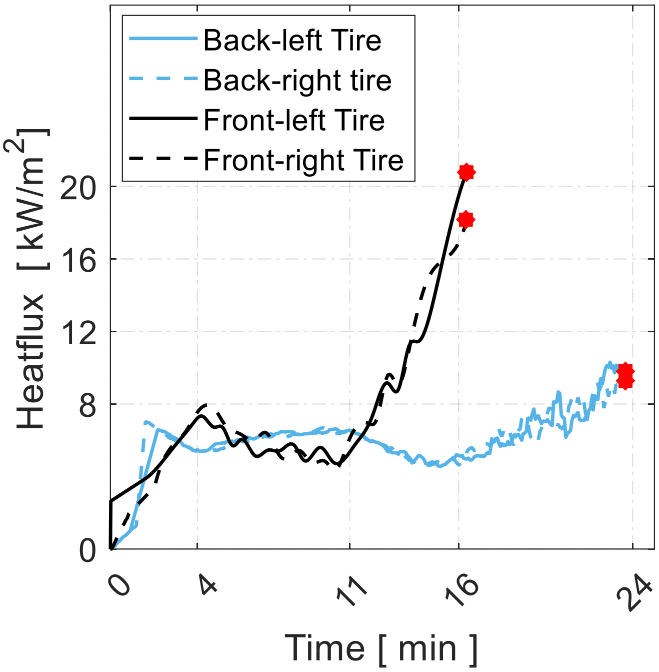

Figure 3.28. Incident surface heat flux at tires during vertical fire spreading

After the analysis on the vertical fire spreading, a fire spreading criteria for both vertical and lateral ways is proposed. When the incident heat flux level is lower than 8 kW/m^2, there is no risk of ignition, whereas the level is higher than 16 kW/m^2, passenger cars start to burn. If the incident heat flux level is between 8 and 16 kW/m^2, adiabatic surface temperature should be checked at the heating phase, because the surface temperature can not be higher than the adiabatic surface temperature. While the adiabatic surface temperature level is lower than the ignition temperature, it can be argued that ignition over a surface does not occur.

3.6. Fire Safety Assessment Criteria of AVPSs

Tower-type automated vehicle parking steel structures are vulnerable to car fires because of their compact designs. Passenger cars are placed close to each other in the horizontal and vertical orientation in AVPSSs. Thus, fire spreading between cars is easier and faster. On the other hand, the temperature rises at structural elements during a fire event may lead parking pallets to dislodge. Although mechanical deformation does not occur at structural elements of an AVPSS, a mechanical strength loss at car pallet is the result of high temperature that can come up with the dislodgement and dropdown of the car pallet. In addition to this, the prevention of fire spreading may not guarantee the dislodgement of parking pallets. The fall down of a parking pallet with a passenger car can cause severe structural damage. When all these situations are taken into consideration, a three-step fire safety doctrine for AVPSS, as shown in Figure 3.29, can be enunciable. Lateral and vertical fire spreading has to be prevented at first. In the second stage, additional measures may be necessary to stay parking pallets fixed. After possible measures for the first two objectives are employed, the overall structural integrity must be tested.

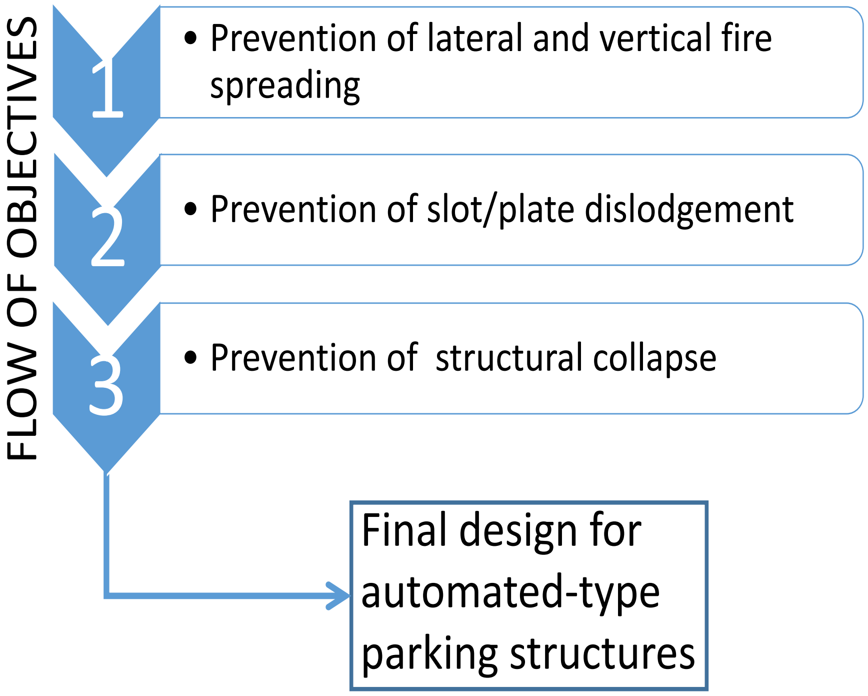

Figure 3.29. Fire safety requirements for AVPSS

4. CASE STUDY

Case studies are based on passive and active fire safety measures to realize the safety doctrine mentioned in Section 3.6. An unprotected AVPS named Case A has been tested in the first step. Then possibilities of passive measures have been inspected; different sprinkler system designs as active methods have been tested later. As cases for passive measures, partially firewalls and fireproof ceilings were applied on the structure in the Case B, fire shutter doors were added on them in the Case C later. Active measures with sprinkler systems were inspected through two different cases that both are subcases of the Case D. At the first stage, the sprinkler layout proposed by AFAC (2018) was simulated in the Case D. Then, a new sprinkler layout was tested. A visual summary of cases is also given in Figure 4.1.

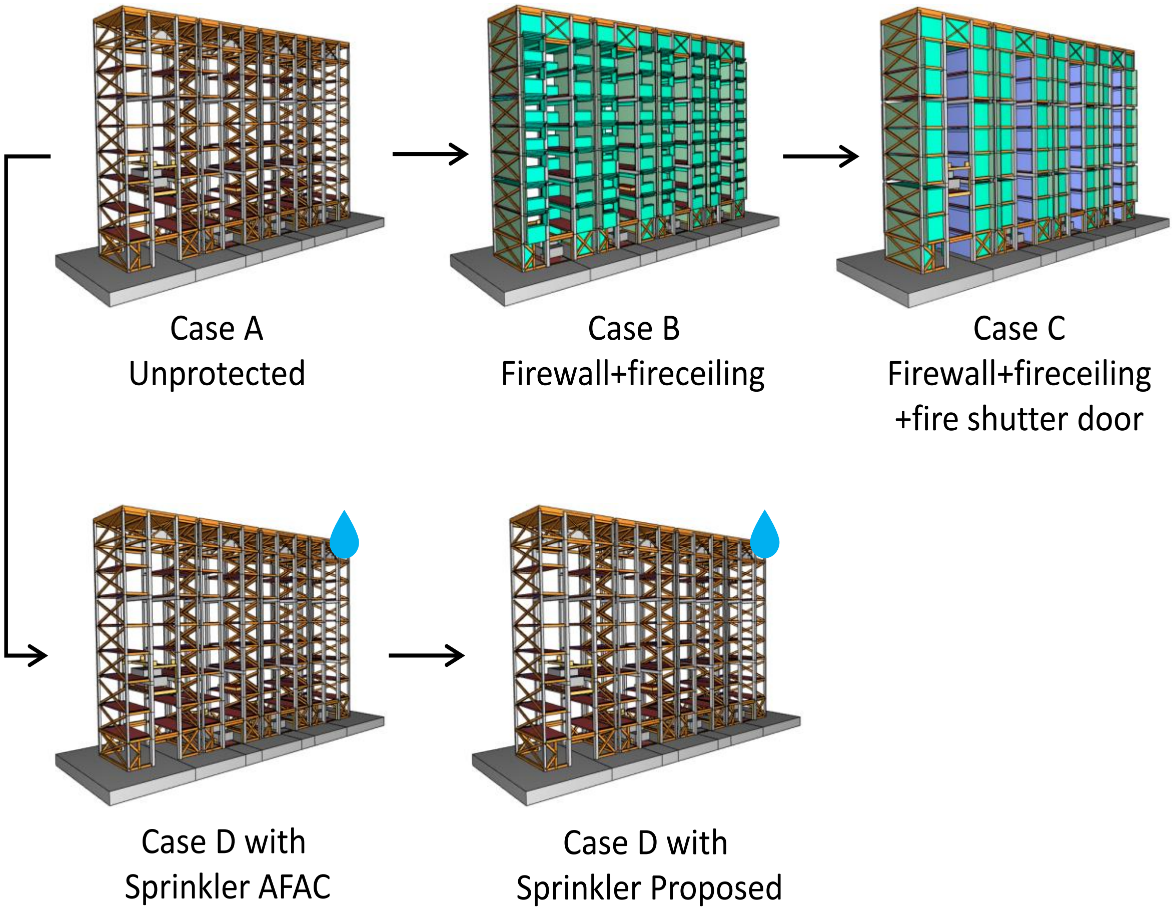

Figure 4.1. Case tree

Due to the modular design of AVPSS, the entire car park design can be expanded vertically and horizontally. An AVPSS with 4x1 unit orientation is chosen as the base structure. The system contains four identical AVPSS units, and they are placed side by side. The gap between units is 30 cm, and there is no physical connection between the units. All units may stand on the same foundation, but this is not one of the topics of this research. Fire design is employed with the Modified Category III curve. Fire location is the left side of the second floor of the third unit. The place is also marked in Figure 4.2. The other passenger cars around the burning car are named: the vehicles at the right side of the fire are marked with ‘R’, the ones at the left side are marked with ‘L’, and the upper cars are tagged with ‘U’. The numbers are also used to define the floor of vehicles relative to the burning one. The fire spreading risk levels are also shown in Figure 4.2. The highest fire spreading risk is marked with yellow, which the zone covers vehicles R0, R1, U1 and partially R2 and U2. It is evident that a burning car can ignite the nearest ones easily. The fire risk level 2 covers the passenger cars of L0, L1 and L2 that are located at the other side of the lift tower. Some unmarked passenger cars are also inside the secondary risk zone.

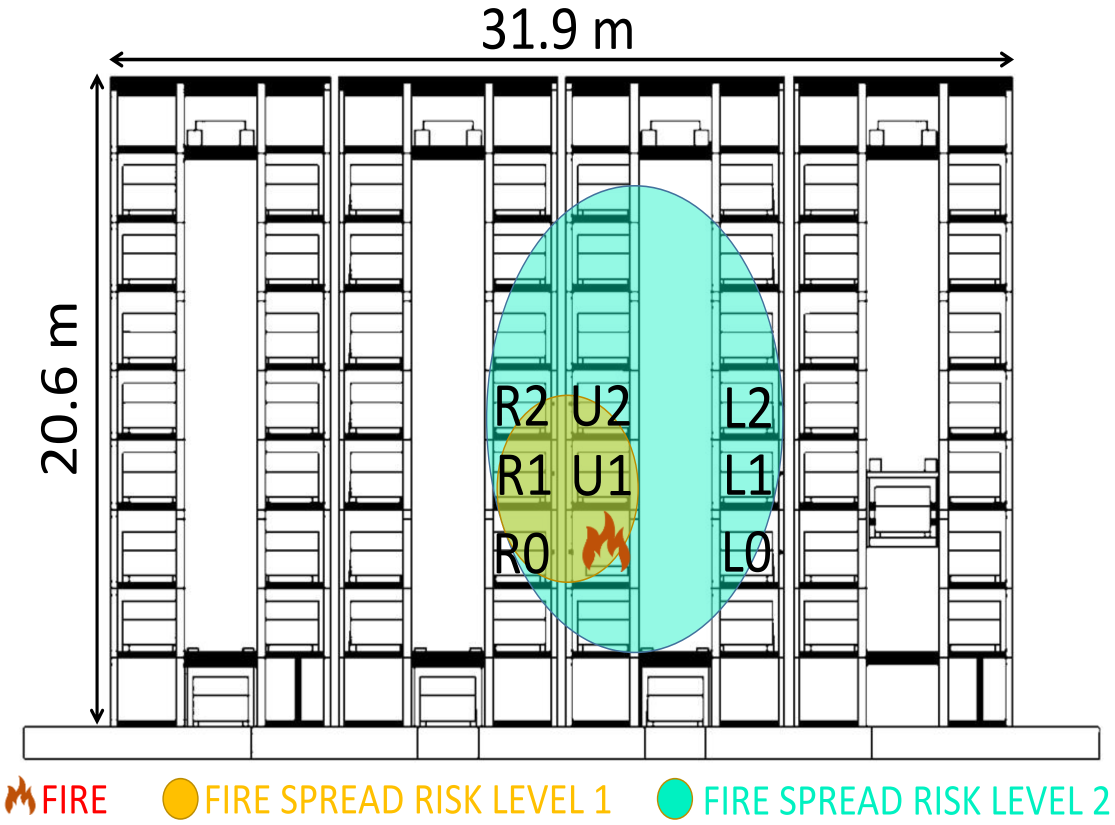

Figure 4.2. AVPSS with 4x1 unit orientation

A fire pool with the size of 1.4x3.1 m is used in unsprinklered fire simulations, whereas the passenger car model, which is given in Figure 3.19a, is employed for simulations containing sprinklers. The entire computational domain has 1,025,304 cells that are in 10 cm in size at the fire spread risk level 1 and 2, and are in 20 cm in length at far distances. The scenario for glass breakage is preserved like mentioned before. However, ignitable materials are not added in order to decrease computational demand. Instead, adiabatic surface temperature and incident heat flux sensors are superimposed on the neighbor vehicles, which positions and names are shown in Figure 4.3. The neighbor vehicles are actually dummy vehicles with basic geometric features. Their dimensions are similar to a mid-size sedan car, 4.4 m in length, 2 m in width and 1.6 m in height. The ground clearance of dummy cars is 20 cm. The main surface material of dummy cars is steel in 2 mm thickness, and their tires are defined as 2 cm rubber. The steel parking pallet in the FDS model is 5.2x2.3 m in size and 0.1 m in thickness. Individual parking space is 2.3x5.2x2 m in size, where there is a gap of 20 cm between the parking pallet and structural beams at both ends of the parking pallet.

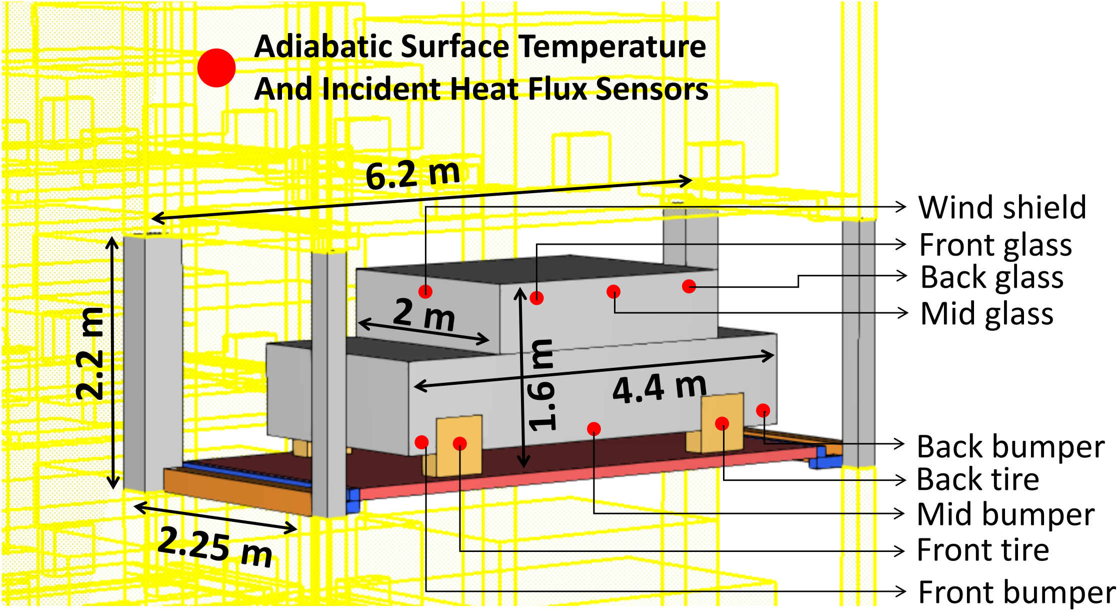

Figure 4.3. Sensor positions on dummy cars

Structural elements around the fire zone are also marked. The marking method is based on the sign convention that is given in the left-bottom of Figure 4.4. The design fire starts at the east side of the second floor, where the related parking pallet is named as P2E, Pallet-2. Floor-East. The upper one is named as P3E. The weak beams are marked with 4-digit keys.

For example, the beam on the third floor at the north façade and on the east side is named B3NE. 3-digit keys refer to strong beams at every three floors. The strong beam just over the fire is marked as B2E. Structural columns are also presented with 4-digit keys, that C3N2 refers to the column on the third floor, at the north façade and at the second place from the east to west.

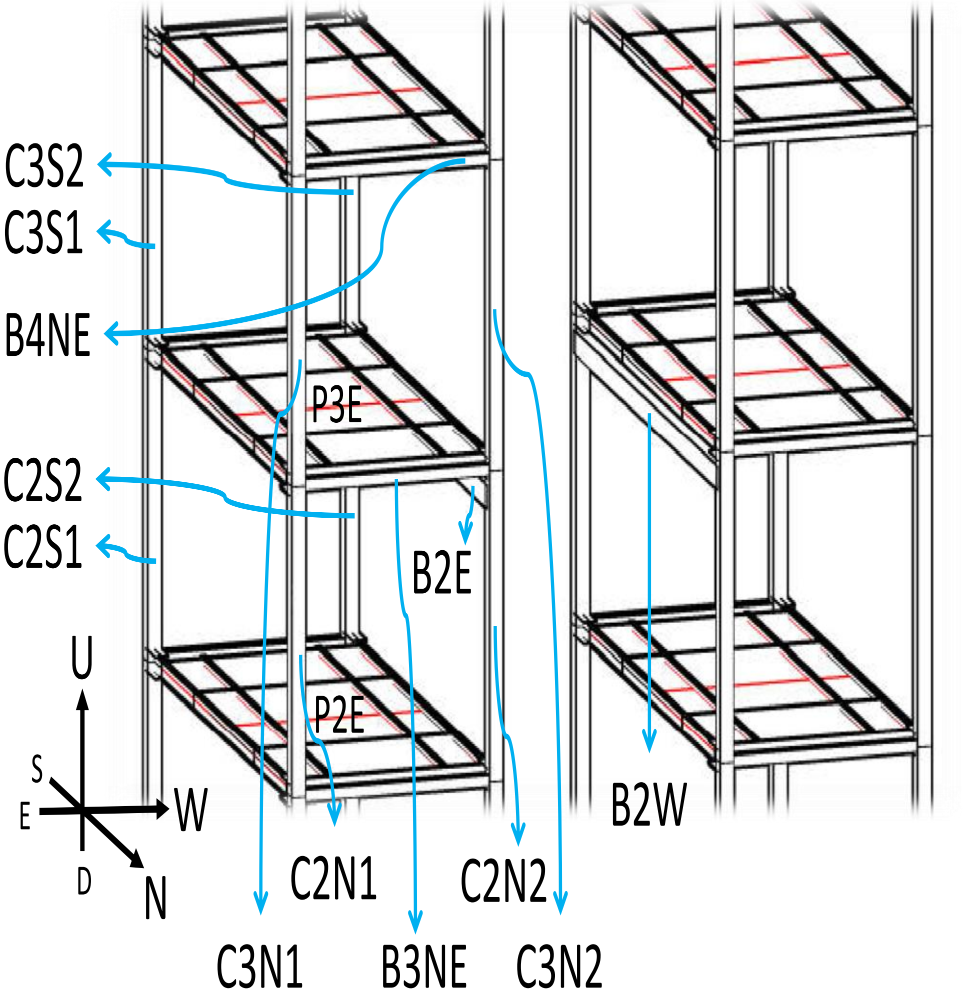

Figure 4.4. Nomenclature of structural elements around the fire zone in the unit

4.1. Case A: Unprotected Design

According to some national fire standards like Turkish Fire Code (BYKHY, 2009), it is legal to construct an open façade AVPSS without active and passive fire safety measurements. The fire safety level of an open façade AVPS is inspected at Case A. The structural system is identical to the one given in Figure 4.2. Fire spread risk, pallet dislodgement and structural healthiness have been examined under the individual Modified Category III fire. A progressive fire due to spreading or flashover has not been included, because the proposed fire safety doctrine already requires to prevent the fire from spreading between passenger cars. The FDS code has been run on an HPC cluster, and 8 cores had been employed for each case.

The first 10 minutes of fire can be manageable in terms of the expanding of hot gases, in which its volume occupies only the parking slot. Vertical temperature maps are also shown in Figure 4.5. When the fire starts to rise again at the 11th minute, hot gases and flames pervade entire parking slot and upper areas. The gas temperature reaches 1000 °C just under the upper parking pallet. It causes the ignition of the underside of the car U1 as inspected in Section 3.5.1. When the HRR level is at the top, Car U1 is fully engulfed by flame, and hot gases at around 1000 °C touch to the left side of car R1. Hot gases with 600 °C are dragged up with buoyancy force and even reach to car U2 and R2. The situation of hot gas-vehicle interaction at the 1500th second is marked with the white circle in Figure 4.5. The distance between car U1 and R1 is 110 cm, and the highest gas temperature at the gap is higher than 1000 °C. This temperature level can cause an ignition on the car R1 and U1 easily. Due to the sequential layout of parking slots, once the fire spreads to n adjacent vehicle at side or upper parking pallet, all vehicles in the automated-type parking structure can start to fire sequentially. Thus, preventing the nearest vehicle/vehicles to ignite should be the rule of thumb as mandated by the fire safety doctrine of AVPS. On the other hand, car L0, L1 and L2 are at a relatively far distance from the fire, where gas temperature is very low. Incident heat flux levels over the cars are under 5 kW/m^2 that is safe according to the doctrine. Incident heat flux levels for car U1, R0 and R1 are given in Figure 4.6. Incident heat flux levels at mid bumpers of upper cars reach over 50 kW/m^2 that causes a fire. The level on the mid glass of car R0 is also high enough to cause a possible ignition. A similar situation has been seen at the full-size car fire test performed by Weissenpacker et al. (2016). Although the hot gases temperature level seems very low around the car R0, radiative heat transfer can lead to a lateral fire spreading within 20 minutes and at a distance of 110 cm.

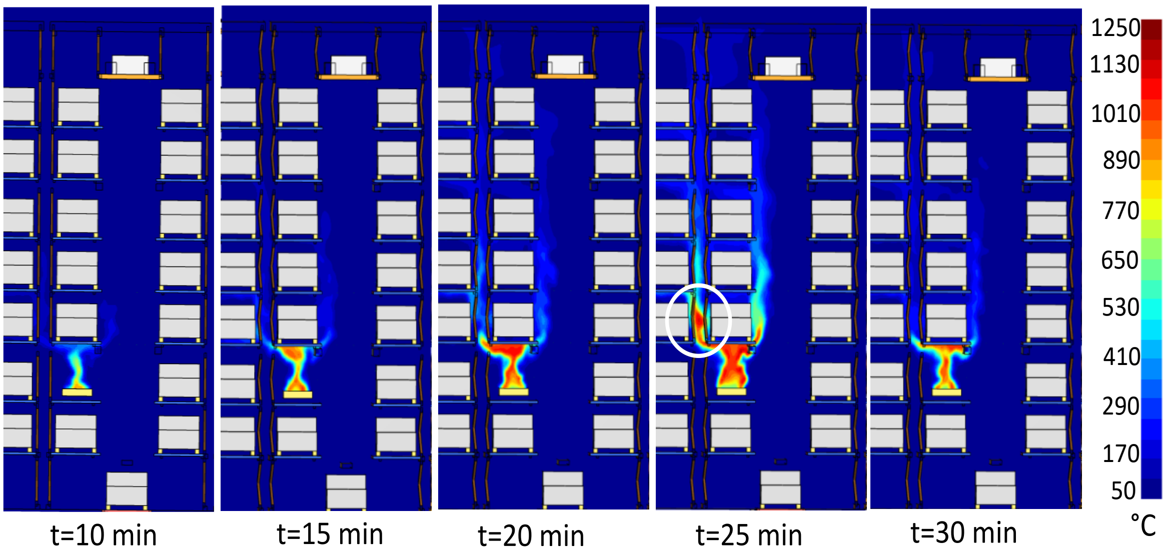

Figure 4.5. Vertical temperature map (Case A)

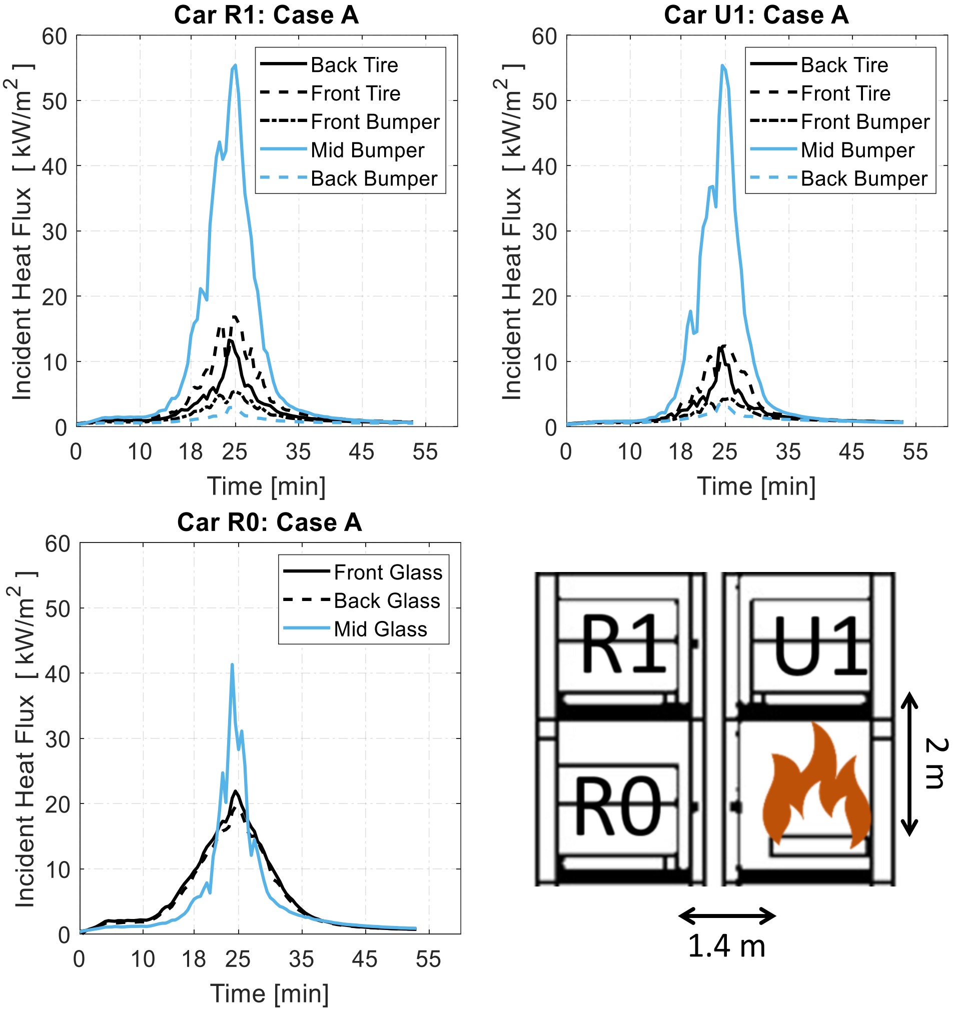

Figure 4.6. Incident heat flux levels at dummy cars(Case A)

After the determining adiabatic temperatures levels around the structural members of AVPSS unit, average temperature change and temperature gradients are calculated with the method given in Section 3.2.1. Calculated temperature levels are also shown in Figure 4.7. Average temperature rise levels are under 100 °C. Because of the lateral distances of columns from the fire pool, the columns are not engulfed by flames. Columns are also exposed to radiative heat partially. As a result of this asymmetric heating, temperature gradients at columns are relatively high, that the gradient levels reach to around 450 °C /m at the column C2N1. Due to the symmetric layout of the AVPSS unit, it is assumed that the temperature levels at C2S1 are identical to levels of C2N1. This assumption based on the symmetric layout is valid for all steel members of the unit. Temperature levels and temperature gradient levels at columns on the third floor are also shown in Figure 4.7. Average temperature rise and temperature gradient levels at the pin-connected beam of B3NE are around 130 °C in average temperature rise, the temperature gradient of -150 °C/m from south to north and over -700 °C/m from up to down. It is an expected result that the lower surface of B3NE is hotter than the upper surface. The pin connections at ends of B3NE cut the moment transfer due to the temperature gradient of T_{DU}; thus, the resultant stress levels on columns is lowered. However, a ball joint or two pins perpendicular to each other can not be used at ends of the B3NE due to earthquake response. Because of the absence of structural slabs in the AVPSS units, one of the main purposes of B3NE is increasing torsional stiffness of the unit. On the other hand, the most significant member is B2E, in that the average temperature rises over 800 °C. At this temperature, the yielding strength and Young’s Modulus of steel drop nearly 90%. The essential purpose of B2E is decreasing the vulnerability of the unit against earthquake loads and buckling of columns. The significant drop in mechanical strength and stiffness is even an advantage for the entire structural stability during a fire event because a drop in Young’s Modulus comes up with a weak level of the moment due to temperature gradient. However, the maximum temperature gradient at B2E from down to up occurs when the average temperature rise is around 500 °C. The $T_{,UD}$ level of 3000 °C/m at the beam is the cause of the major part of torsion on columns C2N2 and C2S2. Average temperature rise at the strong bracings that are placed at the west façade of the second floor is over 400 °C, whereas the one for the third floor is around 750 °C. Temperature gradients from west to east are also high at the strong bracings, 1670 °C/m for the second floor and 3120 °C/m for the third floor. Although strong bracings with the section of TUBO 80x80x8 serve perfectly under earthquake loads, they may be a possible cause for pallet dislodgement during the fire. Thermal expansion of the sections pushes the columns out, and the pallet wheels become distant to each other.

The peak temperature levels are transferred to the finite elements model of AVPS unit in SAP2000. Entire temperature curves are not used. When the average temperature rise is lower than 100 °C, Young’s Modulus of steel stays constant. Thus, peak levels of average temperature rise, and temperature gradients of columns can be used directly for nonlinear static analysis. However, the temperature rises of B2E and B3NE come up with a drop in the Young’s Modulus. The instants when the biggest peak at temperature gradients occur are considered for the beams. The same approach is valid for strong bracings. This problem can not come into view for weak bracings, because cable sections have parameters of average temperature rise and axial force mathematically. The main reason for this approach is the incapability of SAP2000 on temperature-dependent temporal variation of material properties during time-history analyses. In other words, temperature dependent steel properties can not be manipulated during time-history analyses with variable temperature in SAP2000. Then, the most problematics states of members are taken into account for nonlinear static analyses considering spatial variations the structure such as thermal elongation, elastic and plastic deformation with spatially nonlinear material properties.

After the nonlinear static analysis is applied, a collapse or partial collapse at the main structure is not observed. The 20-times amplified deformed shapes are also shown in Figure 4.8. The north side view of the building is given in Figure 4.8(c), and weak bracings are removed to gain a clear view, whereas the east side is shown in the Figure 4.8(b). Due to the high level of temperature gradients and average temperature rise at strong bracing on floor 2 and 3, the highest deformation occurs at the east façade. Nevertheless, the deformation level can not result in structural failure. Only minor plastic hinges are formed at a total of four points. The deformed shape of the third floor is shown in Figure 4.8(a). On floor plans, only weak beams between columns and cantilever beams carrying parking pallets are visible. Parking pallets were not modelled in SAP2000, because parking pallets and the main structure can be decoupled due to the mechanical boundary conditions given in Figure 3.4.

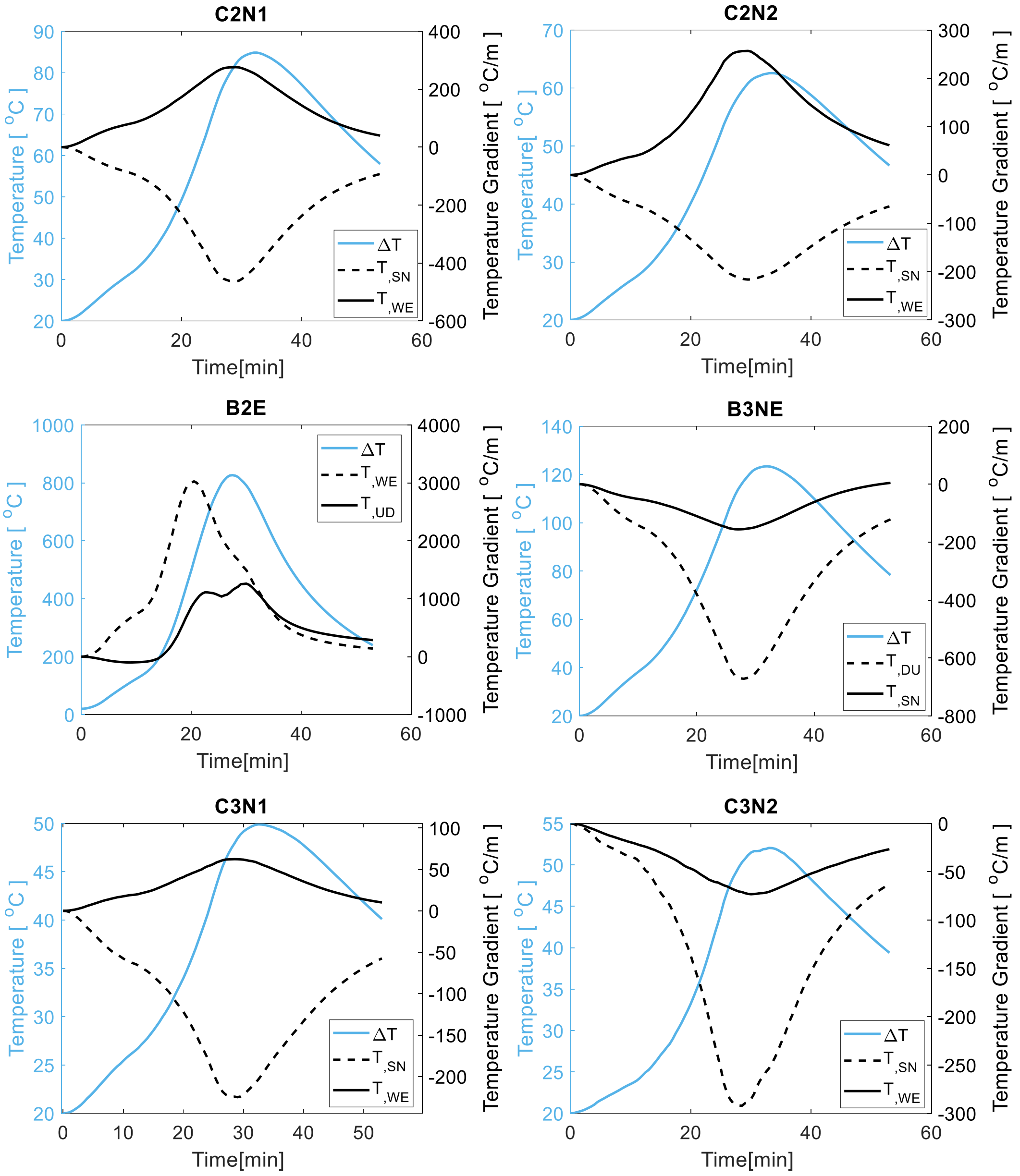

Figure 4.7. Average temperature changes and temperature gradients at steel members

The quarter of total gravity load of parking pallet and passenger car is applied on the tip points of cantilever beams in the plan view in Figure 4.8(a). Replacement distances of tip points of cantilever beams can also be inspected on the figure. The most significant shifting occurs at the east edge of the floor. The maximum change in distance in the y-axis between tip points is 75.1 mm, which is higher than the safety margin of parking pallet. This situation may cause parking pallet dislodgement, but the thermal expansion of parking pallet may also compensate it.

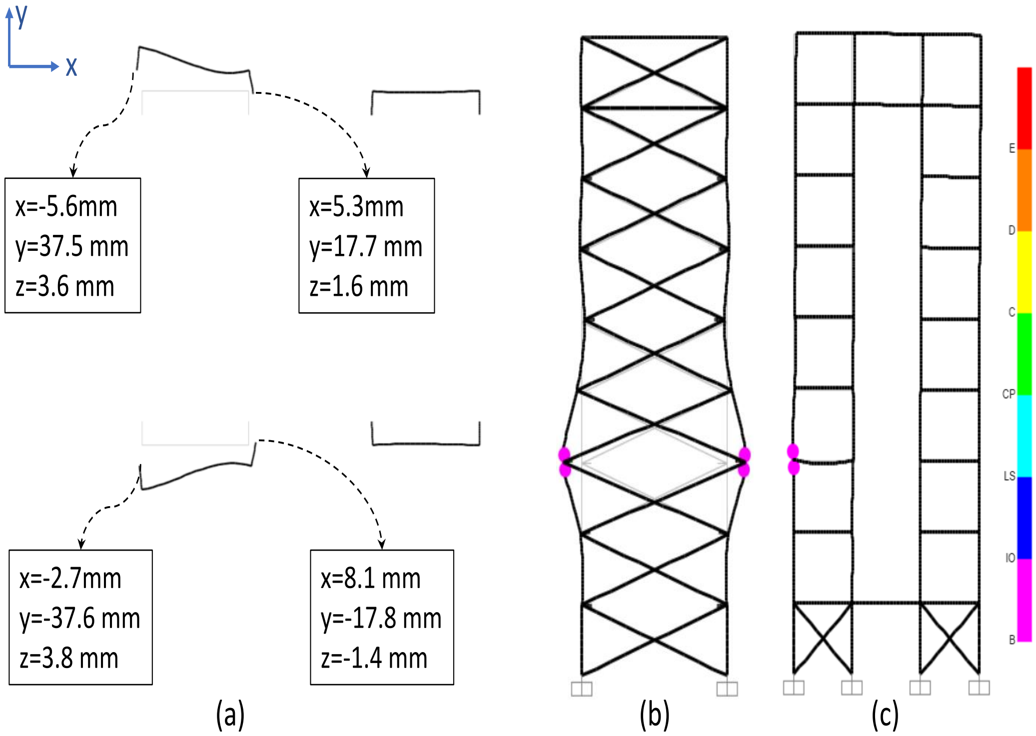

Figure 4.8. Structural fire response (Case A)

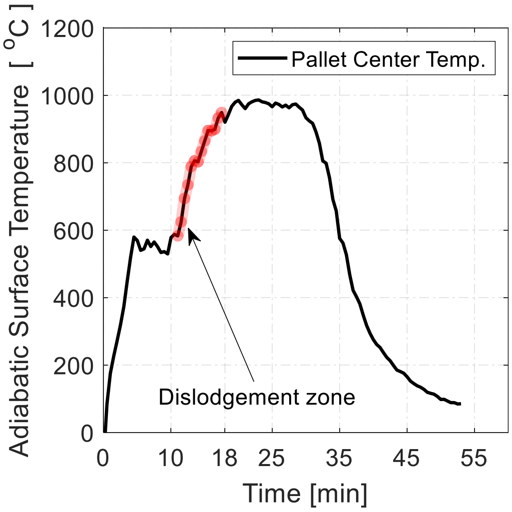

Figure 4.9. Parking pallet mid temperature

Parking pallet dislodgement has been investigated with the method given in Section 3.2.2. The hot gases temperature just under the pallet P3E reach over 1000 °C. The maximum adiabatic surface temperature on the underside the pallet is 1032 °C. The adiabatic surface temperature curve picked at the under-center point of the parking pallet is given in

Figure 4.9. The adiabatic surface temperature (AST) is the upper limit of the surface or member temperature of the section. Thus, using the AST level is a conservative approach. After 10 minutes, the temperature rises above 600 °C and steel members loss 80% of their structural integrity at these temperature levels. A possible dislodgement can occur at the early phase of the fire, which is between 10^{th} to 18^{th} minutes of the fire. The passenger car on parking pallet P3E probably is burning, so the upper side of P3E is already hot. Also, the flames engulf the parking pallet, so its temperature is very close to adiabatic surface temperature levels. Thus, it can be assumed optimistically that the temperature of the parking pallet reaches to 900 °C. Then temperature gradient that causes thermal bowing is calculated as at most 1194 °C/m with 25 W/m^2K of convective heat transfer coefficient and 45.8 W/mK of heat conductivity for steel. Temperature-dependent mechanical properties of construction steel are also defined in EC3 as given in Figure 3.8. Parameters used and calculated with the method are shown in Table 4.1. The midpoint deflection due to gravity load, Δw_P, is 219.5 mm with the assumption that the structure behaves elastically. The one due to thermal bowing, Δw_T, is 49.5 mm. The midpoint deflection normally results in the pallet bracket to drag away from the pallet wheels. However, the thermal expansion of the car pallet has compensated it, and the resultant drag length, $\delta_{\Delta w}$, is negative. When the drag length driven by the deformation of the entire AVPSS unit is taken into account, the total drag, δ, is 46.5 mm that is nearly equal to the safety margin. If a plastic hinge is not formed at the mid of the parking pallet, it may stay on the wheels. However, the moment resistance capacity of the parking pallet at elevated temperature has been calculated as 3.42 kNm. It is lower than the demand. The structure of the parking pallet is not capable of load redistribution. Once a plastic hinge is formed at the midspan, gravity load that is carried by the parking pallet drives the plastic rotation and creates more deflection. Under these condition outlined in Table 4.1, the parking pallet dislodges and drops down. Thus, Case A fails on not only the fire spreading criteria but also pallet dislodgement criteria of the fire safety doctrine for AVPSS. Although the overall structural stability seems safe, an increase in fire load with the spreading between passenger cars may cause structural collapse.

Table 4.1. Car parking pallet fire response (Case A)

$\boldsymbol{E_T}$	$\boldsymbol{\sigma_{y,\Delta T}}$	$\boldsymbol{M_{capacity}}$	$\boldsymbol{M_{demand}}$	$\boldsymbol{\Delta w_P}$	$\boldsymbol{\Delta w_T}$	$\boldsymbol{\delta_{\Delta w}}$	$\boldsymbol{\delta_{\Delta x}}$	$\boldsymbol{\delta < 50}$
14.28 GPa	14.10 MPa	3.42 kNm	25.05 kNm	219.5 mm	49.5 mm	-28.6 mm	75.1 mm	46.5 mm

4.1.1. Improvement of rail-pallet coupling design and its consequences

Structural fire response of columns and beams is given in Figure 4.8, and temperature levels at them are not high to lead a structural collapse. However, parking pallet drops down during the fire. The pallet dislodgement cuts the vertical fire spreading path, but dropping-down of a passenger car is highly dangerous. Pallet dislodgement mechanism must be eliminated for a safer tower-type AVPSS unit. One of the current designs of pallet-rail coupling is shown in Figure 4.10. In this design, plastic wheels which are very vulnerable to fire are mounted to the parking pallet. The rail is a simple L75x75x6 steel beam, and a simple triangular stopper is placed at the end of it. The coupling design does not contain a locking mechanism. Another design that is given in Figure 3.14 is a little bit different. The wheel is mounted to the rail not the parking pallet. However, the wheel is still plastic, and there is no mechanism to prevent parking pallet dislodgement. At first glance, there are two weaknesses of current designs, parking pallet dislodgement and non-fire resistant plastic wheels. To prevent to the parking pallet dislodgement, the pallet-rail coupling mechanism that given in Figure 3.14 has been modified. A hook-like bracket that creates a channel for wheels is added to the end of parking pallet. The design detail is given in Figure 4.11. Several 3D views and technical drawings for the design are also given in Appendix B.

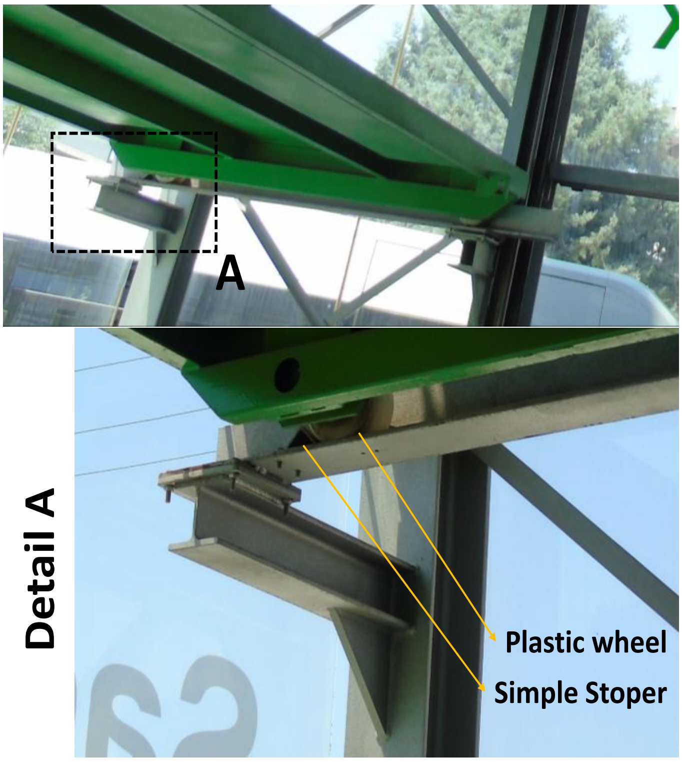

Figure 4.10. Current design of rail-pallet coupling

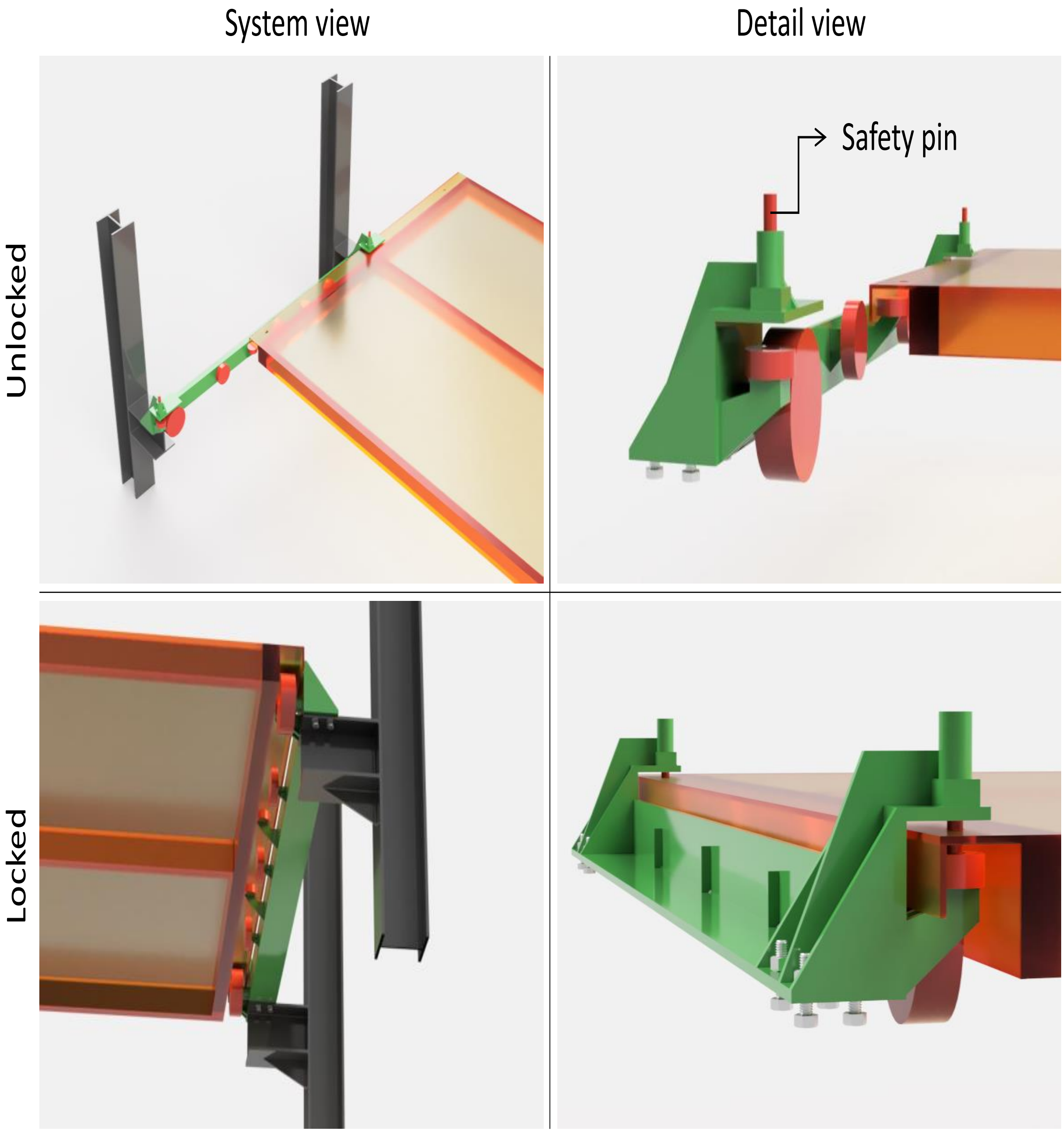

Figure 4.11. Proposed dislodgement free pallet-rail coupling design

Small modifications at the parking pallet design are not sufficient to gain a safer pallet-rail coupling mechanism. The rail design has been improved. Two main and three secondary vertical wheels are placed on the rail with two horizontal guide wheels. A unique ring wheel with safety pin mechanism is added at both ends of the rail. The design is illustrated in Figure 4.12. When the parking pallet is placed on the rail, safety pins close. Safety pins are the first step to prevent pallet dislodgement. If pins fail or pin holes on parking pallet tear-off, the hook-plate of parking pallets hooks to all vertical wheels. This is the secondary safety measure.

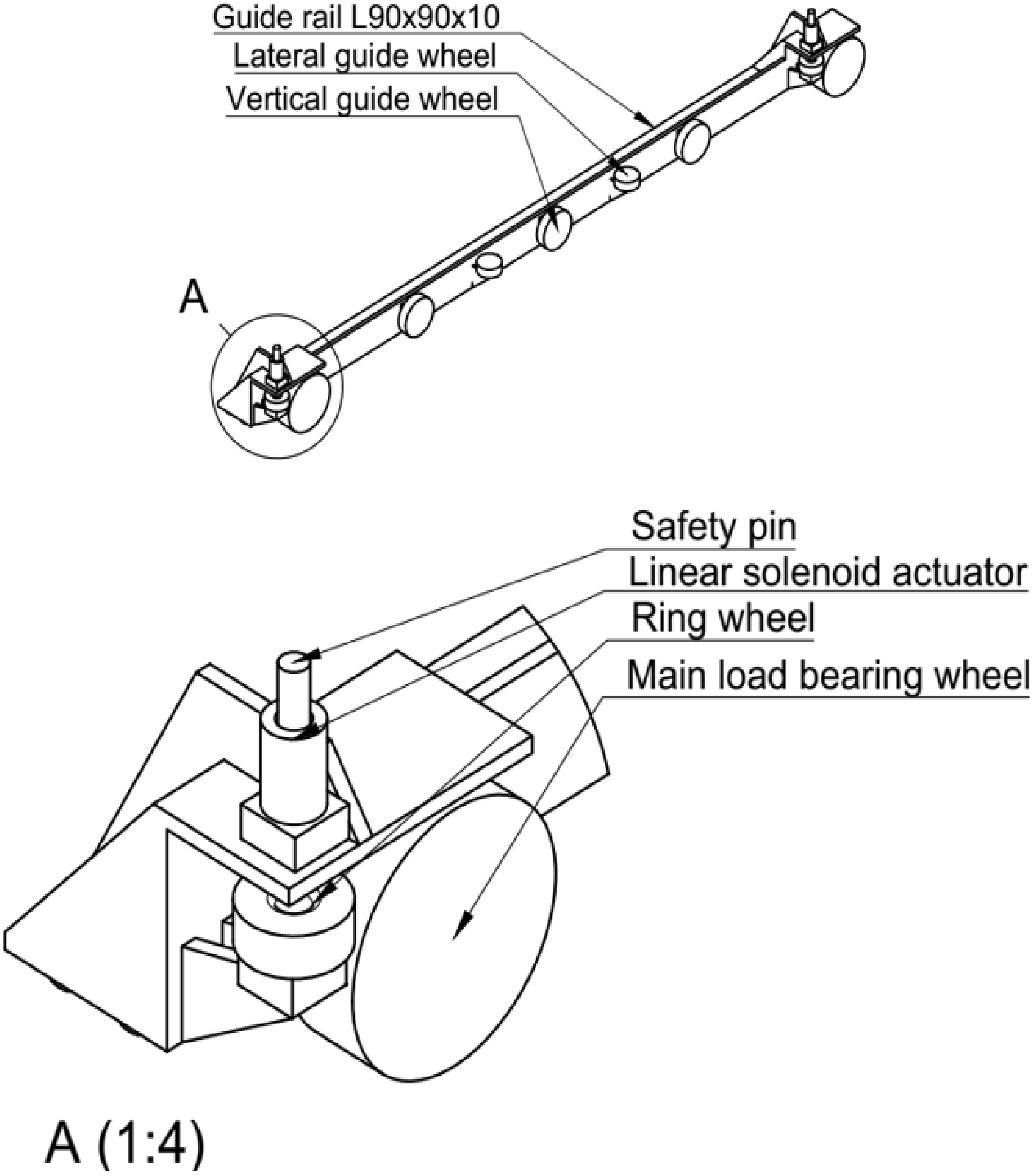

Figure 4.12. Anti-dislodgement rail with safety pin design

Vertical wheels must withstand the pulling force of parking pallet, if safety pins fail. However, the current plastic wheel design can not endure it because the plastic transition point of the wheel is low, and it loses its mechanical integrity during the fire. Actually, the aim of the polymer wheel is absorbing vibration during sliding and reducing rolling noise level. Thus, the polymer wheel is essential for an AVPS. To solve the weakness without removing the polymer material, the design of the wheel has also been improved. Steel is used for the main body, but the outer surface of wheel is covered with a thin polymer ring. The design detail of wheel is given in Figure 4.13.

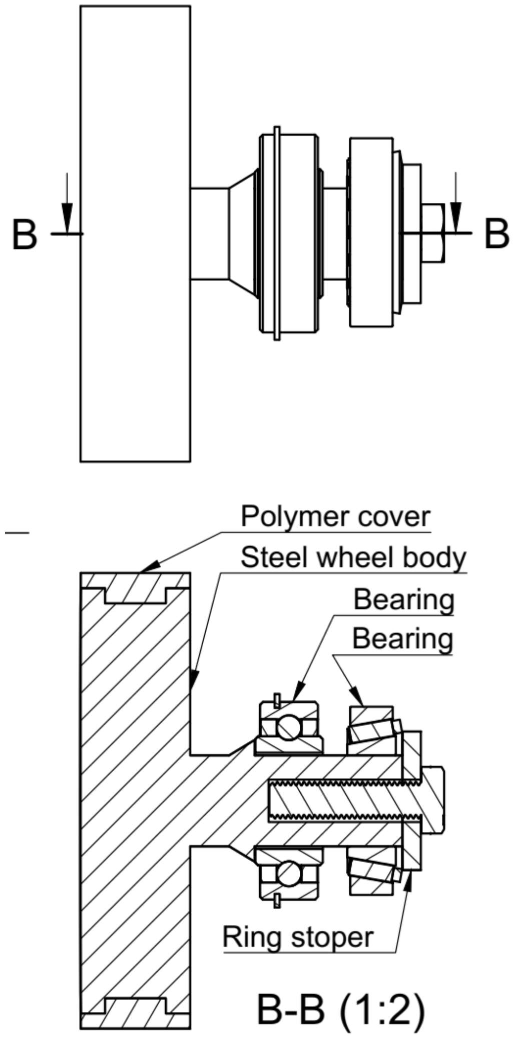

Figure 4.13. Fire proof main load bearing wheel design

Without parking pallet dislodgement, a fire can spread a floor to another sequentially. However, the vertical fire propagation is not simulated in the previous chapter. The vertical fire spreading is examined in Chapter 3.5.1 It is determined that the vertical spreading takes 12 minutes at a two-level car stacker. With a four-minute safety margin, a new fire scenario with 8 minutes vertical fire spreading period for first three floors has been designed, and an individual parking column has been modelled in FDS. Vertical fire spreading periods for higher levels were also shortened. In other words, it is assumed that the vertical fire propagation accelerates while the fire is reaching to upper floors. The setup is given in Figure 4.14. Fire starting times are also given in the same figure. The HRR level reaches to 25 MW by a sequential summation of Modified Category III curves for each passenger cars in the scenario. The resultant HRR curve is given in Figure 4.15. 25 MW peak HRR level is an extreme but possible fire load for this kind of steel frame.

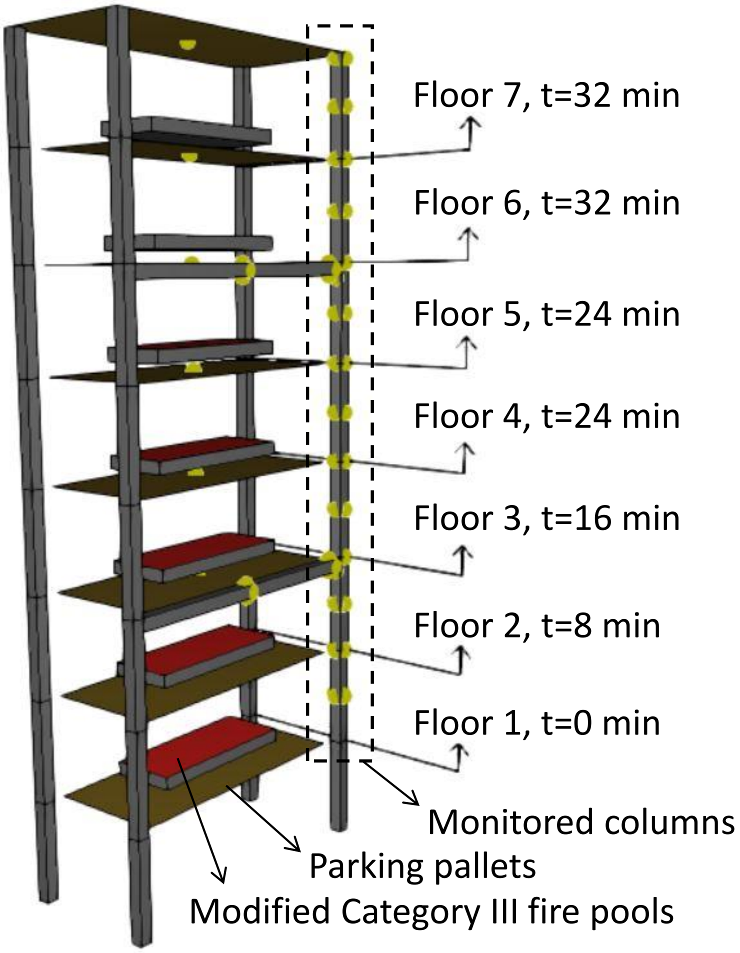

Figure 4.14. Simulation setup for vertical fire spreading

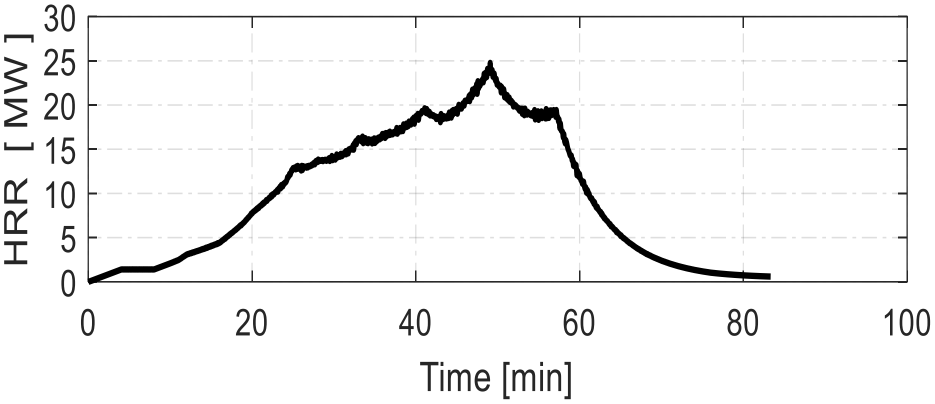

Figure 4.15. HRR curve during vertical fire propagation

It was assumed before the simulation that if average member temperatures of columns are under 400 °C, the structure stays stable. The simulation results show that average member temperatures of columns are under 200 °C. It seems very low and can be though smaller than it actually is. However, the experimental results of Tramoni et al. (2019) given in Figure 2.24 affirm the simulation results. Average column temperatures are given in Figure 4.16. Temperature levels are generally under 150 °C, but average column temperature on floor 7 is about 30% higher. The full ceiling at the top of the structure creates a path to the ceiling jet to reach upper ends of columns on floor 7.

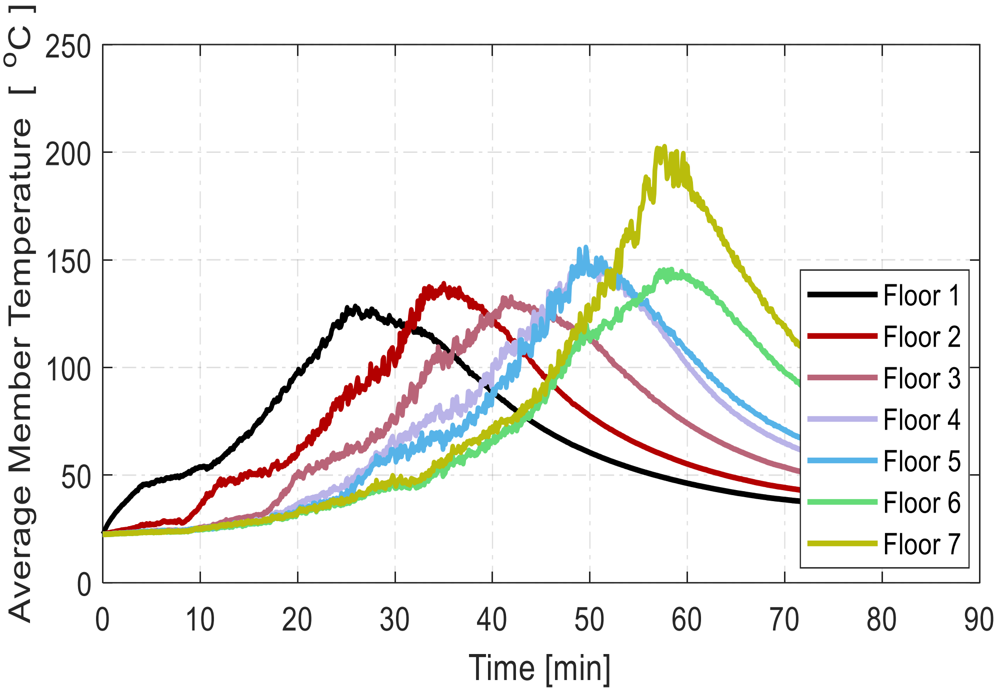

Figure 4.16. Column member temperatures

The structure contains beams per three floors. These beams do not carry any gravity load, and their primary purposes are to make the elevator shaft stable and earthquake resistance. Average member temperatures at beams rise to 650 °C as can be seen in Figure 4.17. This can not cause any structural collapse, because these beams are not exposed to a gravity load except their body loads during a fire. In other words, load demands on the beams are very weak during a fire, whereas their capacities are very high. Main causes of external load demands on inner columns are also thermal bowing and thermal elongation of these beams during a fire event. On the other hand, the situation of pallet rails is very critical. Due to the complex geometry of the proposed design, the AST level at the mid-bottom surface of the rail on floor two is collected. The level is under 330 °C, and the overall change of it is given in Figure 4.18. It can be assumed that the new pallet-rail coupling design does not fail during a fire.

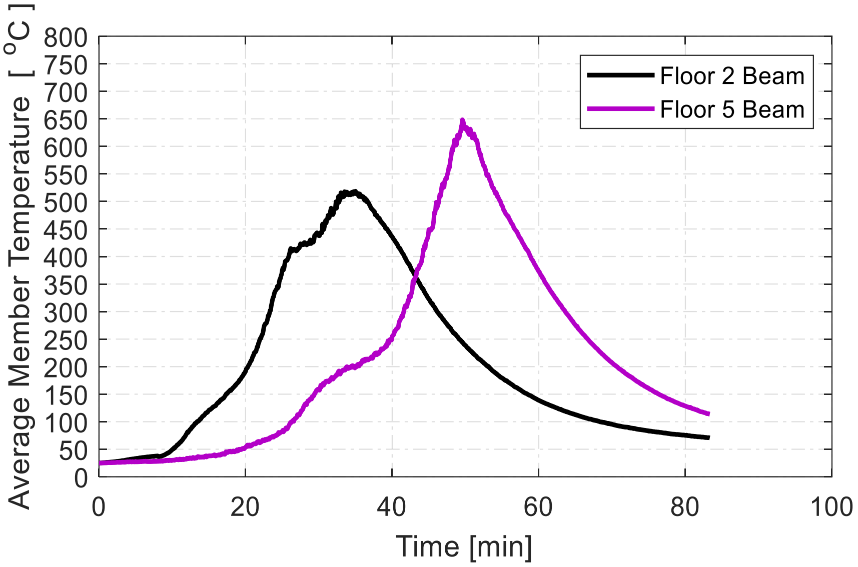

Figure 4.17. Beam member temperatures

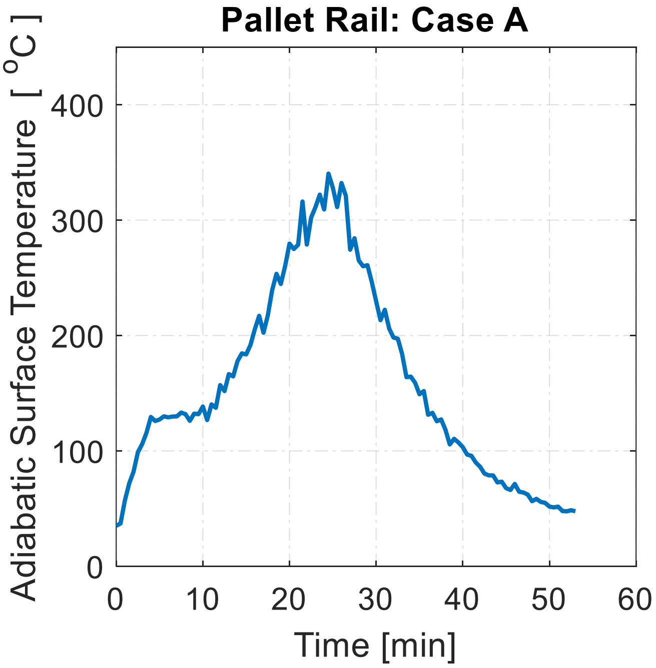

Figure 4.18. Pallet rail temperature at Floor 2

4.2. Case B: Passive Fire Protection with Fire Shields

The results in the previous section have revealed that unprotected AVPSS units with current rail-pallet coupling design are unsafe. In order to improve safety against fire spreading and pallet dislodgement, some passive measures have been applied to the unit. A rigid firewall is placed between passenger cars and outmost columns at first. This wall can both prevent the fire to spread laterally and shield outmost columns. Then, rigid fire ceilings are placed just under parking pallets. It also has a 30-cm overhang at its side. The partial protection design can be seen in Figure 4.19. It is expected that hot gases are channelized between the firewall and the overhang, so hot gases are exhausted out at the north and south façade. A half-length firewall is placed as a heatshield to the north and south sides. It also has an inclined overhang to push smoke and hot gases forward. The material properties and thickness have been chosen fictitiously as 0.05 W/mK in conductivity, 1 kJ/kgK in specific heat and 5 cm in thickness. It is assumed that the thermal properties are not temperature-dependent. The aim is to check to the effectivity of passive measures with fire-rated boards with fictitious but logical thermal properties.

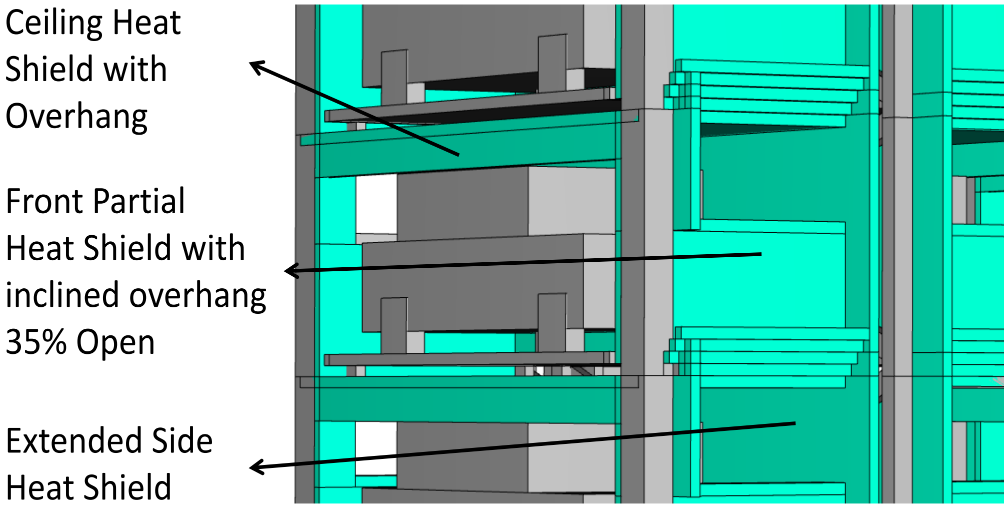

Figure 4.19. Heatshield design for AVPSS units (Case B)

When the temperature map obtained from FDS results given in Figure 4.20 are examined, it can be seen that the firewall and fire-ceiling serve their purpose. However, the 30-cm overhang is not sufficient for the channelization. The flames and hot gases that reach to the upper slot is marked by a white circle in the figure. It is obvious that the 30 cm overhang must be extended to 40 or 50 cm. However, each centimeter of overhang means more wastage of volume and steel. The vertical distance between the upper surface of parking pallet and the lowermost point of overhang can not be shorter than the total height of a passenger car.

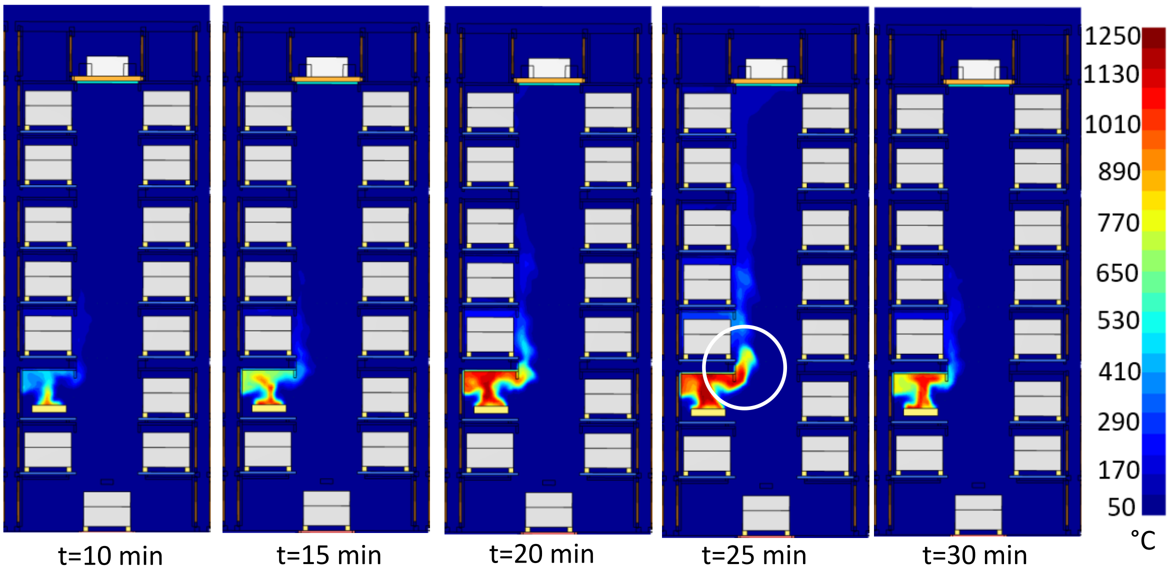

Figure 4.20. Vertical temperature map (Case B)

Incident heat flux levels on the car U1, L0 and L1 are tabulated in Table 4.2. All values are under 16 kW/m^2. The cars L0 and L1 are not in danger. However, mid bumper and front tire of the Car U1 are exposed to an incident heat flux higher than 8 kW/m^2. Then, adiabatic surface temperature levels have been controlled to determine whether ignition occurs or not. Ignitions points for bumpers and tires are defined in Section 3.5.1 as 388 °C and 350 °C. All peak temperature levels on car U1 are also given in Table 4.3. The temperature levels obtained from the fire simulation are 382°C for mid bumper and 392 °C for the front tire. Thus, the car U1 catches fire at its front tire. The design proposal B fails at the first criteria of the doctrine. There is no need to control the criteria 2 and 3.

Table 4.2. Maximum incident heat flux levels on dummy cars (in kW/m^2)

	Bumper			**Tire**		**Glass**		
Car ID	**Front**	**Mid**	**Back**	**Front**	**Back**	**Front**	**Mid**	**Back**
U1	9.30	11.26	5.28	12.76	7.05	6.17	5.86	5.42
L0	3.02	3.54	2.60	3.05	2.08	3.85	3.68	2.8
L1	1.98	2.09	1.69	2.14	1.83	1.53	1.47	1.31

Table 4.3. Maximum adiabatic surface temperature at car U1

	Bumper			**Tire**	
	Front	**Mid**	**Back**	**Front**	**Back**
U1	348	382	252	392	293

4.3. Case C: Hybrid Fire Protection with Fire Shields and Fire Shutter Door

A significant modification has been applied to the previous design. As can be seen in Figure 4.21, all overhangs and openings have been removed in the new design. In addition to this, a fire shutter door has been placed between slots and lift shaft. The fire shutter is actually a steel roller shutter with a fire rating. This design approach is based on turning the fuel-controlled fire into the ventilation-controlled one. In the FDS model, the parking space as a fire compartment is perfectly sealed when the shutter closes. Activation time or triggering mechanism of the fire shutter is an essential fact. Fire shutters can be triggered not only by electronic ways but also by mechanical systems. The roller mechanism is driven by both an electric motor and a muscle force. This fire scenario is based on the worst case. If a triggering mechanism does not exist or it fails, and the electric motor is disabled, the fire shutter may be closed by a human such as a security personal or firefighter. So, 15 minutes of time duration to close the fire shutter is exceedingly enough. There is also no doubt that sensors and an electric motor in proper conditions can close the fire shutter much earlier.

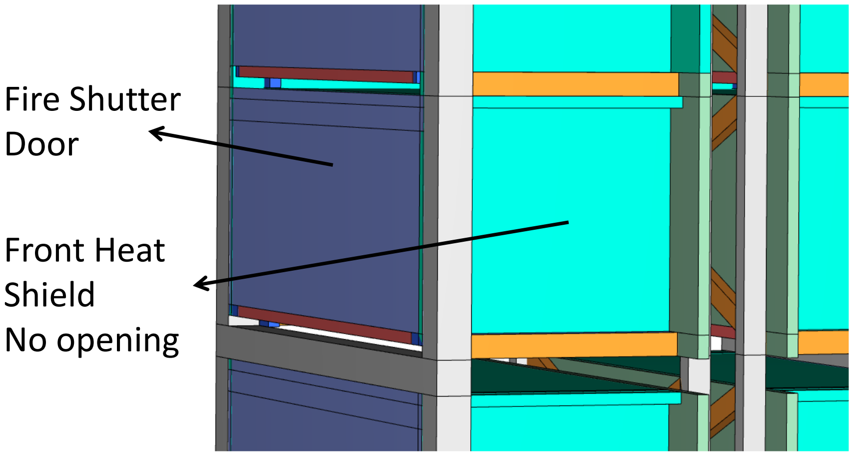

Figure 4.21. Enhanced heat shield design with fire shutter for AVPSS units

Temperature maps resulting from FDS results are given in Figure 4.22. The fire progresses as it should normally be until the fire shutter closes. Temperature levels of hot gases rising to the car U1 are not able to cause an ignition before the 900th second. After the shutter closes, the combustion reaction consumes oxygen in the compartment rapid. Then the fire dies down. The evolution of ventilation-controlled Modified Category III fire curve is given in Figure 4.23. When the HRR level reaches to 2600 kW, it drops down suddenly due to the lack of oxygen. Fire shutter doors close slowly and permit a little air leakage in real-world applications. However, it is evident that the shutter prevents the most portion of air exchange between the outside and the fire compartment. The adiabatic surface temperature levels on the fire ceiling and firewall can be seen in Figure 4.24(b). The temperature data of a gaseous substance from FDS models is zigzagging due to the turbulent nature of combustion. To obtain a clearer vision, the upper envelope of each temperature curve has been plotted. Temperature levels can not reach to 850 °C, and the fire event takes less than half an hour. Thus, ordinary fire-resistant boards and fire shutters with 1-hour fire rating can bear this kind of conditions easily.

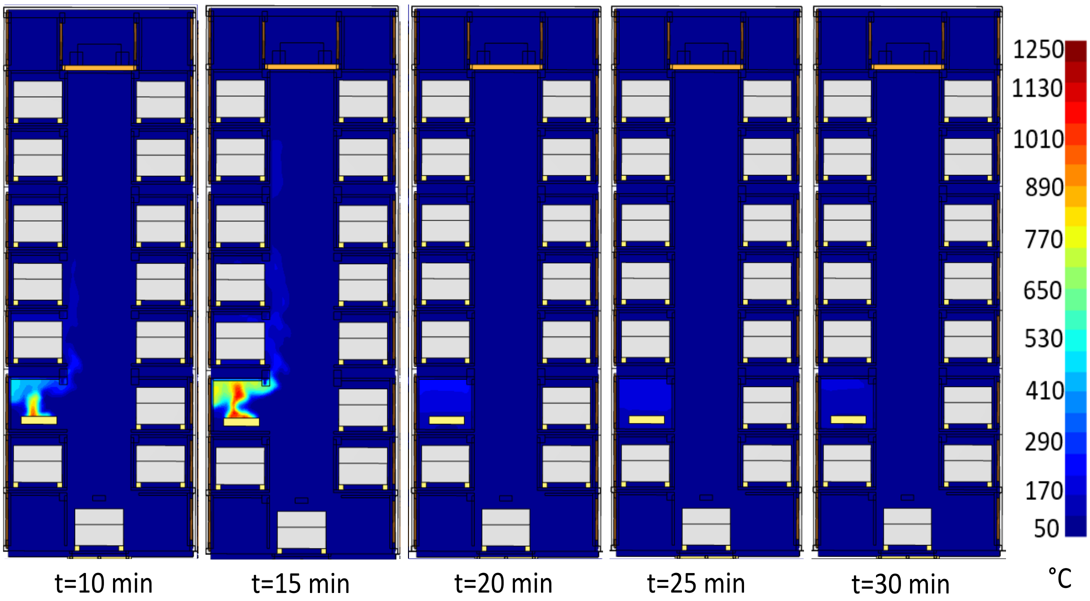

Figure 4.22. Vertical temperature map (Case C)

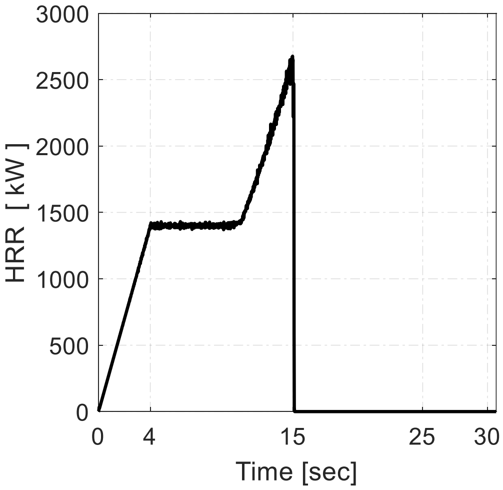

Figure 4.23. Effect of fire shutter on HRR curve (in an ideal case)

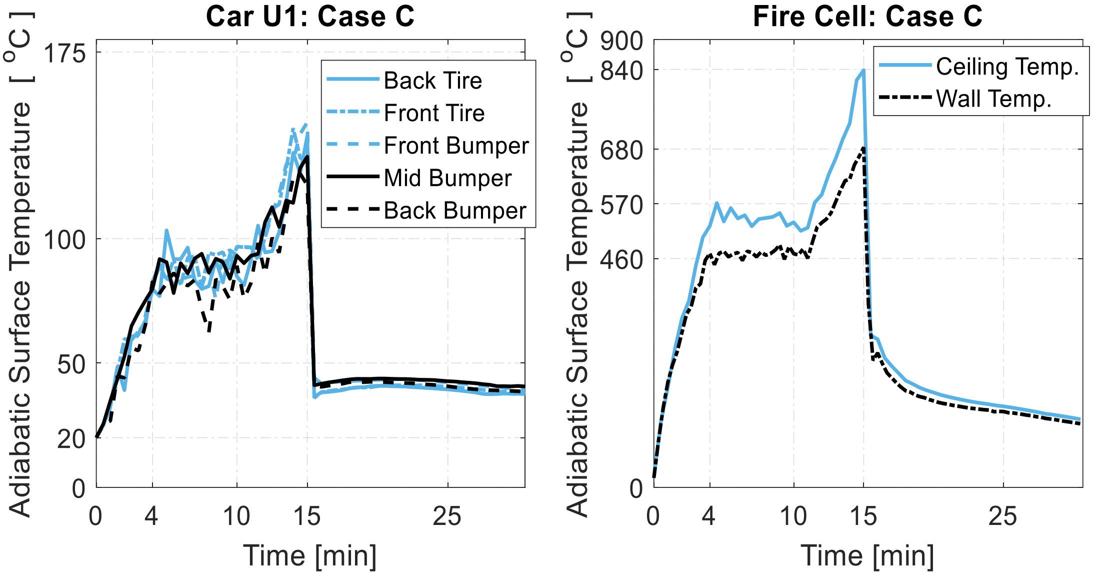

(a)

(b)

Figure 4.24. (a) Temperature levels at car U1; (b) and in fire cell.

Vertical fire spreading risk is nearly zero for case C. The maximum adiabatic surface temperature on the car U1 is lower than 175 °C as can be seen in Figure 4.24(a). The temperature levels at members closest to the fire can be seen in Figure 4.25. Due to the early dying down of fire, average temperature levels and temperature gradients are very low at columns. A relatively high temperature gradient has occurred at the beam B2E. The fire ceiling protects the lower face of it. There is no additional passive protection on the beam, so the east face is exposed until the shutter closes. Hence, a notable temperature gradient level lying on the east to the west is formed. The gradient is around 350 °C/m, which does not cause plastic deformation. Similar to the beam, the firewall protects only one face of each inner column, and their west faces are uncovered. This results in limited temperature gradient levels. All in all, the structural system of the AVPSS unit is not harmed, and the structural deformation is negligible. The maximum value of $\delta_{\Delta x}$ is detected as 0.8 mm between the wheels that close to the beam B2E. By the use of the adiabatic surface temperature curve at the ceiling, the maximum back wall temperature was calculated as 34.9 °C. If it is assumed that the lowest surface of S235 quality beams in parking pallet P3E equals to it, the maximum possible temperature gradient at the beams is 125 °C/m. Average temperatures of them are also lower than 100 °C. Therefore, the mechanical properties of the parking pallet stay constant. Mechanical properties and deflection levels for the parking pallet are given in Table 4.4. Midpoint deflection levels Δw_P and Δw_T are equal to 14.3 and

5.1 mm. However, the resultant drag $\delta_{\Delta w}$ is equal to -1.6 mm with the effect of thermal expansion. Hence, the total drag δ is negative. On the other hands, the moment bearing capacity of pallet P3E is enough, and any plastic hinge is not formed. Thereupon, the design proposal with fire shutter has passed all requirements.

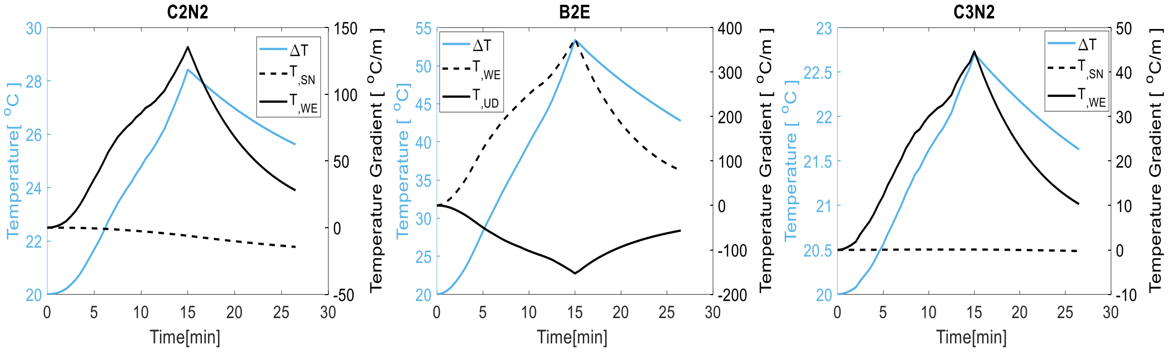

Figure 4.25. Average temperature changes and temperature gradients at steel members

Table 4.4. Car parking pallet fire response (Case C)

E_T	$\sigma_{y,\Delta T}$	$M_{capacity}$	M_{demand}	Δw_P	Δw_T	$\delta_{\Delta w}$	$\delta_{\Delta x}$	$\delta < 50$
210 GPa	235 MPa	57.06 kNm	24.52 kNm	14.3 mm	5.1 mm	-1.6 mm	0.8 mm	-0.8 mm

4.4. Case D: Active Fire Protection with Sprinkler

Fire dynamic simulator is capable of modelling heating and evaporation of water droplets engulfed by hot gases or over a hot surface. Parallel to this, the FDS is adequate to model a reduction in HRR, while water droplets encounter the burning surface with predefined HRR curve. Once the solver meshes the burning surface, the reduction in heat released rate due to water suppression is calculated locally. In other words, it is calculated for each cell that contains a portion of the surface. The main equation that governs the phenomena is given in Eq. 4.1(McGrattan et al.,2015). $\dot{q_o}''(t)$ is the predefined heat release rate per unit area in kW/m^2. The term may be obtained by dividing time-dependent HRR to the area of the fire pool. k is also calculated by Eq. 4.2, in where the term m_W'' is the local mass of water per unit area in kg/m^2. 'a' is an empirical constant in m^2/kg.s. The empirical constant is dependent on water flux, material properties and global geometric features of the burning substance. Thus, it is strictly case-specific, and there is no study that defines 'a' constant for passenger car fires. However, the FDS can be used to compare different sprinkler designs with the same coefficient, a. Also, the overall cooling effect of water droplets from sprinklers is still modelled reasonably by FDS.

$$\dot{q}''(t) = \dot{q_o}''(t)\, e^{-\int k(t)dt} \tag{4.1}$$

$$k(t) = am_W'' \tag{4.2}$$

Two different sprinkler system layouts have been examined and benchmarked. The coefficient ‘a’ has been taken as 0.001 m^2/kg.s which is very small. Hamins and McGrattan had determined the coefficient equal to 1 m^2/kg.s for a rock-storage commodity fire (Hamins et al., 2003). Same sprinkler nozzle has been used in all cases. K factor has been chosen as $160\ L/min\sqrt{atm}$. The activation temperature and operating pressure are 78 °C and 1 atm. Latitude angles of conical jet stream have been defined as 60° and 75° in the sprinkler spray model in FDS. Jet stream velocity is chosen as 5 m/s. The layouts are also given in Figure 4.26. The first layout is marked as ‘AU’. It is the layout proposed in the Doctrine ID 3007 by Australasian Fire and Emergency Service Authorities Council Limited (AFAC, 2018). It contains one sprinkler at corners of each passenger car. The sprinklers are placed at 45 degrees with all principal axes as can be seen in the figure. The second one that is marked as ‘proposed’ also contains four sprinklers per passenger cars but in a different orientation. The sprinklers are placed at edges at 45 degrees with the ground.

Response characteristics of layouts are totally different. The instant that the first sprinkler activated is given in Figure 4.27 for each case. 250 °C isosurfaces are also added on the same figure. In the case of AU, the sprinkler at the south-west corner of the burning car is activated at 191st second. Position of the sprinkler is not on the heat flow path from the gap on the front grill or the partially open window. It is the main reason for the relatively late activation of sprinklers. The isosurface attains to the upper slot and side bracings. The most useful result has been gained in the proposed case due to its sprinkler positions. The generated heat covered by car body can be exhausted from gaps at the front grille, wheel arches and partially open window. All four sprinklers are placed directly on these gaps.

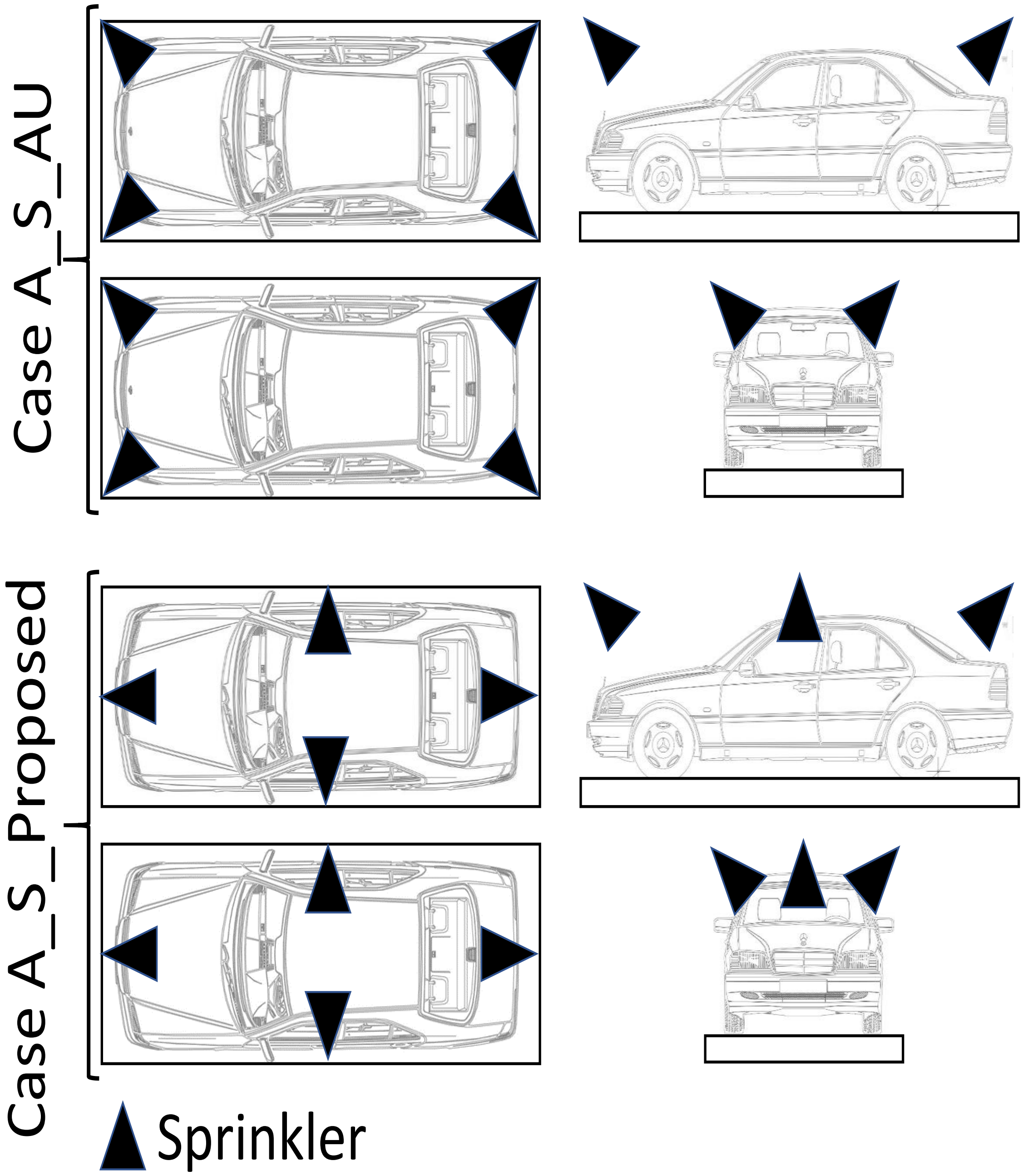

Figure 4.26. Two different sprinkler orientations for parking slots

Even after all windows break, sprinklers block all openings. The sprinkler on the west of burning car is triggered at 41th second. On the other hands, it is crucial that sprinkler water reaches on the ceiling of the passenger car. Water accumulated on the roof drips into the cabin and suppresses the combustion inside the passenger car. Changes in the layouts also differ the overall responses of the sprinkler system. For example, sprinklers at the upper slot are activated earlier than ones in other cases.

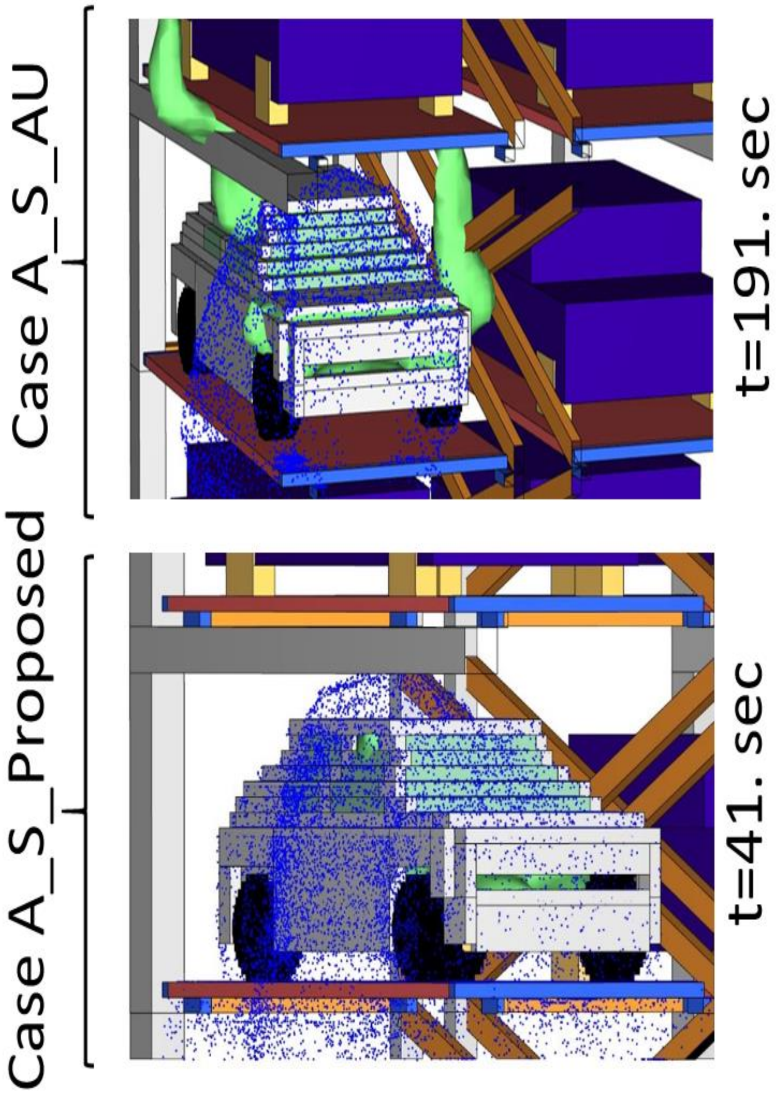

Figure 4.27. First sprinkler activations

The reduction in HRR is directly related to the amount of water penetrating on the fire surface. The amount depends on not only the number and orientation of sprinklers but also the vehicle geometry and windows. Change in the HRR with different sprinkler layouts are shown in Figure 4.28(a) comparatively. The layout AU is less effective because sprinkler water does not reach to the burning surface, which is inside the car body. Sprinkler water absorbs an important portion of total convective heat during its heating up and evaporation, as shown in Figure 4.28(b). Adiabatic surface temperature and incident heat flux levels on surrounding vehicles for both two cases are shown in Figure 4.29. The performance of the layout AU is good. Fire spreading risk is eliminated for car U1 and R0 and, nearly 80% of convective heat is absorbed. However, the incident heat flux on the mid bumper of car R1 is still over 20 kW/m^2. Thus, the layout can not prevent to fire spreading for all surrounding passenger cars.

Conversely, the proposed layout can not only prevent the fire to spread but also suppress it. The side sprinklers just above windows cover sides of the passenger car, and sprinkler water enters into the cabin. Parallel to this, side sprinklers are in an excellent position to face convective heat which is exhausted from side windows directly. When it comes together with the reduction in the HRR level, the convective heat transfer rate drops to zero. Convective heat transfer rates and HRR curves for the proposed layout can be seen in Figure 4.28(b) and (a). Incident heat flux levels on all surrounding cars shown are Figure 4.29 are under the level of 8 kW/m^2, and all adiabatic surface temperatures can not reach to ignition points.

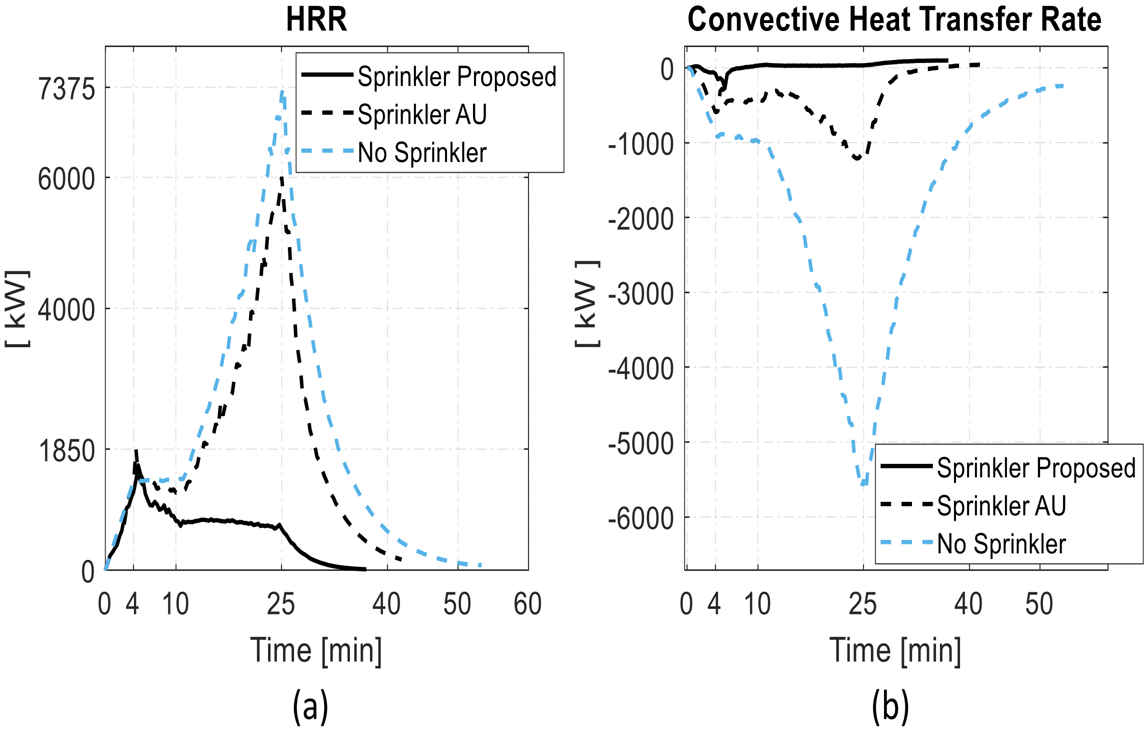

Figure 4.28. (a) Effect of sprinklers on HRR; (b) and convective heat transfer.

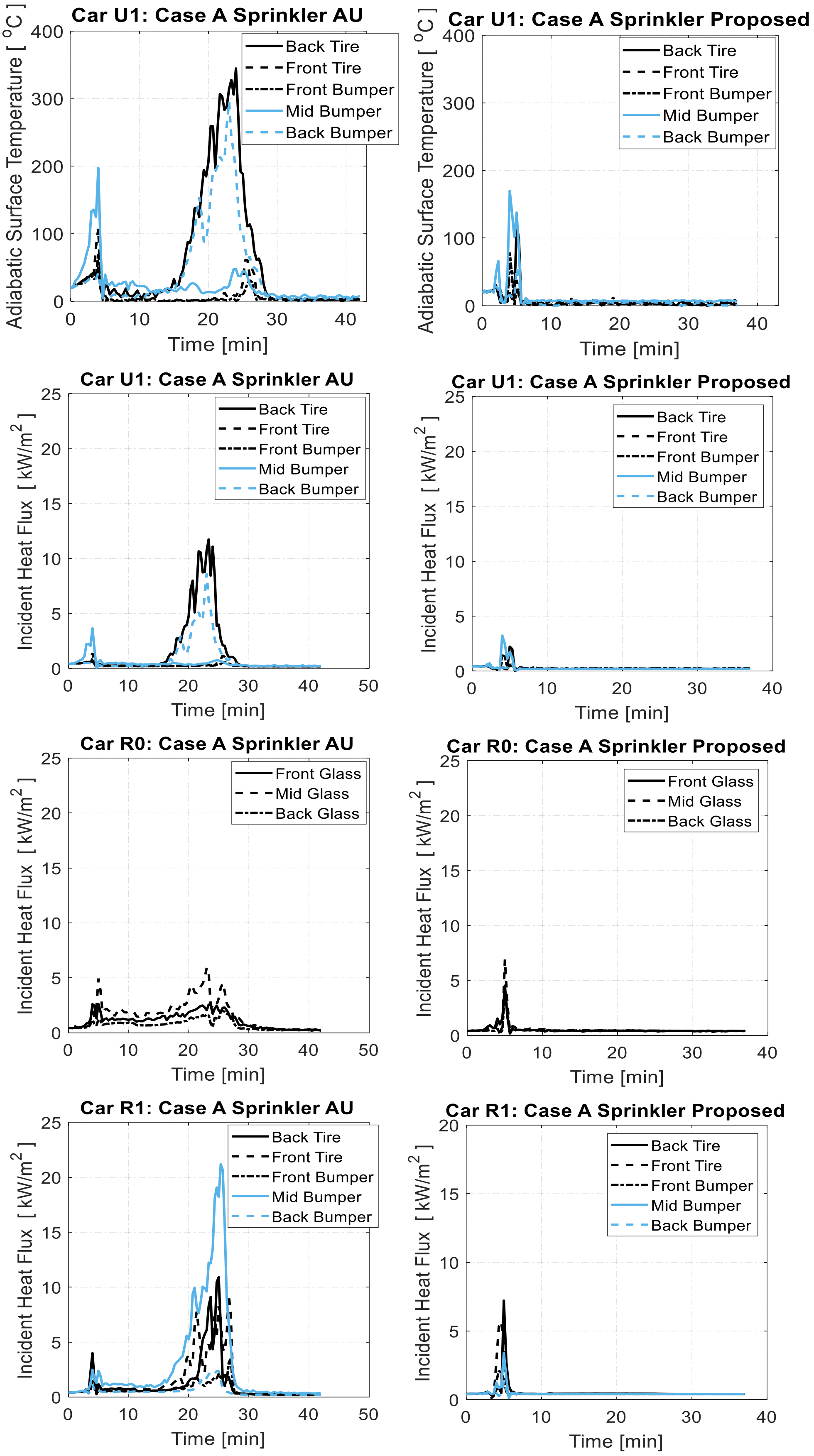

Figure 4.29. Incident heat flux and temperature levels at dummy cars

Temperature levels on columns and the beam B2E are shown in Figure 4.30 comparatively. At first glance, all layouts can protect the main structure. Average temperature levels and temperature gradients in columns are minimal in all cases. The levels can be inspected in Figure 4.30. Significant changes occur in the beam B2E and the car pallet P3E. The average temperature of the beam B2E reaches 125 °C at the case AU, whereas the level drops under 30 °C at the proposed one. The main reason for this significant drop is side sprinklers. Side sprinklers also protect beams, and temperature levels on them are also limited. Adiabatic temperature levels under the parking pallet P3E strongly depend on sprinkler layout. The maximum temperature on P3E reaches 530 °C at the case AU, at which the yielding strength of steel decreases around 45%. It is a dangerous situation because the safety factor of parking pallet is already 2. The parking pallet can dislodge, if the proposed pallet-rail coupling design is not employed. Controversially, the maximum adiabatic surface temperature on the pallet is only 162 °C at the proposed one, in which the reduction in HRR as much as the convective cooling of sprinkler water affects this situation.

All in all, the best result is gained from the proposed case. Resultant deformation of the unit is given in Figure 4.31 for the proposed layout. It is at a negligible level, in which columns and beams almost do not deform. The maximum change in distance between pallet wheels occurs at the east side due to thermal expansion of strong bracings, in which the change is 4.7 mm. The detail of the deformed shape of the 3rd floor is given in Figure 4.31a. The main cause of deformation at the 3rd floor is the thermal expansion in strong bracings and the thermal bowing of beam B2E. Additionally, the results of pallet dislodgement analysis are shown in Table 4.5. The upper surface temperature of parking pallet P3E is assumed constant, and 20 °C due to the cooling effect of sprinkler water, and the lower one is assumed to equal the adiabatic surface temperature. Thus the thermal gradient at parking pallet P3E is 1183 °C/m. Midpoint deflections of the pallet Δw_P and Δw_T are 15.3 and 48.1 mm, therefore the resultant drag, δ, is calculated as 0.6 mm with the effect of thermal elongation of the parking pallet. When all these facts are examined, it can be concluded that the pallet dislodgement can not occur at the proposed layout with the current pallet-rail coupling design, and the design passes all three criteria of the fire safety doctrine of AVPS.

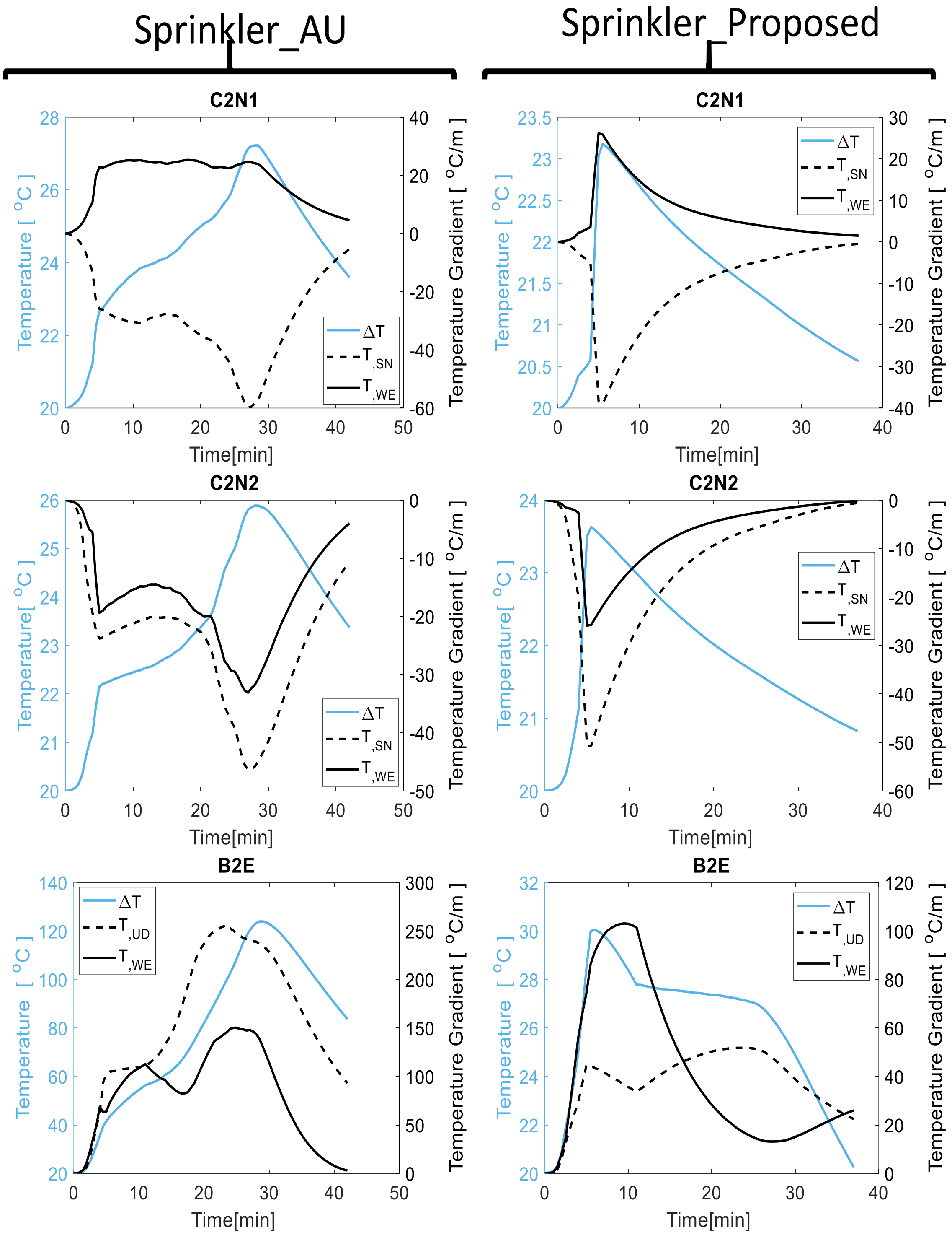

Figure 4.30 Average temperature changes and temperature gradients at steel members

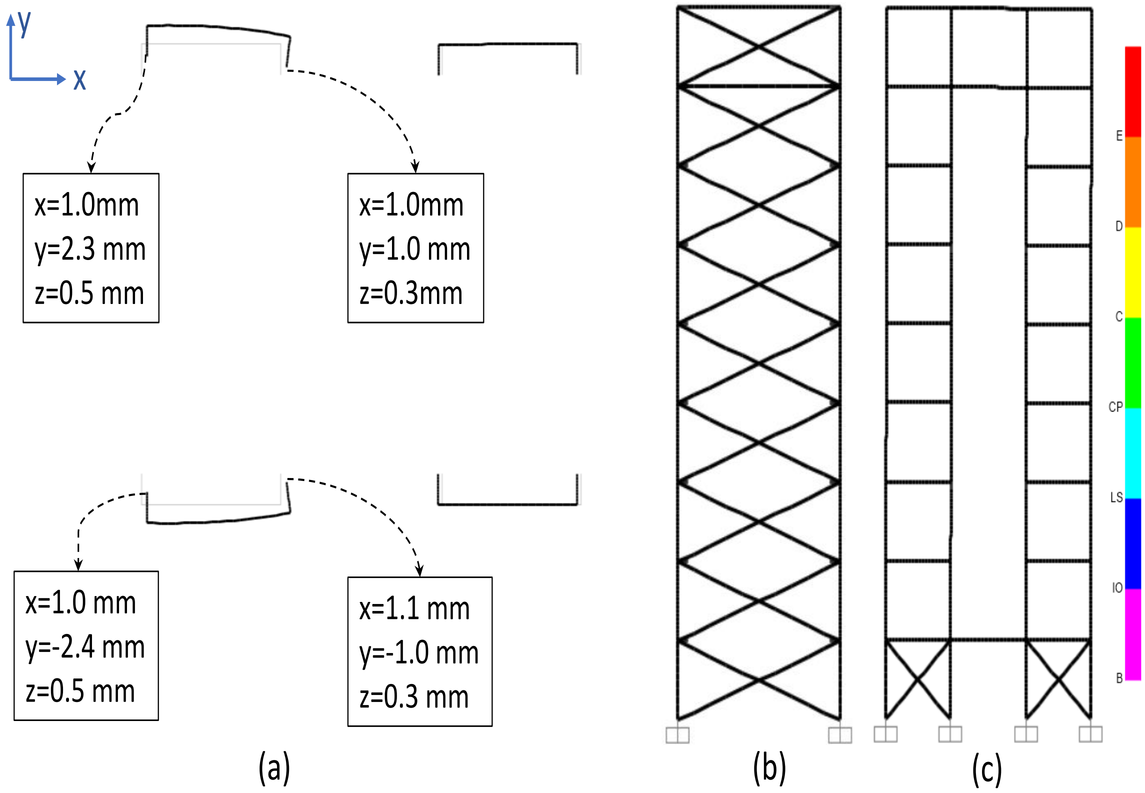

Figure 4.31. Structural fire response

Table 4.5. Car parking pallet fire response

E_T	$\sigma_{y,\Delta T}$	$M_{capacity}$	M_{demand}	Δw_P	Δw_T	$\delta_{\Delta w}$	$\delta_{\Delta x}$	$\delta < 50$
210 GPa	235 MPa	57.06 kNm	24.55 kNm	15.3 mm	48.1 mm	-4.1 mm	4.7 mm	0.6 mm

5. CONCLUSIONS AND RECOMMENDATIONS

In this study, the structural fire performance of a tower-type automated vehicle parking structure has been studied. Firstly, the structural design of an 8-floor AVPS unit based on an existing structure in Balıkesir, Turkey has been modelled for both thermomechanical and fire-driven computational fluid dynamic analyses. Fire Dynamic Simulator (FDS) has been used for fire simulations. Before fire simulations, Category the III fire curve that is a widely used design curve for family size passenger cars has been modified to obtain a computationally more efficient design curve with negligible trade-offs in thermal results. Criteria for vertical fire spreading between passenger cars that not mentioned in the literature have also been defined. After fire models and before structural calculations, a heat transfer analysis model for structural members with the concept of adiabatic surface temperature (AST) that is used to decouple fire and structural models has been developed. The validity of the model has also been criticized. Lastly, peak levels of average member temperature and temperature gradients, that are calculated by the model after fire simulations have been transferred to a 3D finite-element model of the structure in SAP2000. A comprehensive time-history analyses with SAP2000 could not be done, because SAP2000 does not have a capability to update temperature-dependent steel properties during time-history analyses. Temperature-dependent properties of steel that are defined in EC3 have also been used for only peak member temperature levels. After this chain of analyses for tower-type AVPSs, weaknesses of the structure have been identified. The main structural systems consist of columns and beams have been concluded as safe. However, parking pallets and current pallet-rail coupling designs have been seen as vulnerable. It has also been found that existing parking pallet locking mechanisms are not effective during a fire and parking pallets can dislodge easily. Passive and active fire protection measures have been designed to minimize these weaknesses. A new fireproof pallet-rail coupling mechanism has been developed within this scope. A group of firewalls, fire ceilings and fire shutter doors have been proposed as another passive measure. Lastly, the sprinkler layout design proposed by AFAC (2018) has been improved as an active fire safety measure for tower-type AVPSs.

The following conclusions can be drawn on the basis of the fire simulations, the structural performance of tower-type AVPSs, sprinkler layout designs and the proposed fire safety doctrine.

- Fire safety requirements for tower-type AVPSSs by national standards are either out of coverage or inadequate. Without active and passive fire protection measures, tower-type AVPSs are very vulnerable to fire. It was observed that the first collapse mechanism is started at 10th to 12th minute of fire. After the 20th minutes of a car fire, hot gas with 1000 °C and flames start to engulf upper parking slots, which such a thermal conditions can trigger a fire spreading mechanism between passenger cars.

- Vehicle fires within unprotected open car parks had caused structural collapses in steel car parks. A reinforced concrete slab that is carried by not only steel beams but also reinforced concrete ones can not withstand fully developed car park fires in big facilities. Similarly, parking pallets are probably not robust against a passenger car fire within unprotected systems. Adiabatic surface temperature levels under parking pallets can reacht to 1000 °C before the 18th minutes of fire. 12 minutes after a car fire starts, at least one plastic hinge at the mid of parking pallet starts to be formed. At this stage, the moment bearing capacity of parking pallets drops significantly to 3.42 kNm, while the demand due to gravity load of the passenger car and dead load of the parking pallet is about 25 kNm. Apart from this, due to the current design itself, parking pallets cannot redistribute their dead and live loads. The proposed pallet-rail coupling design must be employed within AVPSs, because the new design can redistribute the load after a plastic hinge formed at the midspan of parking pallet.

- When results from the proposed pallet dislodgement model are examined, it can be concluded that the vertical displacement due to gravity load, Δw_P, is generally higher than the one due to fire load, Δw_T. The levels for unprotected Case A are 219.5 mm for Δw_P and 49.5 mm for Δw_T before a plastic hinge formed at the midspan of parking pallet. In addition to this, drag length due to the main structural deformation, $\boldsymbol{\delta}_{\Delta x}$, was calculated as 75.1 mm and the one due to deformation of parking pallet, $\boldsymbol{\delta}_{\Delta w}$, was calculated as -28.6 mm with the effect of thermal expansion of the parking pallet. Hence, the thermal expansion of parking pallet may compensate for some portion of the total drag length.

- Columns within such an AVPS are robust against fire, even the fire spreads to other cars and grows. The calculated maximum member temperature in columns in all cases is under 200 °C. If a fire can not make a change to spread to other cars, the value is under 100 °C. Because there is no ceiling jet impinging to columns, and columns are relatively far away from the car fire. Parallel to this, temperature gradients within columns are also very limited. Maximum temperature gradient levels are under 500 °C /m.

- Internal beams in an AVPS are not robust against fire. Member temperatures within such structural elements can reach 800 °C. A steel member loses nearly 90% of its load-bearing capacity at such a temperature level. In contrary, beams located on the façade are safe. The peak member temperature detected on them is similar to the one for columns due to the same reason. Maximum temperature and temperature gradients detected at outmost beams are under 130 °C and 650 °C/m.

- Sprinklered and unsprinklered car stacker fire tests of the BRE are not adequate for tower-type AVPSSs. A very significant knowledge gap on tower-type AVPSs is the overall sprinkler performance within the structure. Only full-size fire tests can fill these knowledge gaps. Fire simulations with FDS can not give totally accurate results without experimental verification.

- Heat transfer paths during a passenger fire must be examined carefully. The effect of ceiling jets is very important for conventional car parking structures. However, it is not important for tower-type AVPSSs. Fire plumes and their vertical paths around the parking pallet just above the burning car are very critical. The paths must be blocked physically or blocked with a sprinkler head.

- FDS can be used for benchmarking of sprinkler layouts. A few well-though-out sprinkler layouts have been proposed in AS 2118.1:2017 (Australia) and NZS 4541:2020 (New Zealand). However, these are more generic layouts, and neither of them is suited to open-façade tower-type AVPSSs. Sprinkler heads must be placed at the backside, frontside and sides of cars; not corners of cars. When sprinkler heads are placed on the side of passenger cars, total water mass flux penetrating into the car cabin increased. Also, if windshield and back window are not broken during the fire, sprinklers at corners are insufficient to control the fire.

- The only way to control or suppress a passenger car fire in an unsprinklered AVPS is turning the fire into a ventilation-controlled fire. An adequate design is possible with using firewalls, fire ceilings and fire shutter doors. A robust design has also been proposed in this thesis.

- The investment cost of an open tower-type AVPS is around 8000 USD per parking slot, whereas an ordinary brand-new passenger car is worth about 20000 USD. So, protecting vehicles rather the structure from fire and fire spreading is a logical approach, if the tower-type AVPS has a low parking capacity. On the other hand, the floor number of a tower-type AVPS can be as much as 35. This equals almost to the height of a 25-floor apartment. A structural collapse or pallet dislodgement at such an AVPS may turn into a life safety issue.

- 'NFPA-1710: Standard for the Organization and Deployment of Fire Suppression Operations, Emergency Medical Operations, and Special Operations to the Public' by Career Fire Departments mandates 5:20 minutes response criteria for passenger car fires. If a passenger car fire is intervened by the fire brigade within 5:20 minutes, the fire can not result in a fire spread or pallet dislodgement at unprotected open-façade tower-type AVPSs. However, the performance of fire detection systems within AVPSs is a vital issue for the first intervention by the fire brigade. The mandated response duration starts after when the fire brigade is being informed about the fire. The fire brigade must be alerted in at most 4 or 5 minutes after the fire initiated.

- Effects of fuel tank failures during a passenger car fire event in a tower-type AVPSS is not mentioned in this thesis as well as the entire fire safety literature. A fuel tank failure in such a structure may lead the fire to spread downward. Because parking pallets are surrounded by vertical openings, and the fuel may spill down.

REFERENCES

AFAC, 2018, *Fire Safety Requirements for Automated Vehicle Parking Systems,* Retrieved 13 June 2020, from https://www.afac.com.au/docs/default-source/doctrine/fire-safety-requirements-for-automated-vehicle-parking systems.pdf ?sfvrsn=6 &download=true

AFAD, 2018, *Revised Probabilistic Seismic Hazard Map of Turkey*, Available at: https://tdth.afad.gov.tr/

Arcelor Mittal, 2007, "*Parkings Aériensmét Alliques Large Mentventilés*", Les carnets de l'acier.

Bennetts, I.D., D. Proe, R. Lewins, and I.R. Thomas, 1986, "Open-vehicle park fire analyses", *Proceedings of the Pacific Structural Steel Conference*, Aukland, New Zealand.

bin Mohd Tohir, M., 2015, *Multiple Vehicle Design Fire Scenarios in Car Parking Buildings*, Ph.D. Thesis, University of Canterbury.

BRE, 2009, *Sprinkler Protected Car Stacker Fire Test* . Technical report, London, UK: BRE - The British Automatic Fire Sprinkler Association.

BRE, 2010, *Fire spread in car parks* -BD2552. Technical report, London, UK: BRE - Department for Communities and Local Government.

BSI, 2015, BS EN 12845:2015 Fixed firefighting systems – Automatic sprinkler systems – Design, installation and maintenance.

Churches, C.H., E.W.J. Troup, C. Angeloff, 2003, Steel Design Guide 18: Steel-Framed Open-Deck Parking Structures, American Institute of Steel Construction, Inc., Chicago, Illinois.

Cook, Daniel R. and S. Pessiki, 2008, *Analytical Investigation of Fire Loads for Steel-Framed, Open-Deck Parking Structures*, ATLSS Reports. ATLSS report number 08-12: http://preserve.lehigh.edu/engr-civil-environmental-atlss-reports/108

CSE Combustion Science & Engineering, (Producer), 2020, *Modern Vehicle Hazards in Parking Garages and Vehicle Carriers*, NFPA funded webinar from https://players.brightcove.net/1640544031001/default_default/index.html?videoId=6161601923001

Çengel, Y., 2004, *Heat transfer : A practical approach* (2nd ed.), McGraw-Hill, New York:

Dobson, D. E., 1974, “Fire risks in parking garages”, *Batiment International, Building Research and Practice Journal*, Vol. 3(2), pp. 93-97.

European Committee for Standardization, 2005, Eurocode 3: Design of Steel Structures - Part 1-2 General Rules - Structural Fire Design - EN 1993-1-2, European Committee for Standardization, Brussels, Belgium.

FESG., 2020, *FESG provides explanation on Stavanger car park fire - News* , FESG., Retrieved 1 June 2020, from https://www.fesg.be/en/news/fesg-stavanger-car-park-fire

Fraud, C., B. Zhao, 2003, *Guide pour la verification du comportement au feu de parcs de stationnement largement ventilés en suprestructure metallique*, Internal Communication CTICM-Arcelor.

Franssen, J.-M, 2005, “SAFIR, A thermal/structural program modelling structures under fire”, *Engineering Journal*, Vol. 42, pp.143–158.

Ggwash.org, 2020, *64 years ago, the world’s first driverless parking garage opened in DC*, Retrieved 1 June 2020, from https://ggwash.org/view/40165/64-years-ago-the-worlds-first-driverless-parking-garage-opened-in-dc

Hamins, A., K. McGrattan, 2003, “Reduced-scale experiments on the water suppression of a rack-storage commodity fire for calibration of a CFD Fire model”, *Fire Safety Science*, Vol. 7, pp.457–468.

Hirashima, T., Y. Wang, and H. Uesugi, 2003, Large Scale Fire Tests Of A 4-story Type Car Park Part 2 Analysis Of The Thermal Stresses And Deflections, *Fire Safety Science*, Vol. 7, pp.655-666.

Hrabovský, L., T. Mlčák, & G. Kotajný, 2019, “Forces Generated in the Parking Brake of the Pallet Locking System”, *Advances in Science and Technology Research Journal*, Vol. 13(4), pp.181-187.

Joyeux, D., 1997, *Natural Fires in closed Car Parks - Car Fire Tests*. Technical Report. CTICM - Department Incendie et Essais.

Joyeux, D., J. Kruppa, L.G. Cajot, J.B. Schleich, P. Van de Leur, L.Twilt, 2001, *Demonstration of real fire tests in car parks and high buildings*, European Research Contract no 7215, Final report.

Kitano, T., O. Sugawa, H. Masuda, T. Ave, and H. Uesugi, 2000, “Large Scale Fire Tests of 4-Story Type Car Park Part 1: The Behavior of Structural Frame Exposed to the Fire at the Deepest Part of the First Floor”, *Prooceeding of 4th Asia-Oceania Symposium on Fire Science and Technology,* Tokyo, Japan, 24-26 May 2000.

Li, D., G. Zhu, H. Zhu, Z. Yu, Y. Gao, X. Jiang, 2017, “Flame spread and smoke temperature of full-scale fire test of car fire, Case Study” *Therm. Eng.*, Vol. 10, pp. 315–324.

MathWorks, 2020, *MATLAB*, Retrieved 2 June 2020, from https://au.mathworks.com/products/matlab.html.

Márton, T., A. Dederichs, L. Giuliani, 2016, “Modelling of Fire In An Open Car Park”, *Prooceeding of Applications of Structural Fire Engineering,* Dubrovnik, Croatia, October 2015, McGrattan, K., R. McDermott, C. Weinschenk & G. Forney, 2013, *Fire Dynamics Simulator, Technical Reference Guide*, Sixth Edition, Retrieved September 2019, https://www.nist.gov/publications/fire-dynamics-simulator-technical-reference-guide-sixth-edition

McGrattan, K., R. McDermott, C. Weinschenk & G. Forney, 2013, *Fire Dynamics Simulator, Validation Guide*, Sixth Edition.

Merceyside Fire and Rescue Service, *Kings Dock Car Park Fire*, 2018, Retrieved 3 June 2020, from https://www.bafsa.org.uk/wp-content/uploads/bsk-pdf- manager /2018/12/Mersey side-FRS-Car-Park-Report.pdf

Mohd Zahirasri Mohd Tohir, 2015, *Multiple Vehicle Design Fire Scenarios in Car Parking Buildings*, PhD Thesis, University of Canterbury.

National Fire Protection Association, 2019, NFPA 13:2019 Standard for the Installation of Sprinkler Systems, Quincy, MA.

National Fire Protection Association, 2019, NFPA 88A:2019 Standard for Parking Structures, Quincy, MA.

National Fire Protection Association, 2019, NFPA 220:2019 Standard on Types of Building Construction, Quincy, MA.

National Fire Protection Association, 2019, NFPA 1710:2019 Standard for the Organization and Deployment of Fire Suppression Operations, Emergency Medical Operations, and Special Operations to the Public by Career Fire Departments, Quincy, MA.

Noordijk, L., T. Lemaire, 2005, "Modelling of fire spread in car parks", *TNO Centre for Fire Research, Delft, the Netherlands, HERON*, Vol. 50(4), pp.1-8.

Okamoto, K., N. Watanabe, Y. Hagimoto, T. Chigira, R. Masano, H. Miura, 2009, "Burning behavior of sedan passenger cars", *Fire Safety Journal*, Vol. 44(3), pp.301-310.

Park, Y., J. Ryu, H.S. Ryou, 2019, “Experimental Study on the Fire-Spreading Characteristics and Heat Release Rates of Burning Vehicles Using a Large-Scale Calorimeter”, *Energies*, Vol.12(8), pp.1465-1475.

Parking-net.com, 2020, Retrieved 1 June 2020, from https://www.parking-net.com/parking-industry-blog/get-my-parking/history-of-the-automated-parking-system.

Pearce, E.M., 1985, “Polymer Flammability”, *Am. Chem. Soc. Polym. Prepr. Div. Polym. Chem.*, Vol. 15, pp.26-198.

Polipark, *Asansörlü Otopark Otomatik Park Sistemleri* , 2020, Retrieved 22 July 2020, from https://www.polipark.com.tr/sayfa.php?detay=apart-otopark

Pope, Nicholas D., 2005, *Computational fluid dynamics modelling of large-scale compartment fires*, Ph.D. Thesis, The University of Manchester, UK.

PyroSim, 2020, Thunderheadeng Inc., Retrieved 1 June 2020, from https:// www. thunderheadeng.com/pyrosim/

Republic of Turkey Ministry of Environment and Urbanization, 2009, Binaların Yangından Korunması Hakkında Yonetmelik, Turkish Official Journal, 27344, 45, Turkey.

SAP2000, 2019, Computers and Structures Inc., Berkeley, California, U.S.A.

Schleich, J., 1999, *Development of design rules for steel structures subjected to natural fires in closed car parks. Luxembourg*, Office for Official Publications of the European Communities.

Standards Australia, 2017, AS 2118.1:2017 Automatic fire sprinkler systems-General Systems.

Standards New Zealand, *2020, NZS 4541:2020*, Automatic fire sprinkler systems.

Strenchock, K., S. Pessiki, 2008, *Multiple-Vehicle Fire Loads for Precast Concrete Parking Structures* , ATLSS Report No. 08-03, Lehigh University.

TBDY, 2018, Türkiye Bina Deprem Yönetmeliği, Afet ve Acil Durum Yönetimi Başkanlığı, Ankara, 2018

Tramoni J-B, C. Thauvoye, F. Hanus, B. Poutrain, M. Suzanne, A. Thiry, 2020, "Temperature assessment of steel members subjected to fire generated by alternative fuel vehicles: Experimental tests", *Fire and Materials*, Vol. 41, pp.1-10.

USATODAY, 2020, *Robot parking garage to open in New York,* Retrieved 1 June 2020, from http://usatoday30.usatoday.com/tech/news/techinnovations/2007-01-30-robotic-garage_x.htm.

Web-japan.org, 2020, *Hidden Like Secret Bases – Automated Multistory Parking Facilities, Tech & Life, Trends in Japan,* Retrieved 1 June 2020, from https://web-japan.org/trends/11_tech-life/tec170223.html

Weisenpacher, P., J. Glasa, L. Halada, 2016, "Automobile interior fire and its spread to an adjacent vehicle", *Journal of Fire Sciences*, Vol. 34(4), pp.305-322.

Wickstrom Ulf, S.N., D. Duthinh, K. Mcgrattan, 2007, "Adiabatic Surface Temperature for Calculating Heat Transfer To Fire Exposed Structures", *11th Proceedings of Interflam 2007 International Interflam Conference*, London, September 3-5 2007.

Zanon, R. , M. Sommavilla, O.Vassart, L. Cajot, R. Zandonini, F. Gadotti, 2010, "Analysis of steel-framed open car parks under localized fire", *Proceedings of Urban Habitat Constructions under Catastrophic Events,* Taylor & Francis Group, London, ISBN 978-0-415-60685-1.

Zhao, B., J.Kruppa, 2004, "Structural behavior of an open vehicle park under real fire scenarios," *Fire and Materials*, Vol. 28, pp. 1-12.

APPENDIX A: DERIVATION OF EQUATIONS FOR PARKING PALLET DISLODGEMENT

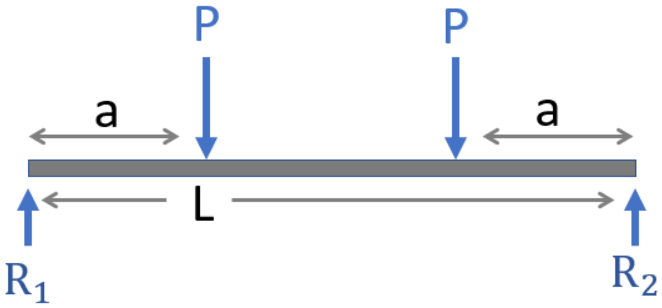

Figure A1. Symmetrically loaded and simply supported beam

$$\Delta \mathrm{w}_{\mathrm{midspan}} = \frac{\mathrm{Pa}}{24\mathrm{EI}}\,(3L^2 - a^2) \tag{A1}$$

Symmetrically two-point loaded simply-supported beam can be used to model the mechanic response of parking pallet under the gravity load of a passenger car. The free body diagram of the beam is shown in Figure A1. Midpoint deflection of the beam can be calculated by Eq. A1. This equation is widely used and derived from the Bernouilli Beam Theory. It can be found at every book of structural mechanics. By that parameters within the Eq. A1 are converted to related parameters given in Figure A2, the midpoint deflection of parking pallet can be calculated. These parameters are $\mathrm{L}_{\mathrm{P},\Delta\mathrm{T}}$, L_{a} and W_{car}, which refer the thermally expanded length of parking pallet, the length of wheelbase of passenger car and the weight of passenger car. Transformations of parameters are given in Eq. A2, A3 and A4. After the transformation, Eq. A1 changes in Eq. A5. The Young’s Modulus, E, in Eq. 5 is temperature-dependent, that as like defined in EC3.

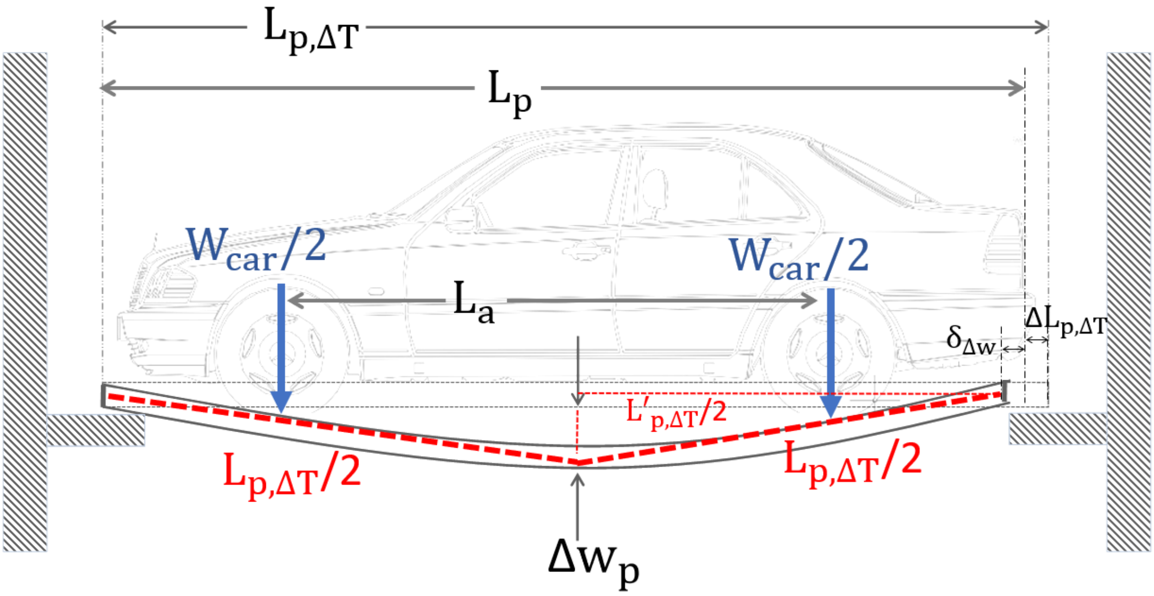

Figure A2. Symmetrically loaded and simply supported parking pallet on wheels

$$a = \left(L_{P,\Delta T} - L_a\right)/2 \tag{A2}$$

$$L = L_{P,\Delta T} \tag{A3}$$

$$P = W_{car}/2 \tag{A4}$$

$$\Delta w_P = \frac{W_{car}}{96EI}\left[\left(L_{P,\Delta T} - L_a\right)\left(2{L_{p,\Delta T}}^2 - {L_a}^2 + 2L_{P,\Delta T}L_a\right)\right] \tag{A5}$$

The lateral shift of end brackets of the parking pallet is a function of the midpoint deflection and thermally elongation of parking pallet. The resultant midpoint deflection, Δw, is the summation of the midpoint deflection due to gravity load, Δw_P, and the midpoint deflection due to thermal bowing, Δw_T, as given in Eq. A6.

$$\Delta w = \Delta w_P + \Delta w_T \tag{A6}$$

With the assumption that the deformed shape of parking pallet is a symmetric ‘V” shape as illustrated red-dashed line in Figure A2, the lateral shift length, $\delta_{\Delta w}$, is calculated by Eq. A7. Where L_p is the original length of parking pallet and $L'_{p,\Delta T}$ is the projection length of the deformed and thermally expanded parking pallet on its original position. The term of $L'_{p,\Delta T}$ is simply calculated by Pythagorous' Theorem and the calculation is given in Eq. A8. Lastly, Eq. A7 turns into Eq.A9.

$$\delta_{\Delta w} = L_p - 2L'_{p,\Delta T} \tag{A7}$$

$$L'_{p,\Delta T} = \sqrt{\left(\frac{L_{p,\Delta T}}{2}\right)^2 - \Delta w^2} \quad .\text{(A8)}$$

$$\delta_{\Delta w} = L_p - 2\sqrt{\frac{{L_{p,\Delta T}}^2}{4} - \Delta w^2} \quad .. \quad \ldots\text{(A9)}$$

APPENDIX B: DISLODGEMENT PROOF PARKING PALLET RAIL DESIGN DETAILS

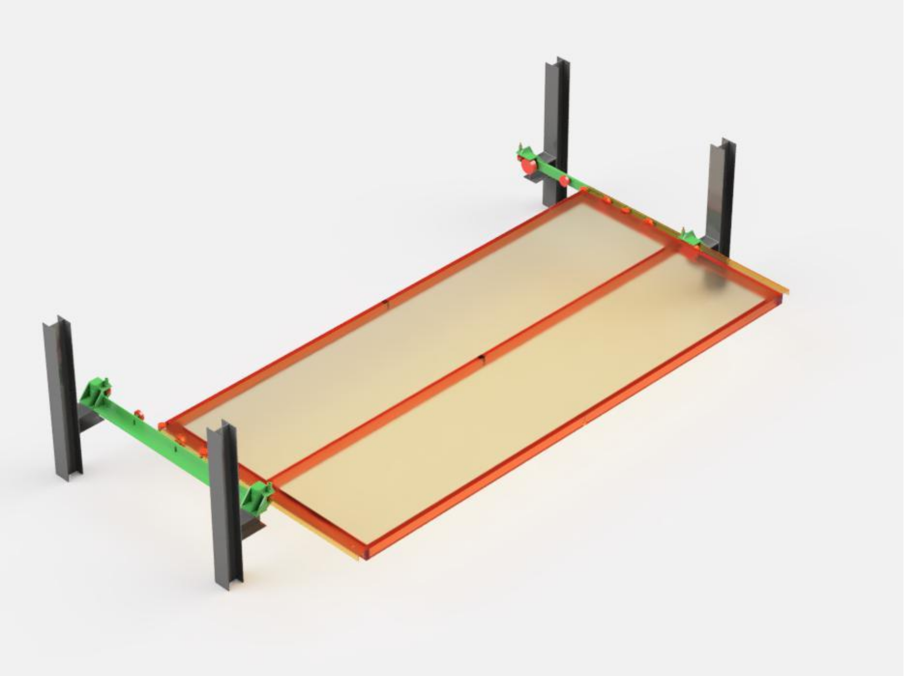

Figure B1. General view

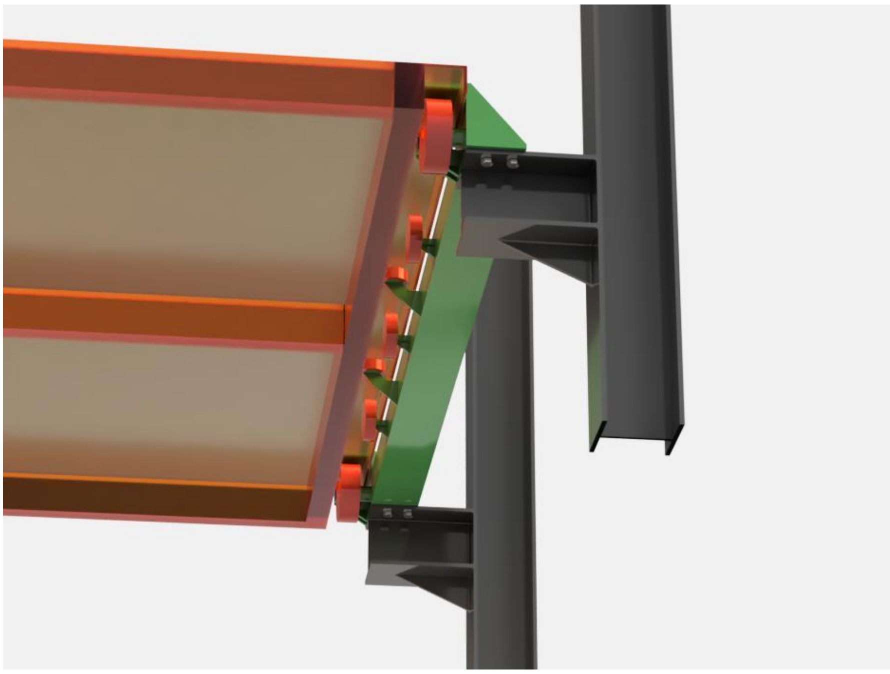

Figure B2. Rail-pallet coupling detail 1

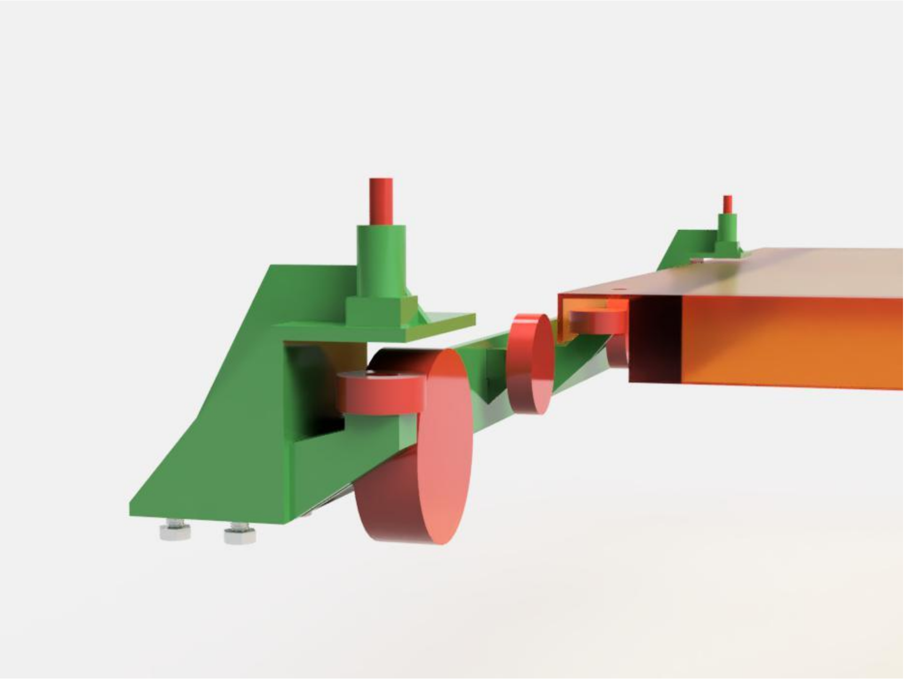

Figure B3. Rail-pallet coupling detail 2

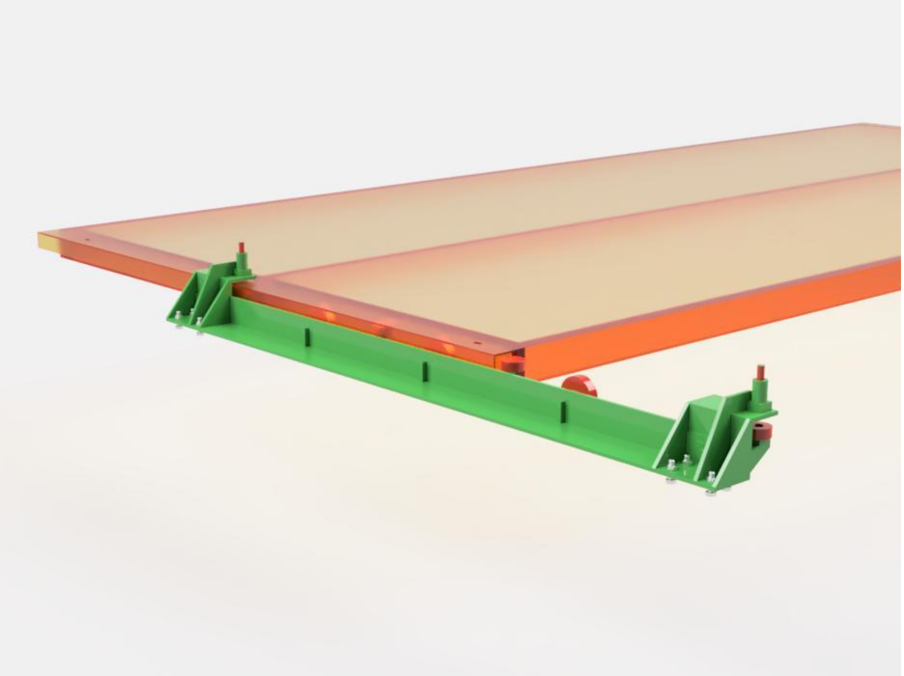

Figure B4. Rail-pallet coupling detail 3

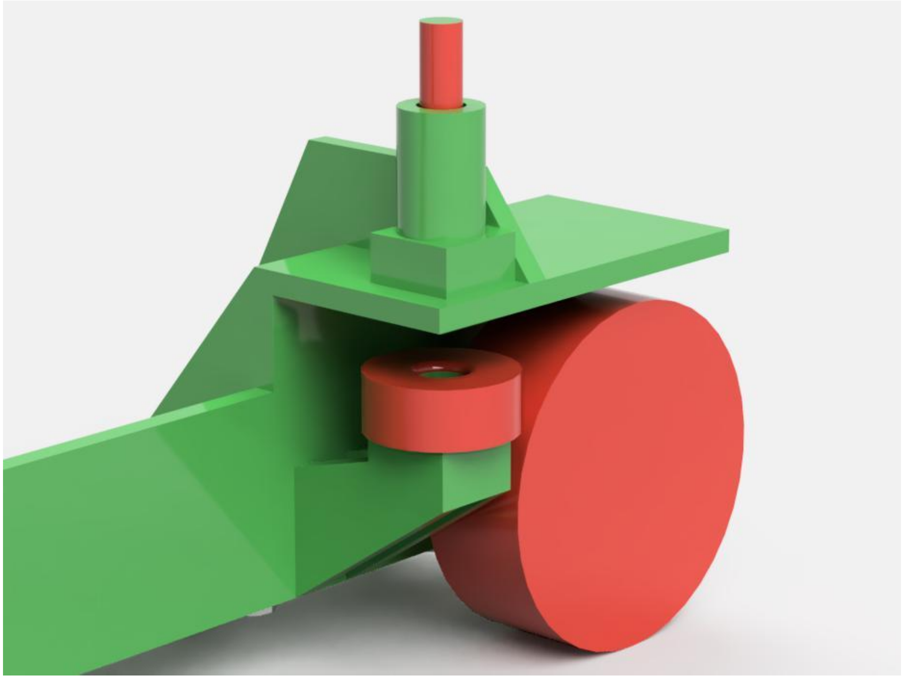

Figure B5. Locking mechanism detail

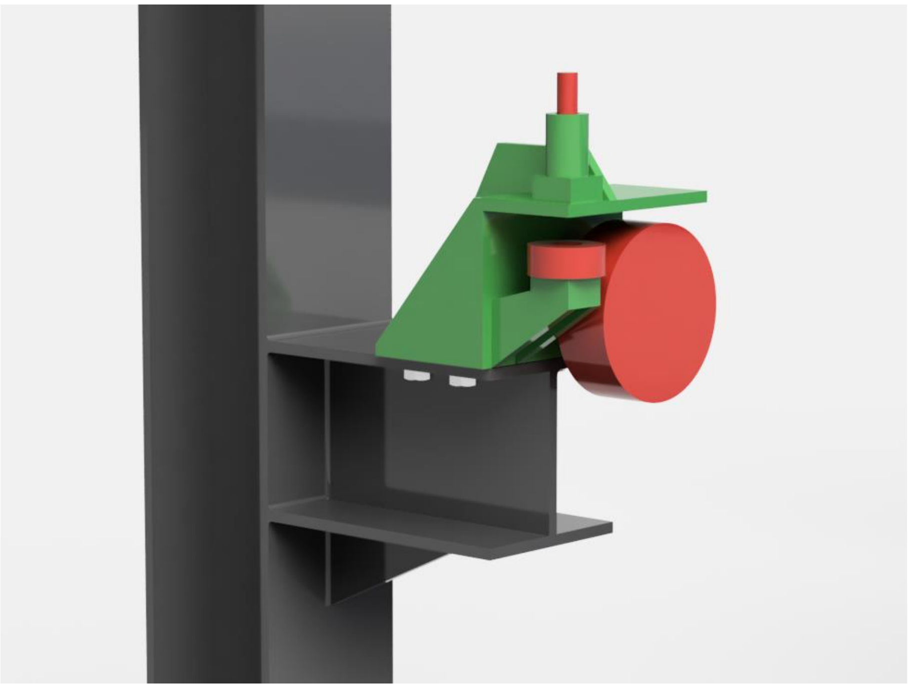

Figure B6. Locking mechanism – frame connection

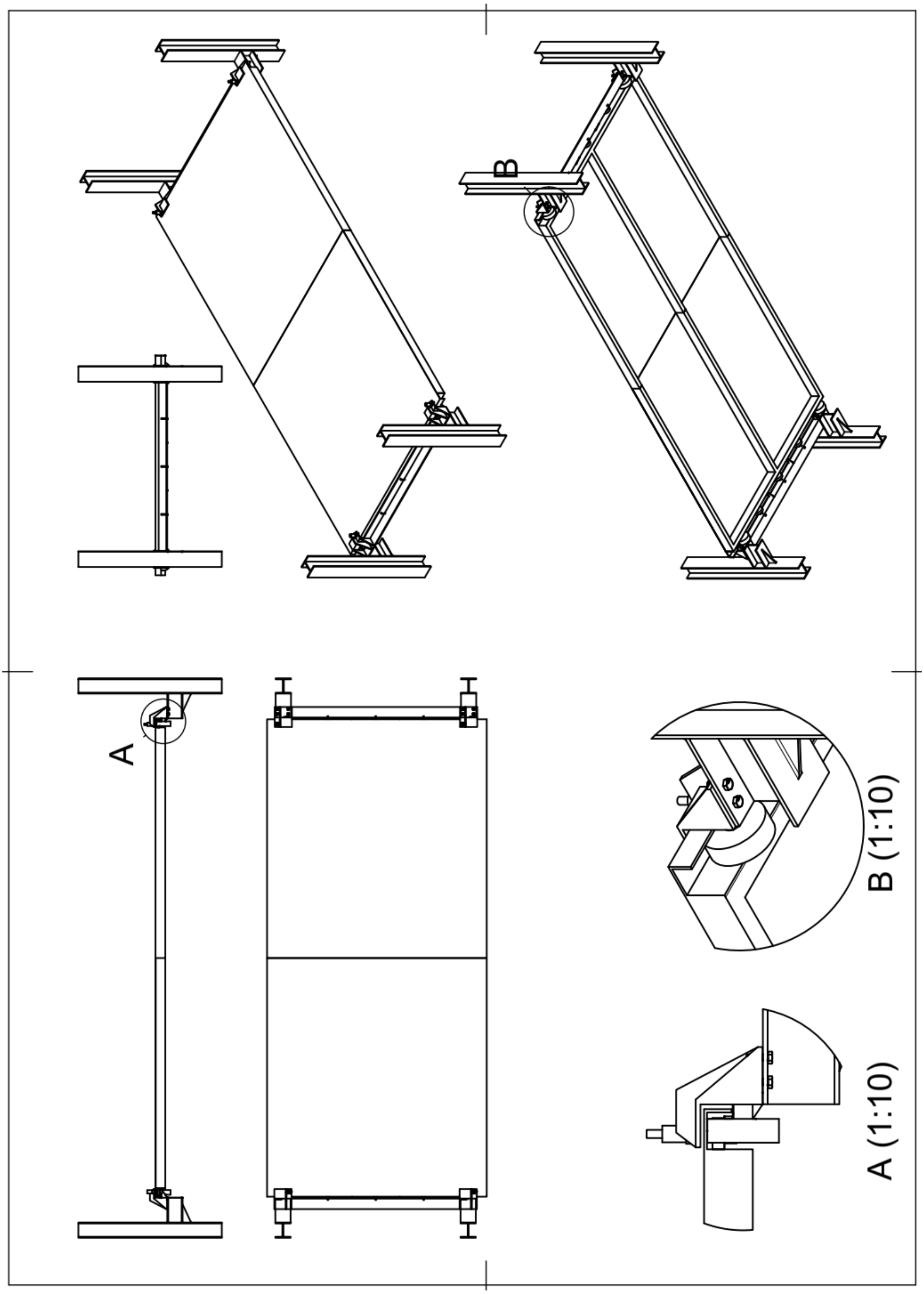

Figure B7. Technical drawing 1

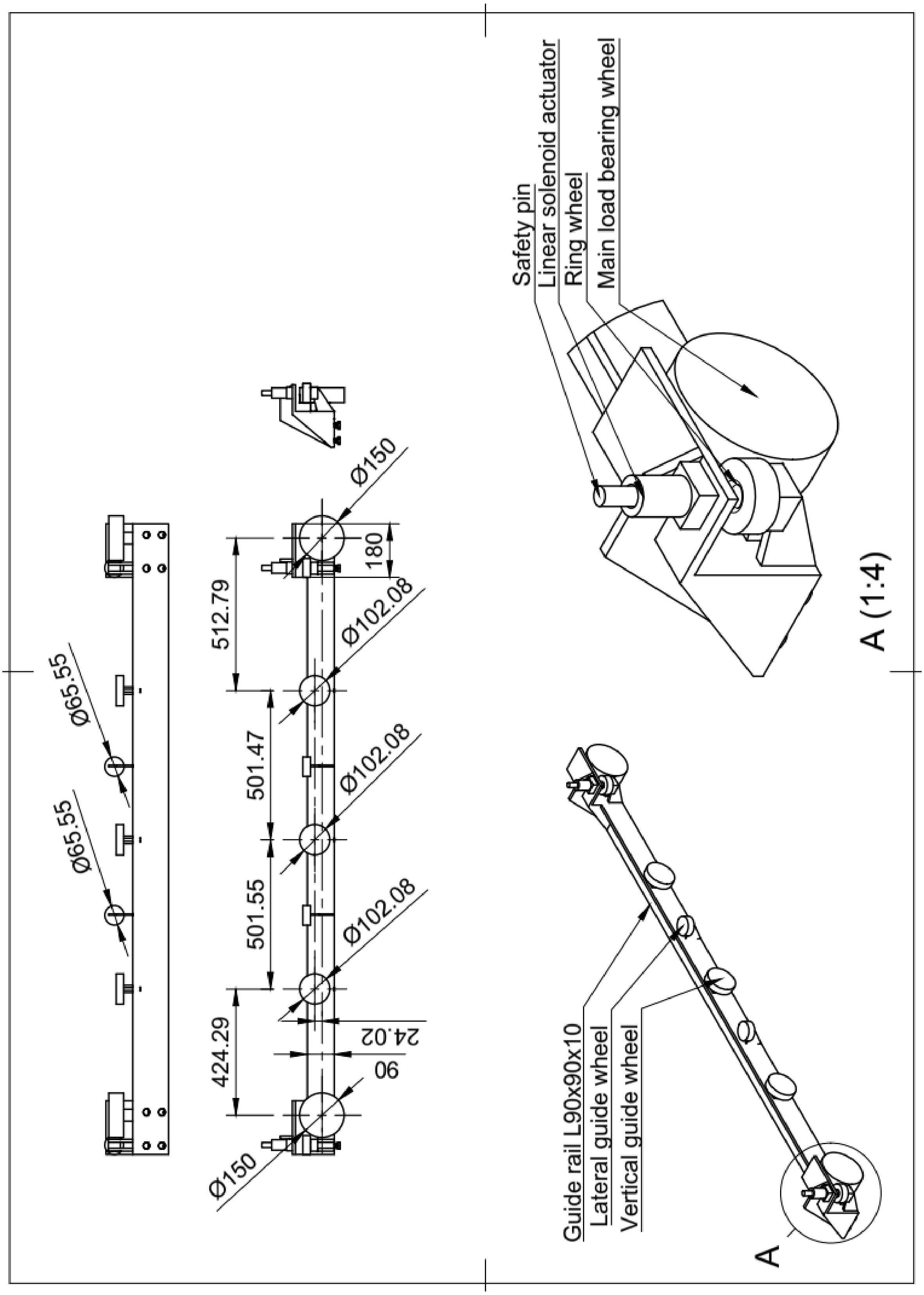

Figure B8. Technical drawing 2

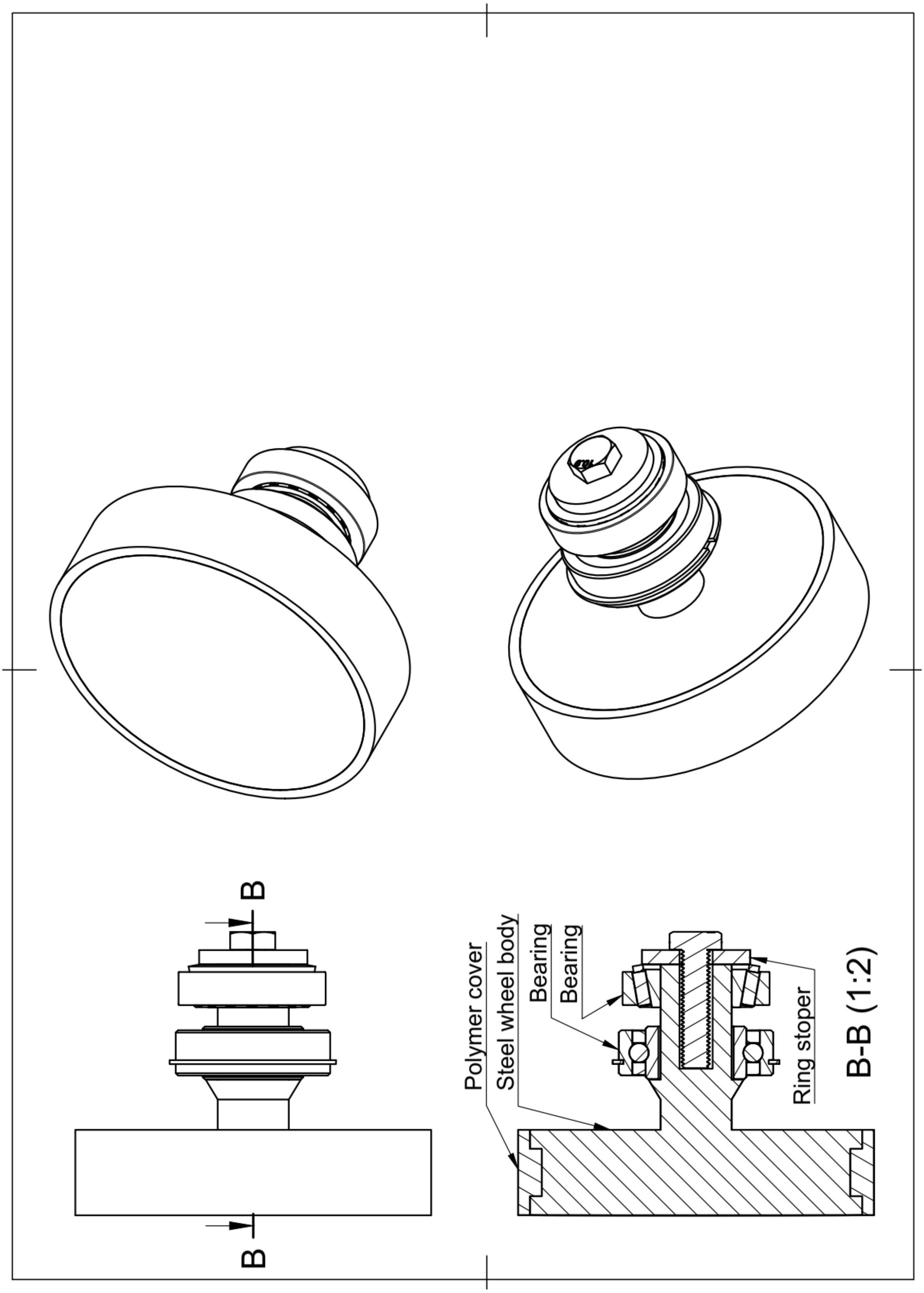

Figure B9. Technical drawing 3

APPENDIX C: ARCHITECTURAL PLAN of BALPARK AVPS in BALIKESIR

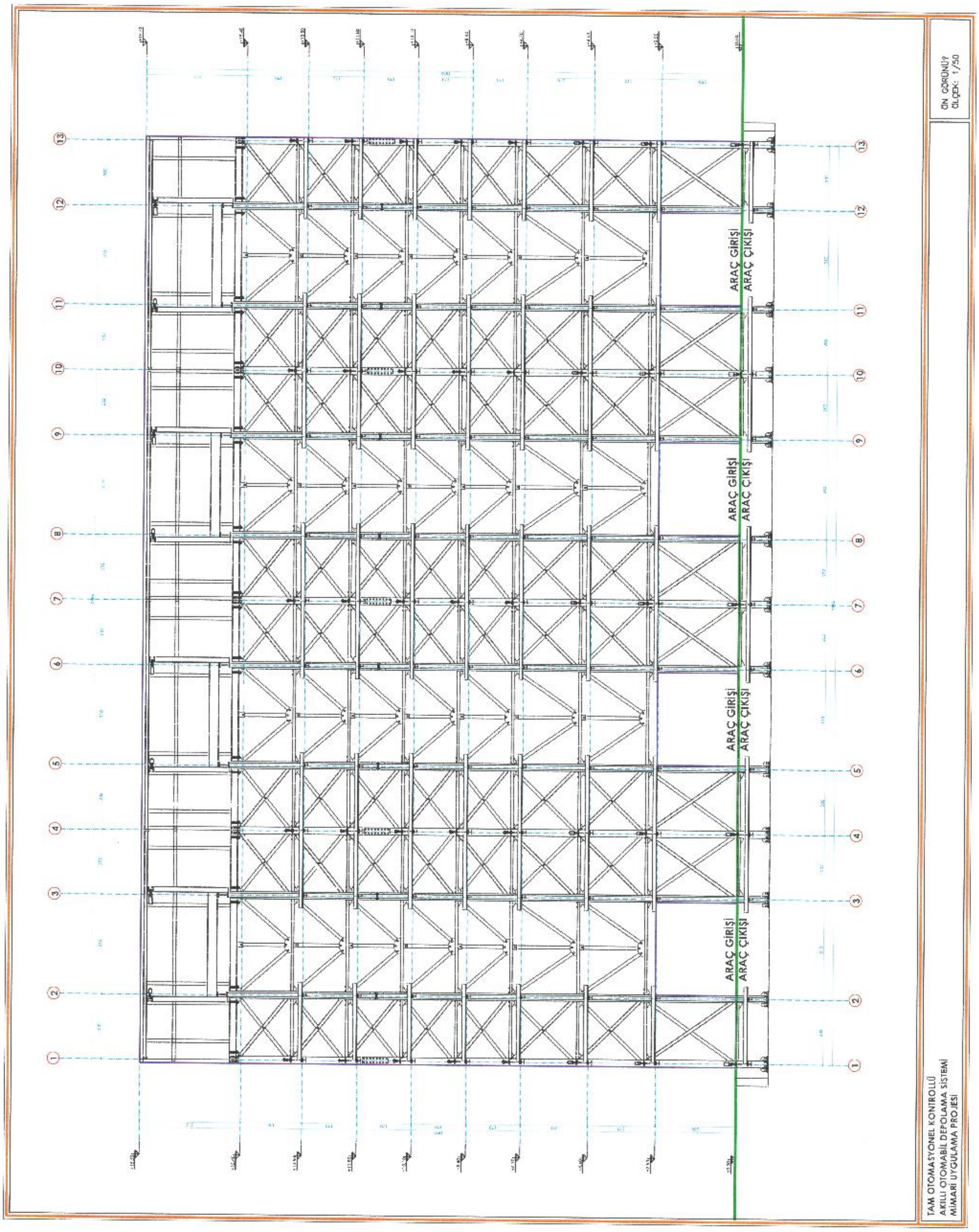

Figure C1. Balikesir Balpark 4x14 Tower Type AVPS front view

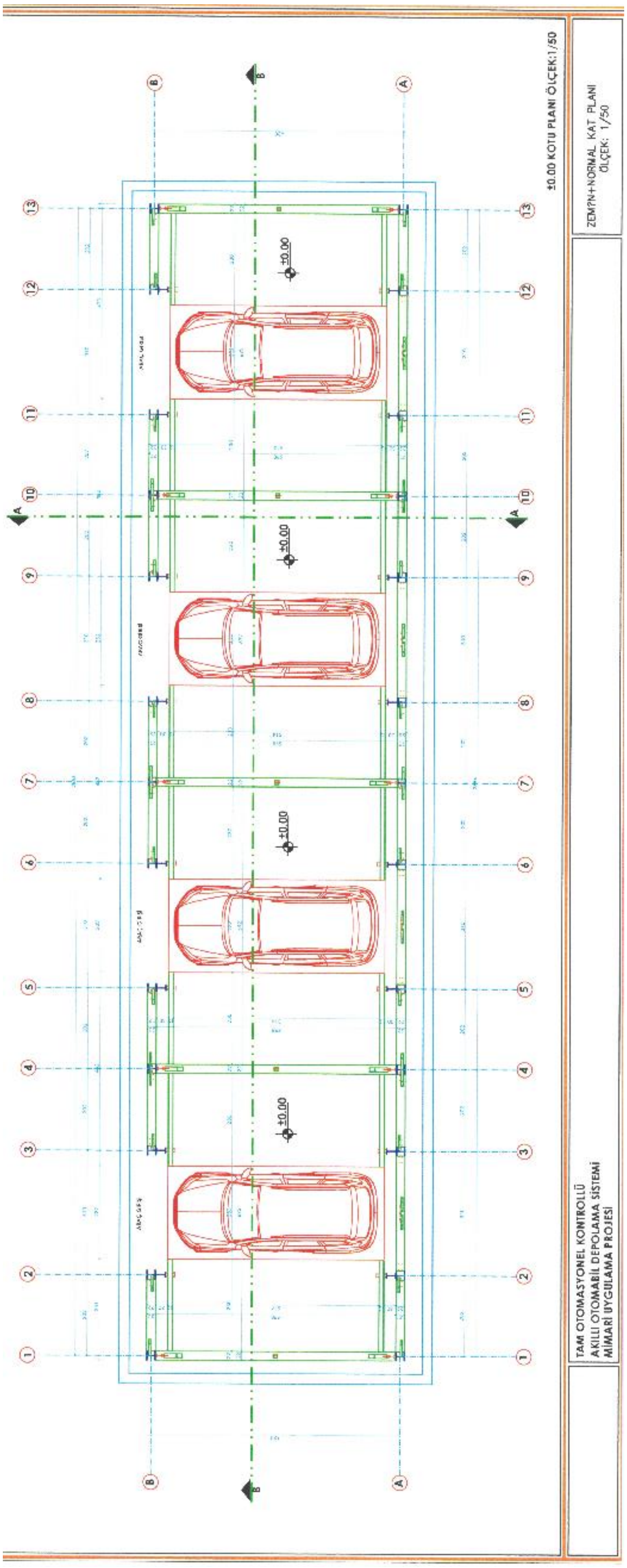

Figure C2. Balikesir Balpark 4x14 Tower Type AVPS plan view

APPENDIX D: MATLAB CODES

1-)Backwall temperature calculation with adiabatic back surface

```
function [Tback] = backwall(T,t)
cp=1000; ro=800; delx=0.05; k=0.05;
[n,y]=size(T)
Tback=20*ones(n,1);
for i=2:1:n
    delt=t(i)-t(i-1);
Tback(i)=Tback(i-1)+k*delt*(T(i-1)-Tback(i-1))/(ro*cp*delx*delx);
End
```

2-)The Code for Pallet Drop

```
clc
close all
clear all

Tz=125;
T=27.5;
Ereduction=210/210;
Yreduction=235/235;
x=0.0008;

alpha=12e-6;
W=19600;
La=2.7;
Lo=5.2;
I=4*3.178e-6;
Wp=60.7;
Y=235;
Lp=Lo*(1+alpha*T)

E=Ereduction*210e9;
M=W*(Lp-La)/2
Mcap=4*Wp*Y*Yreduction
sigmaY=Y*Yreduction;
capacity_ratio=(M)/Mcap
wP=W/(96.*E.*I)*((Lp-La)*(2.*Lp.*Lp-La.*La+2.*Lp.*La))
wT=(Lp.*Lp)*(alpha*Tz)/8
w=wT+wP
del_w=Lo-2*(Lp.*Lp/4-w.*w)^(1/2)
del_x=x;
delta_dislodgement=(del_x+del_w)
```

3-)SHS Section Finite Difference Code

```
function [Tdata, delT,gradT_SN, gradT_WE] = SHS_fire_response(t,S,E,N,W,W_mean,del_st,h )
hu=4; %EC1 propose 4 w/m2k convective heat transfer coef. for unexposed surfaces
ro_st=7850;
cp_st=460;
k_st=45.8;
eps=0.95;
sigma=5.67e-8;
[n,jj]=size(N);
T_Sin=20*ones(n,1);
T_Sout=20*ones(n,1);
T_Win=20*ones(n,1);
T_Wout=20*ones(n,1);
T_Ein=20*ones(n,1);
T_Eout=20*ones(n,1);
T_Nin=20*ones(n,1);
T_Nout=20*ones(n,1);
```

```
delT=20*ones(n,1);
gradT_SN=0*ones(n,1);
gradT_WE=0*ones(n,1);

for i=1:1:n-1


   delt=t(i+1)-t(i);

   for jj=1:1:10

   % T_Nout
  q1=k_st*W_mean*(T_Nin(i)-T_Nout(i))/del_st;
  q2=k_st*del_st/2*sqrt(2)*(T_Wout(i)-T_Nout(i))/(W_mean);
  q3=k_st*del_st/2*sqrt(2)*(T_Eout(i)-T_Nout(i))/(W_mean);
  q4=W_mean*0.95*(5.67e-8)*((N(i)+273)^4-(T_Nout(i)+273)^4)+W_mean*hu*(N(i)-T_Nout(i));
   T_Nout(i+1)=T_Nout(i)+ delt/((ro_st*cp_st*(W_mean+del_st/2)*del_st/2)) * (q1+q2+q3+q4);

   % T_Nin
  q1=k_st*W_mean* (T_Nout(i)-T_Nin(i)) /del_st;
  q2=k_st*del_st/2*sqrt(2)* (T_Ein(i)-T_Nin(i)) / (W_mean-2*del_st);
  q3=k_st*del_st/2*sqrt(2)* (T_Win(i)-T_Nin(i)) / (W_mean-2*del_st);
  qrr=0.3*(W_mean-2*del_st)*eps*eps*sigma*((T_Ein(i)+273)^4-(T_Nin(i)+273)^4);
  qrl=0.3*(W_mean-2*del_st)*eps*eps*sigma*((T_Win(i)+273)^4-(T_Nin(i)+273)^4);
  qrd=0.4*(W_mean-2*del_st)*eps*eps*sigma*((T_Sin(i)+273)^4-(T_Nin(i)+273)^4);
   T_Nin(i+1)=T_Nin(i)+ delt/ (ro_st*cp_st*(W_mean-del_st/2)*del_st/2) * (q1+q2+q3+qrr+qrl+qrd);

   % T_Sout
  q1=k_st*W_mean*(T_Sin(i)-T_Sout(i))/del_st;
  q2=k_st*del_st/2*sqrt(2)*(T_Wout(i)-T_Sout(i))/(W_mean);
  q3=k_st*del_st/2*sqrt(2)*(T_Eout(i)-T_Sout(i))/(W_mean);
  q4=W_mean*0.95*(5.67e-8)*((S(i)+273)^4-(T_Sout(i)+273)^4)+W_mean*h*(S(i)-T_Sout(i));
   T_Sout(i+1)=T_Sout(i)+ delt/((ro_st*cp_st*(W_mean+del_st/2)*del_st/2)) * (q1+q2+q3+q4);


 % T_Sin
  q1=k_st*W_mean*(T_Sout(i)-T_Sin(i))/del_st;
  q2=k_st*del_st/2*sqrt(2)*(T_Ein(i)-T_Sin(i))/(W_mean-2*del_st);
  q3=k_st*del_st/2*sqrt(2)*(T_Win(i)-T_Sin(i))/(W_mean-2*del_st);
  qrr=0.3*(W_mean-2*del_st)*eps*eps*sigma*((T_Ein(i)+273)^4-(T_Sin(i)+273)^4);
  qrl=0.3*(W_mean-2*del_st)*eps*eps*sigma*((T_Win(i)+273)^4-(T_Sin(i)+273)^4);
  qrd=0.4*(W_mean-2*del_st)*eps*eps*sigma*((T_Nin(i)+273)^4-(T_Sin(i)+273)^4);
   T_Sin(i+1)=T_Sin(i)+ delt/(ro_st*cp_st*((W_mean-del_st/2)*del_st/2)) * (q1+q2+q3+qrr+qrl+qrd);

   % T_Wout
  q1=k_st*W_mean*(T_Win(i)-T_Wout(i))/del_st;
  q2=k_st*del_st/2*sqrt(2)*(T_Sout(i)-T_Wout(i))/(W_mean);
  q3=k_st*del_st/2*sqrt(2)*(T_Nout(i)-T_Wout(i))/(W_mean);
  q4=W_mean*0.95*(5.67e-8)*((W(i)+273)^4-(T_Wout(i)+273)^4)+W_mean*h*(W(i)-T_Wout(i));
   T_Wout(i+1)=T_Wout(i)+ delt/((ro_st*cp_st*(W_mean+del_st/2)*del_st/2)) * (q1+q2+q3+q4);

    % T_Win
  q1=k_st*W_mean*(T_Wout(i)-T_Win(i))/del_st;
  q2=k_st*del_st/2*sqrt(2)*(T_Nin(i)-T_Win(i))/(W_mean-2*del_st);
  q3=k_st*del_st/2*sqrt(2)*(T_Sin(i)-T_Win(i))/(W_mean-2*del_st);
  qrr=0.3*(W_mean-2*del_st)*eps*eps*sigma*((T_Nin(i)+273)^4-(T_Win(i)+273)^4);
  qrl=0.3*(W_mean-2*del_st)*eps*eps*sigma*((T_Sin(i)+273)^4-(T_Win(i)+273)^4);
  qrd=0.4*(W_mean-2*del_st)*eps*eps*sigma*((T_Ein(i)+273)^4-(T_Win(i)+273)^4);
   T_Win(i+1)=T_Win(i)+ delt/(ro_st*cp_st*((W_mean-del_st/2)*del_st/2)) * (q1+q2+q3+qrr+qrl+qrd);

   % T_Eout
  q1=k_st*W_mean*(T_Ein(i)-T_Eout(i))/del_st;
  q2=k_st*del_st/2*sqrt(2)*(T_Sout(i)-T_Eout(i))/(W_mean);
  q3=k_st*del_st/2*sqrt(2)*(T_Nout(i)-T_Eout(i))/(W_mean);
  q4=W_mean*0.95*(5.67e-8)*((E(i)+273)^4-(T_Eout(i)+273)^4)+W_mean*h*(E(i)-T_Eout(i));
   T_Eout(i+1)=T_Eout(i)+ delt/((ro_st*cp_st*(W_mean+del_st/2)*del_st/2)) * (q1+q2+q3+q4);
```

```
    % T_Ein
   q1=k_st*W_mean*(T_Eout(i)-T_Ein(i))/del_st;
   q2=k_st*del_st/2*sqrt(2)*(T_Nin(i)-T_Ein(i))/(W_mean-2*del_st);
   q3=k_st*del_st/2*sqrt(2)*(T_Sin(i)-T_Ein(i))/(W_mean-2*del_st);
   qrr=0.3*(W_mean-2*del_st)*eps*eps*sigma*((T_Nin(i)+273)^4-(T_Ein(i)+273)^4);
   qrl=0.3*(W_mean-2*del_st)*eps*eps*sigma*((T_Sin(i)+273)^4-(T_Ein(i)+273)^4);
   qrd=0.4*(W_mean-2*del_st)*eps*eps*sigma*((T_Win(i)+273)^4-(T_Ein(i)+273)^4);
    T_Ein(i+1)=T_Ein(i)+ delt/(ro_st*cp_st*((W_mean-del_st/2)*del_st/2)) * (q1+q2+q3+qrr+qrl+qrd);
    end
    delT(i)=(1/8)*(T_Eout(i)+T_Ein(i)+T_Wout(i)+T_Win(i)+T_Sout(i)+T_Sin(i)+T_Nout(i)+T_Nin(i));
    gradT_SN(i)=(0.5/W_mean)*((T_Nout(i)+T_Nin(i))-(T_Sout(i)+T_Sin(i)));
    gradT_WE(i)=(0.5/W_mean)*((T_Eout(i)+T_Ein(i))-(T_Wout(i)+T_Win(i)));
end
    Tdata=[T_Eout,T_Ein,T_Wout,T_Win,T_Sout,T_Sin,T_Nout,T_Nin];
end
```